Preliminary Analysis of an Internal Annuloplasty Ring for the Aortic Valve

Neda Sadeghi Malvajerdi

Thesis submitted to the

Faculty of Graduate and Postdoctoral Studies

in partial fulfillment of the requirements

for Masters of Applied Science in Mechanical Engineering

Department of Mechanical Engineering

Ottawa-Carleton Institute for Mechanical and Aerospace Engineering

University of Ottawa

Ottawa, Canada

May 2017

Abstract

Among the four valves of the heart, the aortic valve (AV) is frequently affected by disease. When progressive dilatation of the valve produces a leak when the valve should close (regurgitation), repair may be possible. AV repair is a desirable option because, contrary to AV replacement using a prosthesis, it does not require life-long anticoagulation treatment, and retains the original tissues that naturally combat structural degradation. All the AV repair procedures developed by cardiac surgeons require a good stabilization of the ventriculo-aortic junction (VAJ) diameter, through annuloplasty or reimplantation, for long-term success. In the present work, a preliminary design for a new type of annuloplasty ring is proposed that surgeons could tailor to the each valve's shape and suture inside the VAJ. The design consists in wrapping a commonly available surgical biomaterial into a ring of controlled radial flexibility. For sizing and material selection, several models of increasing complexity were created to account for the anisotropic, hyperelastic nature of all the materials involved. First, an analytical model was programmed in MATLAB to assess the radial flexibility of annuloplasty rings formed with different biomaterials and select those that could match the physiological VAJ radial flexibility between systolic and diastolic pressures. The same program was also used to reproduce the experimental radial and longitudinal stretches of the human VAJ from 0 to 140 mmHg pressures. The analytical models were used to calibrate the parameters of independent finite element (FE) models of the VAJ and ring. Finally, the FE approach was extended to simulate the ring after suturing inside the VAJ, to determine the radial flexibility of the assembly under pulsatile pressure. Supple Peri-Guard® bovine pericardium patches used in transverse orientation emerged as the best currently available material option for the proposed ring, although a material providing more physiological radial flexibility would be desirable.

Acknowledgments

I owe my knowledge and deepest gratitude to my supervisor Professor Michel Labrosse for his technical, helpful advice, and great patience with endless source of knowledge and experience.

Most of all, I take this opportunity to express my words to my best friend and supportive husband Majid for his deepest love, patience and for his tremendous encouragement and support in all aspects of my life. His role has been indispensable and cherished in my achievements. My deepest thanks go to my parents, Rahmat and Mahnaz for their invaluable sacrifices, love and unconditional support. Although they are far away, without them I couldn't have made it up to this point. I wish them all the best and long life.

Table of Contents

List of Figures

List of Tables

List of Symbols

AV	Aortic valve
B	Fillet radius
c_i	Material constant
CC	CardioCel®
E_i	Green strain in direction i
FE	Finite element
H	Strut width
J	Jacobian matrix
L	Strut length
N	Number of strut
nelT	Number of elements across strut thickness
OD	Outer diameter
P	Penalty factor (or Lagrange multiplier)
PG	Peri-Guard®
sele	Size of elements along strut ends
self	Size of elements along fillet radius
sell	Size of elements along strut length
SJM	St Jude Medical®
SPG	Supple Peri-Guard®
STJ	Sinotubular junction
T	Thickness
VAJ	Ventriculo-aortic junction
W	Strain energy function

Chapter 1 Introduction

1.1 General

Heart diseases affect the lives of many people. For example, in Canada, according to the lasts numbers available, heart diseases caused about 48,000 deaths in 2012. Among heart diseases, diseases of the aortic valve, one of the four valves of the heart, are quite common [1]. Because the research work presented in this thesis focuses on the aortic valve, the present chapter will describe in more detail the heart, the aortic valve anatomy and physiology, and prevalent aortic valve diseases. In addition, valve repair procedures and annuloplasty ring designs will be presented. Finally, the thesis objectives will be outlined.

1.2 Heart anatomy and physiology

The heart is a muscular organ that pumps blood throughout the body and beats almost 80 million times per year without stopping. The heart is divided into four chambers: the left and right ventricles, and the left and right atria. Four valves ensure the unidirectional circulation of blood [2].

The purpose of the circulatory system is to bring oxygen-rich blood to and collect carbon dioxide from all the tissues in the body (Figure 1.1). Numbers 1 to 6 in Figure 1.1 show the blood circulation within the heart. Oxygen-poor blood from the inferior and superior vena cave returns to the right atrium; the right atrium fills and contracts, causing the tricuspid valve to open and blood to flow into the right ventricle. The right ventricle then contracts, causing the tricuspid valve to close and the pulmonary valve to open, sending blood through the pulmonary artery to the lungs where blood gets rid of carbon dioxide, and binds with oxygen. When the right ventricle relaxes, the pulmonary valve closes to prevent back-flow. Oxygen-rich blood from the lungs fills the left atrium; the left atrium contracts, causing the mitral valve to open and blood to flow into the left ventricle. The left ventricle then contracts, causing the mitral valve to close and the aortic valve to open, sending oxygen-rich blood through the aorta to reach all parts of our body. When the left ventricle relaxes, the aortic valve closes to prevent back-flow. The time when both the right and left ventricles contract is called systole, while the time when both ventricles relax is called diastole.

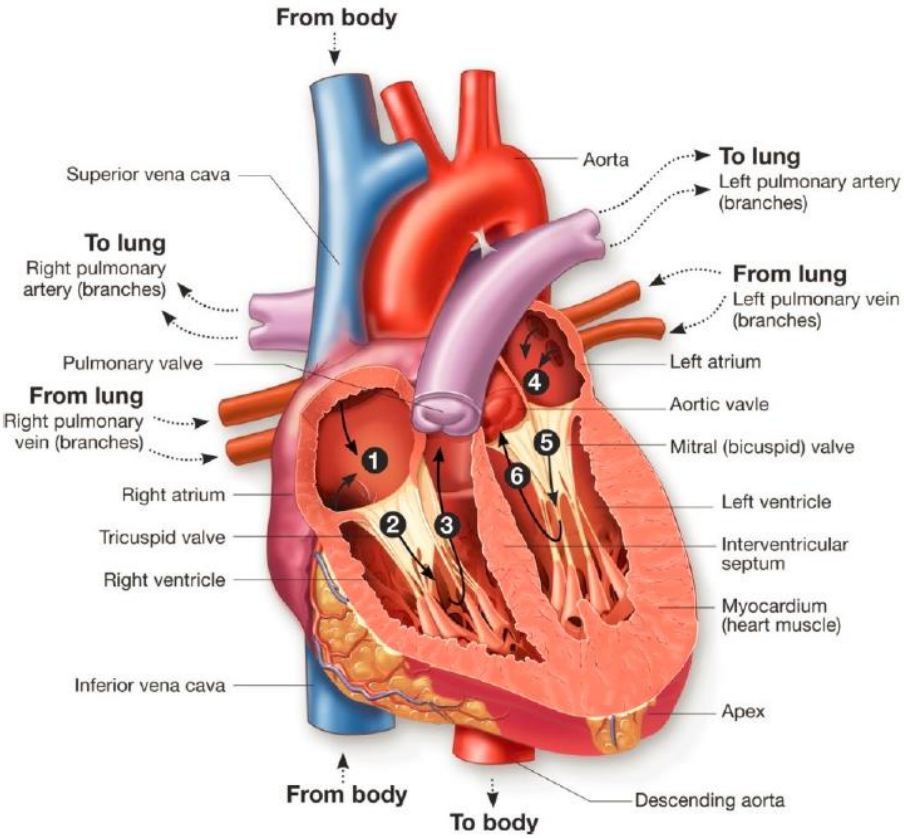

Figure 1.1: Heart anatomy and blood circulation through the heart [3]. According to anatomical convention, left and right are with respect to the person laying face up.

1.3 Aortic valve anatomy and physiology

As mentioned above, a healthy human heart includes four valves (Figure 1.2): the tricuspid and pulmonary valves in the right side of the heart, and the mitral and aortic valves in the left side of the heart [2]. All these valves let blood flow into and out of the heart.

Of particular interest in the present work, the aortic valve (AV) sits between the left ventricle and the origin of the aorta, called the aortic root. As can be seen in Figure 1.3, the AV consists of the ventriculo-arterial junction (VAJ) sinotubular junction (also called basal ring or surgical annulus), three aortic sinuses which correspond to outside bulges of the aortic root, three aortic leaflets, and the sinotubular junction (STJ) delimiting the aortic root from the ascending aorta.

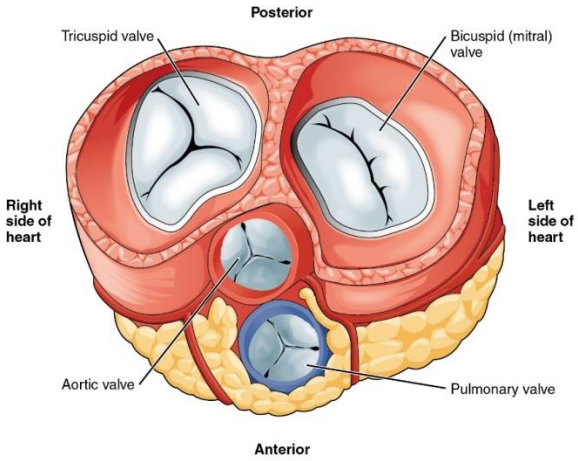

Figure 1.2: Human heart valves [4].

During diastole, the three aortic leaflets (or cusps) come together to close the AV and prevent the reflux of blood from the aorta into the left ventricle; conversely, during systole, the AV leaflets opens fully to allow proper flow of blood from the left ventricle into the aorta.

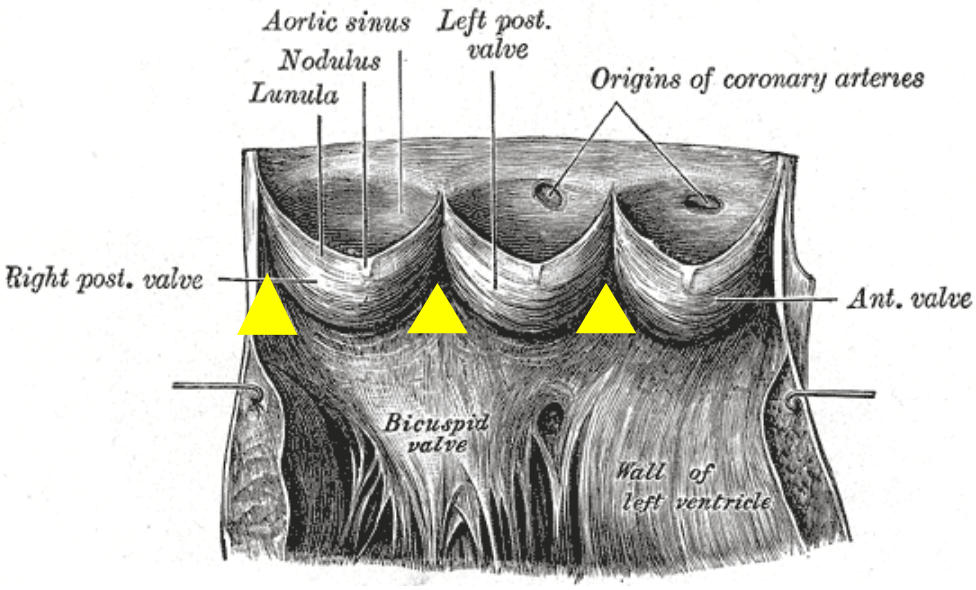

Figure 1.3: Anatomy of aortic valve: the aortic root has been opened through a longitudinal incision and unrolled flat to expose the three aortic leaflets of th eaortic valve inside it, as well as the fibrous triangles (in yellow) between them [5].

1.4 Aortic valve diseases

Aortic valve diseases are divided into two main types: stenosis and regurgitation.

1.4.1 Aortic stenosis

As illustrated in (Figure 1.4), aortic stenosis is present when the aortic valve cannot open completely during systole, causing the heart to work harder than it normally would to circulate the same amount of blood. A frequent cause of stenosis is hardening and thickening (due to calcium deposition) of the leaflets that compose the valve [6].

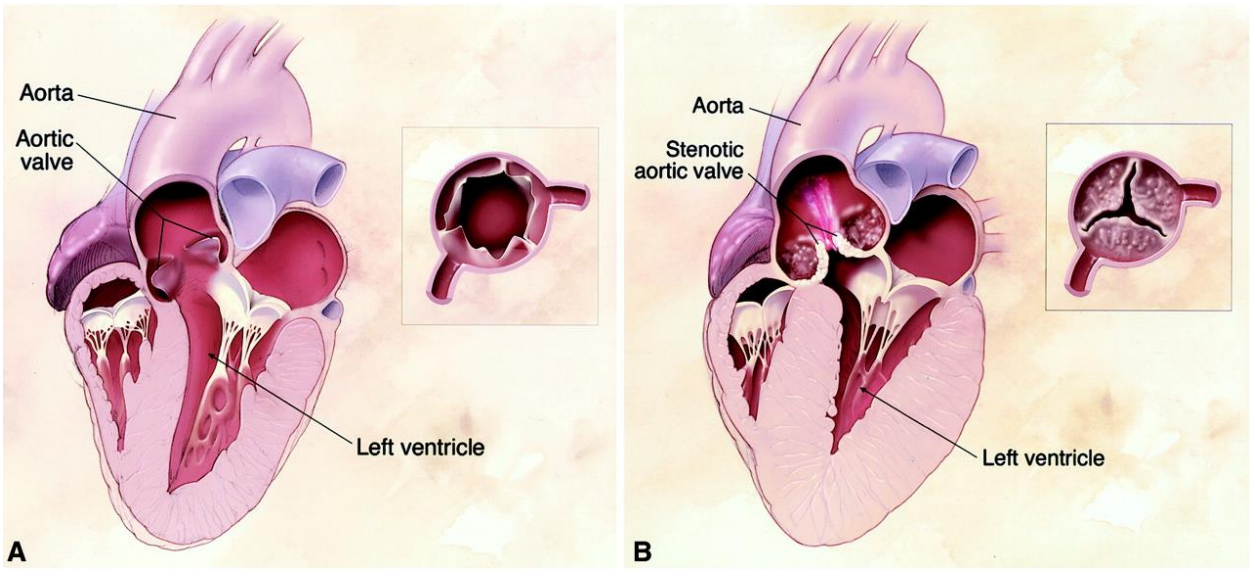

Figure 1.4: (A) Normal aortic valve; (B) Patient with aortic stenosis [6].

1.4.2 Aortic regurgitation

As can be seen in Figure 1.5, aortic regurgitation occurs when the AV does not fully close during end diastole, causing some blood to flow back into the ventricle, and rendering heart beats inefficient. A frequent cause of aortic regurgitation is the dilatation of the aortic root, to the point that the leaflets become too small to close the valve [6].

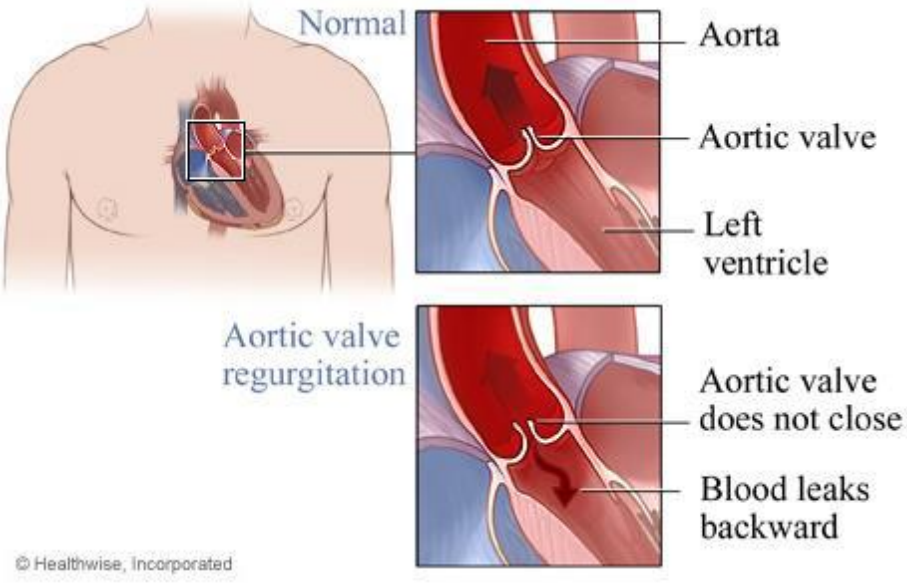

Figure 1.5: Top: Normal AV; Bottom: Aortic regurgitation [6].

1.5 Aortic valve disease treatment

When AV disease becomes so severe that surgical intervention is necessary, different options are available depending on the type of pathology. With aortic stenosis, the leaflets are generally so badly damaged that the only option is AV replacement with a prosthetic valve. However, with aortic regurgitation, and only when the leaflets look functional, aortic valve repair may be performed instead of aortic valve replacement [7]. Either way, open heart surgery is required, with a heart-lung machine and cardio-pulmonary bypass to maintain circulation throughout the body while the heart is arrested and operated on.

1.5.1 Aortic valve replacement

As illustrated in (Figure 1.6), there are two general types of prostheses available for AV replacement: tissue valves or mechanical valves [8]. Mechanical heart valves are made of rigid man-made materials and are extremely durable. However, because the rigid materials damage red blood cells and induce blood clotting, the patients who receive mechanical heart valves need to be treated with life-long anti-coagulation therapy. On the other hand, tissue valves are derived from porcine or bovine aortic valves, after tissue-fixation treatment to destroy any living cells and avoid rejection by the patient's immune system. Without living cells, the tissues of the implanted valves cannot

repair themselves as normal living tissues do, and as a result, tissue valves degrade over time (10-15 years), and present risks of calcification and tears [9,10]. In the case of aortic regurgitation, given the shortcomings of the AV prostheses used in AV replacement, surgeons may prefer to turn to aortic valve repair procedures as an alternative [7].

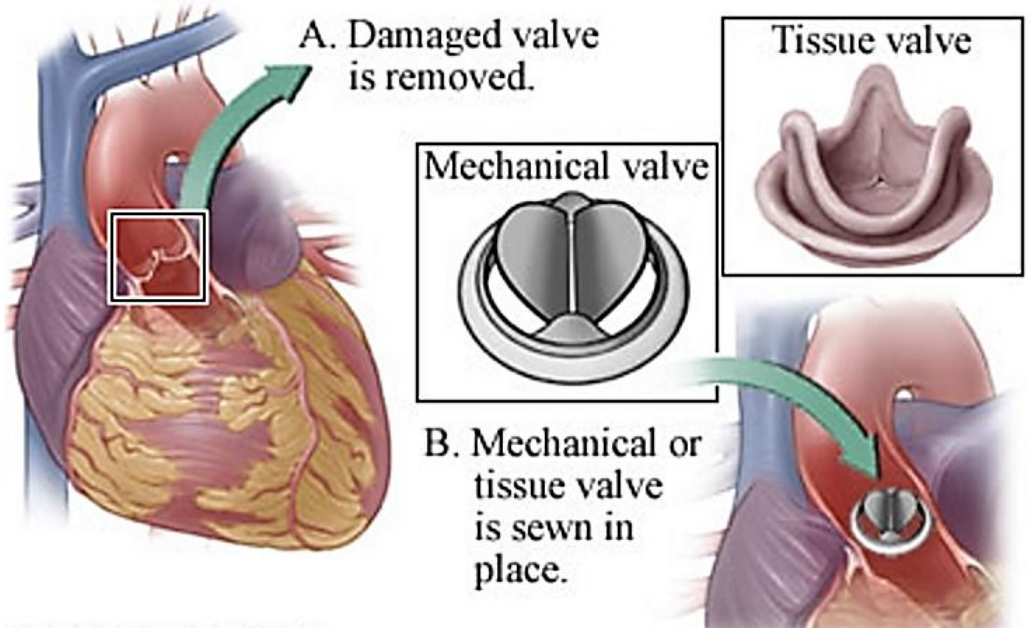

Figure 1.6: Aortic valve replacement techniques [8].

1.5.2 Aortic valve repair

AV repair means that the original deficient valve is not removed. Instead, it is left in place, and modifications are made to it, as deemed appropriate by the surgeon. Because the AV is unpressurized during surgery, it exhibits dimensions that are significantly different from those in vivo. In addition, no two AV are the same, making AV repair only feasible by highly trained and skilled surgeons.

There are two broad techniques of AV repair (Figure 1.7): reimplantation of the aortic valve or remodeling of the aortic root [11]. In the reimplantation technique, the generally dilated aortic root geometry is replaced with a prosthetic tube (Dacron graft) of normal diameter. This graft extends down to the base of the valve, providing full and long-term dimensional control of the repaired aortic root dimensions.

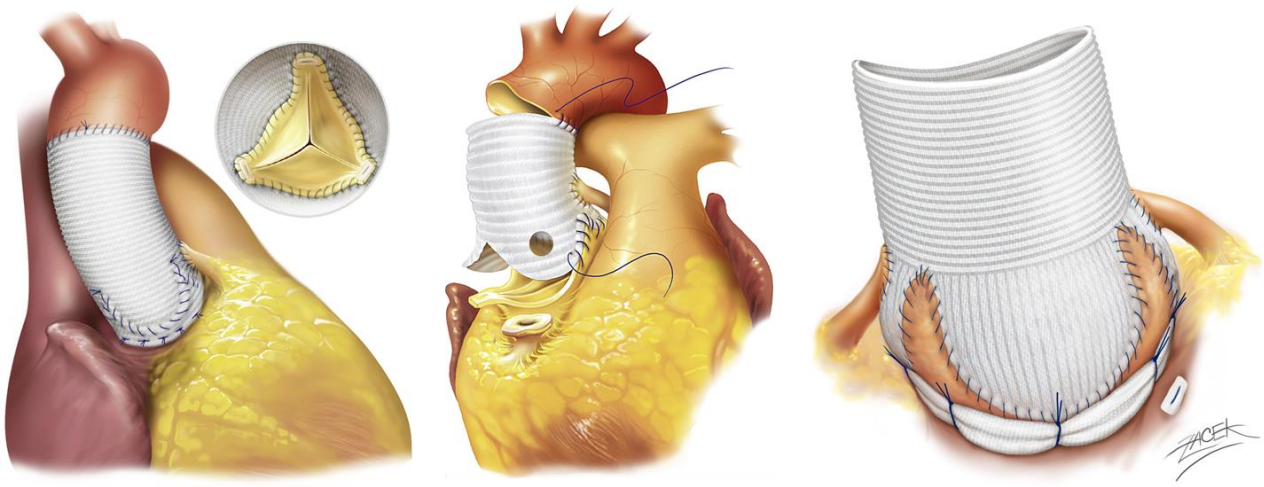

Figure 1.7: Left: reimplantation of the aortic valve; Middle: remodeling of the aortic root; Right: remodeling with an external annuloplasty ring [11].

By contrast, in the remodeling technique, the generally dilated aortic root geometry is also replaced with a prosthetic tube graft of normal diameter, but the commissures of the valve (the regions where two neighbouring leaflets attach to the aortic root) are not constrained by the graft. Although the root remodeling technique tends to be simpler and less time-consuming than the reimplantation technique, it does not stabilize the diameter of the ventriculo-aortic junction (VAJ) as well as the reimplantation technique does. To help stabilize the VAJ diameter, surgeons then often resort to so-called annuloplasty rings [12]. However, as will be detailed in the next chapter, the current annuloplasty rings available to surgeons do not provide full satisfaction. This realization, prompted by direct discussions with Dr. Munir Boodhwani, cardiac surgeon at the University of Ottawa Heart Institute, has given rise to the present work.

1.6 Thesis objectives

The purpose of this study is to 1) come up with a list of basic and functional requirements that a new annuloplasty ring would need to satisfy to achieve to potentially meet with greater acceptance

from the surgical community than the existing models currently enjoy; and 2) propose a tentative design that satisfies these requirements.

1.7 Thesis overview

This thesis includes six chapters, including the present one introducing general knowledge of the heart and AV anatomy and physiology. The literature review in Chapter 2 will give a detailed description of the annuloplasty rings currently available for the mitral valve (annuloplasty of the mitral valve being very common), and the few types of annuloplasty devices available for the AV. This chapter will help identify where improvements can be made, and will culminate in a list of design requirements. During the course of the work, one design was first developed and analyzed, but proved unsuccessful. However, as it is felt that even unsuccessful attempts might be worth recording (at the very least to avoid repetition), Chapter 3 will describe the analysis of the unsuccessful concept, while Chapter 4 will focus on the analysis of a more promising concept. Both chapters include finite element (FE) analyses with different software packages, so particular attention will be paid to the geometry, material properties, loading, and boundary conditions applied to the models. In Chapter 5, comparisons will be made between analytical solutions and FE analysis for the more promising design, and further elaborate on the results from the FE analysis. In the final Chapter 6, conclusions of the work will be developed, as well as recommendations for future work.

Chapter 2 Literature review

2.1 General

This chapter first presents a review of materials commonly used for the construction of prosthetic heart valves (Section 2.2). Given the similarity of biocompatibility and durability requirements as well as location in the body, such materials are natural candidates for constructing an annuloplasty ring. In spite of a thorough literature search, it appeared that relatively few annuloplasty rings have been designed for the AV (Section 2.4). Therefore, it will be relevant, as a potential source of inspiration, to first consider the more numerous annuloplasty rings that have been designed for the mitral valve (Section 2.3).

2.2 Materials traditionally used in heart valve prostheses

Mechanical heart valves, at their introduction in the mid-1960s, used Lucite (methacrylate), nylon, silicone elastomer rubber (initially without and later with heat curing) and stainless steel. More materials were progressively introduced, such as stellite (an alloy of cobalt, chromium, molybdenum and nickel), Silastic rubber (a proprietary Dow Corning's silicone rubber), titanium, high molecular weight polyethylene. Finally, pyrolytic carbon, originally developed for the encapsulation of nuclear fuel rods, has become the principal biomaterial for virtually all mechanical valves [12].

Successful bioprosthetic heart valves, on the other hand, are usually made of porcine or bovine pericardium for the valve leaflets, while the leaflets supports, when present (in so-called stented valves), are made of molded silicone rubber, cobalt-chromium-tungsten (Haynes alloy), stellite, or stainless steel. In more recent valves, the stent/frame tends to be made of cobalt-nickel alloy (Elgiloy), polypropylene, acetyl homopolymer (Delrin), acetyl copolymer (Celcon), or titanium. The base ring and stent/frame can be exteriorized by Dacron, pericardium, polytetrafluoroethylene, or some other polyester fabric, at the level of the base ring [13].

Given the experience accumulated with the materials listed above, one can state that any of them would exhibit the required biocompatibility and durability to be inserted in the body without concern for the short and long-term safety of the patient.

2.3 Annuloplasty rings for the mitral valve

While repair of the AV is still largely under-developed when compared to aortic replacement, the situation, to a large extent, is opposite with the mitral valve (MV), whose anatomy is vastly different from that of the AV. The MV apparatus consists of two asymmetrical leaflets, the annulus along which the leaflets are attached to the left ventricular wall, chordae tendineae (string-like structures) that suspend the leaflets, and two papillary muscle heads that originate from the bottom and sides of the left ventricle to anchor the chordae. The MV leaflets open in diastole to let blood in from the left atrium into the left ventricle. The MV function is to close and prevent backflow during systole [2].

For the MV, repair is recognized and practiced as a very successful approach to MV disease. The American College of Cardiology/American Heart Association guidelines demonstrate that success rate of mitral valve repair reaches more than 90% [15,16]. MV replacement, on the other hand, increases the risk of thromboembolism (formation of potentially lethal blood clots); therefore, most patients need anticoagulation after valve replacement [17,18]. In addition, they may also need to undergo repeated valve surgeries during their lifetimes.

Typically, a mitral annuloplasty ring is sutured into a dilated mitral valve annulus to prevent future annular dilatation and restore the normal shape and diameter of the valve [19]. In a mitral valve that is no longer dilated, the leaflets can seal more efficiently during systole, and open more widely in diastole. Insertion of an annuloplasty ring is expected to decrease the stress generated in the leaflets and sutures [20,21]. As the general final step in MV repair (e.g. after sutures, such as the Alfieri stitch [22], are applied to the leaflets), the insertion of an annuloplasty ring is an important cornerstone, where selection of the proper device, adequate sizing and suturing technique all play important roles [20,23].

There are many different annuloplasty devices available for the MV (Figure 2.1). They can be categorized according to geometry, structure, indication and function [24]. As illustrated in

Figure 2.1, rings are typically available in four different geometries: complete or D- shape, partial or C-shape, and 2D or 3D shaped rings. Annuloplasty rings come in rigid (typically complete or D-shape), and semirigid or flexible (typically partial or C-shape) implementations. 3D shape rings are intended to reproduce the natural saddle-shape outline of the MV annulus. There have been studies to explore which type of ring would be better, rigid or flexible. For example, Chee et al. [25] found that using flexible annuloplasty rings improved left ventricular systolic function, while the rigid ones had a negative impact on it. They also found that flexible rings were not as efficient as rigid ones in preventing future dilatation of the mitral annulus, pointing to the possibility of recurrence of mitral regurgitation (leakage) when using flexible annuloplasty ring. Still, from a clinical perspective, many different rings tend to be associated with the same outcomes [20], and their apparent diversity may stem more from various suppliers trying to differentiate themselves in a crowded market than from evidence-based analysis [20].

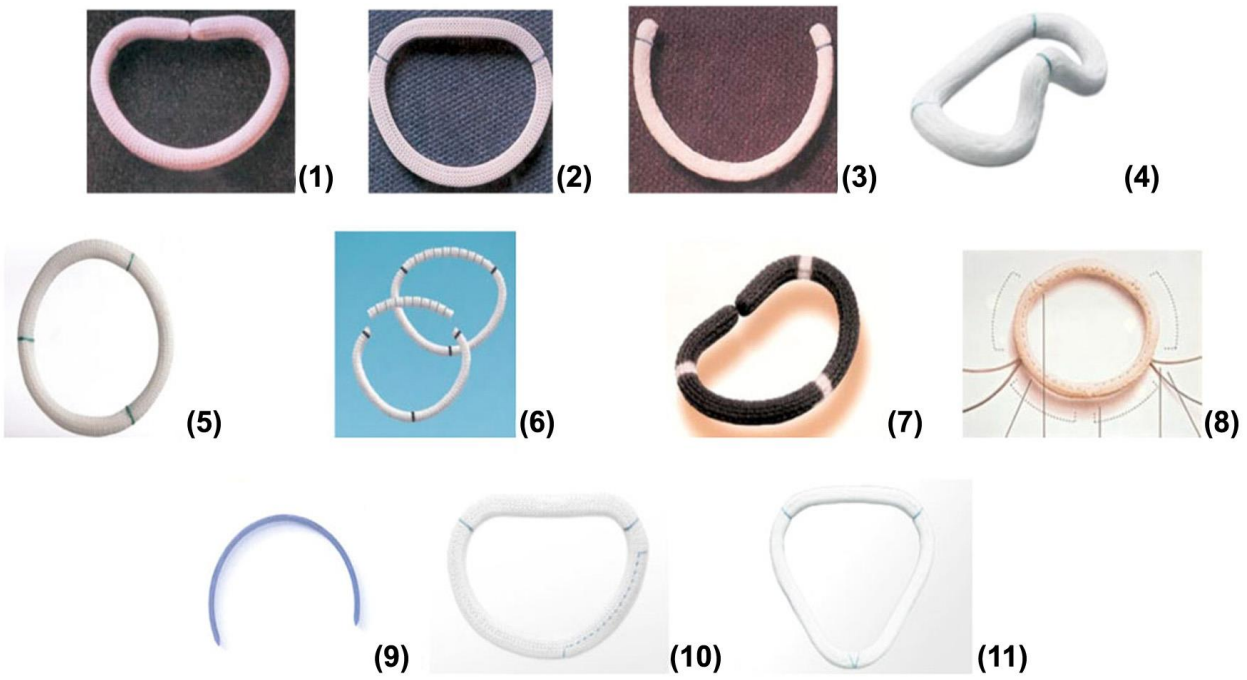

Figure 2.1: 1. Carpentier-Edwards classic annuloplasty rings. 2. Carpentier-Edwards physio annuloplasty ring. 3. Cosgrove-Edwards annuloplasty system. 4. Edwards GeoForm annuloplasty ring. 5. Medtronic-Duran flexible annuloplasty ring. 6. St Jude tailor annuloplas annuloplasty ring and band. 7. Sorin-CarboMedics Flo annuloplasty ring. 8. Genesee Sculptor annuloplasty ring (adjustable). 9. Kalangos Bio-ring. 10. Carpentier- McCarthy-Adams IMR ETlogix. 11. Edwards Myxo ETlogix [24].

Even then, as can be seen from Figure 2.1, all rings present a common feature in the form of a fabric sewing cuff to allow for easy suturing to the surrounding structures. Indeed, this is a feature that any annuloplasty ring, for any valve, must have to be acceptable in the operating room.

The mitral valve size is unique to each patient. Therefore, the ring sizes can be selected from a list of available dimensions or possibly tailored during surgery [24].

The number of sutures used to implant an annuloplasty ring depends on the ring geometry. For example, for the D-shape ring, the required sutures number is at least 10-12, while this number decreases to 8-10 for a partial ring. For a ring used to shrink the mitral valve annulus (in a process called undersizing, rather than just stabilizing), more sutures are used [23].

2.4 Annuloplasty rings for the aortic valve

Chief among recognized causes of aortic regurgitation are the combined or individual dilatation (i.e. permanent enlargement) of the VAJ diameter and/or the STJ diameter [26]. As discussed previously, surgical repair approaches following the reimplantation technique [27,11] provide inherent stabilization of the VAJ diameter, because the prosthetic graft goes all the way down to the VAJ level. However, with more sutures and more tissue dissection needed around the valve, reimplantation takes more time to perform than remodeling, and because every minute counts in the operating room as the patient is unconscious and under cardio-pulmonary bypass, remodeling has been favoured by many surgeons. Still, repair approaches following the remodeling technique [28,11] do not stabilize the VAJ diameter, hence the need for additional stabilization in the form of annuloplasty ring for the aortic valve. Aortic annuloplasty devices may be external or internal, as detailed below. Please note that, contrary to MV annuloplasty rings, the selection currently available to surgeons is extremely limited. The only models that were identified after a thorough literature search are described below, and only Lansac's Extra-Aortic^{TM} annuloplasty ring and Rankin's HAART 300 aortic annuloplasty device are available on the market.

2.4.1 External annuloplasty devices for the AV

In 2009, Lansac et al. suggested to combine the remodeling and reimplantation techniques by adding an external annuloplasty ring to stabilize the VAJ diameter, and possibly including another

annuloplasty ring to stabilize the STJ diameter (Figure 2.2) [14]. As can be seen in Figure 2.3, the expansible external aortic ring designed by Lansac et al. is made of two silicone elastomer cores sheathed within a polyester material. The elasticity of the ring was claimed to increase the sealing capability of the leaflets through recoil during diastole, while accommodating physiological root expansion during systole [14]. Indeed, over the course of every heartbeat, the aortic root normally dilates and retracts by some amount, as dictated by the changes in aortic pressure between diastole (80 mmHg) and systole (120 mmHg) (Figure 2.4). The ring must be designed to allow for this normal aortic compliance, and avoid degenerative and tearing issues. Lansac et al. reported radial flexibility values of 10% from diastolic to systolic aortic diameters after AV repair in animal models (sheep) [14].

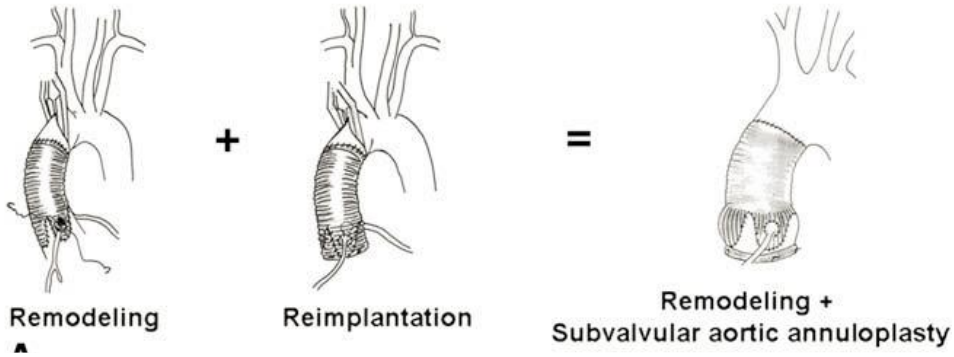

Figure 2.2: Remodeling associated with a complete subvalvular aortic ring to combine the advantages of both the original remodeling and reimplantation techniques [14].

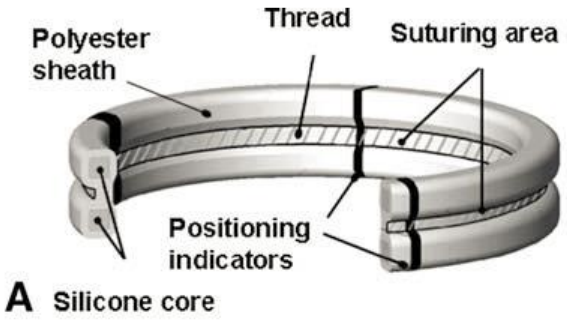

Figure 2.3: Extra-Aortic^{TM} flexible external annuloplasty ring [14].

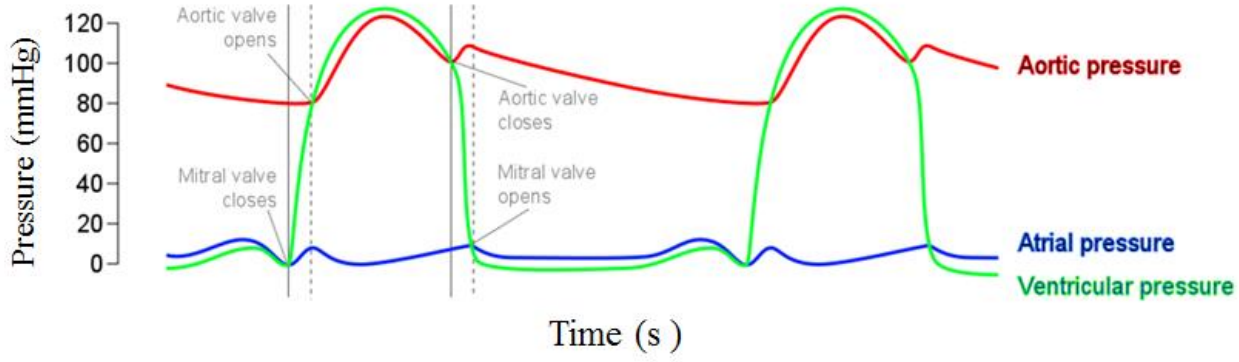

Figure 2.4: Cardiac cycle in the left side of the heart (Redrawn by the author from [2]).

The Extra-Aortic^{TM} ring has demonstrated durable stabilization of the VAJ as well as elastic properties after implantation in humans [29,30]. However, in 10 humans (51 years of median age), the immediate as well as middle-term (median of 21 months after operation) radial flexibility from diastolic to systolic aortic diameters was between 2 and 4%, as measured by careful measurements of the annuloplasty ring base diameter using computed tomography imaging [30]. This means that, even though the ring is capable of a radial flexibility of 10%, only on average 3% is needed in humans, which defines 3% as the target value for the effective radial flexibility of any new annuloplasty ring design after implantation.

Given difficulties with tissue dissection around the valve during surgery (in particular, damaging certain areas or electrical conduction, and leading to cardiac fibrillation, a potentially life-threatening condition) it remains a challenge for surgeons to implant an external ring such as the Extra-Aortic^{TM} ring at a level that is low enough to truly achieve VAJ stabilization rather than deformation of the mid-sinus region (roughly at the mid-height of the valve) [30].

In 2011, Scharfschwerdt et al. proposed an open external annuloplasty ring to be implanted at the base of the aortic root [31]. The outer layer of the ring is covered in Dacron for easy suturing. The inner core of the ring is made of metal, with a rise in the portion that will meet with the area of the heart where any compression or damage may lead to heart fibrillation (Figure 2.4). In tests, this annuloplasty device was able to reduce the volume of blood leakage through the valve in diastole; in addition, the height of sealing contact between leaflets was favorably increased [31].

However, specific attention needed to be paid to the suturing method used because the ring was prone to cause damage to the coronary arteries [31].

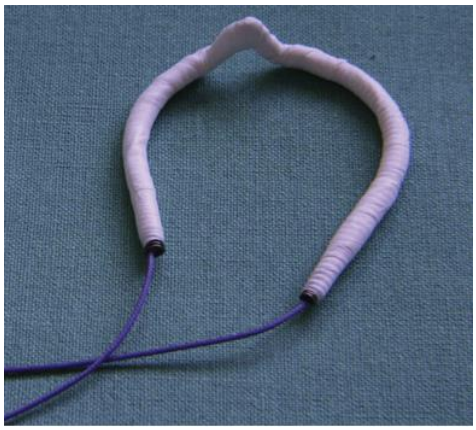

Figure 2.4: External annuloplasty ring [31].

2.4.2 Internal annuloplasty devices for the AV

In contrast to external annuloplasty, internal implantation has the potential of completely circumventing the issue of surgical dissection of the tissues around the AV. In addition, if the profile of the device is thin enough, no significant impact on the quantity and quality of blood flow throw the AV is expected. Scharfschwerdt and his research team modified their external ring design to generate a closed flexible annuloplasty ring meant to be implanted inside the VAJ. It was made of wire frame covered in a Dacron layer (Figure 2.5) [31]. A significant issue reported about this device was its proper positioning to achieve effective VAJ stabilization without interfering with the motion of the aortic leaflets [31]. Another issue was the difficulty in custom-sizing the ring to the patient's geometry.

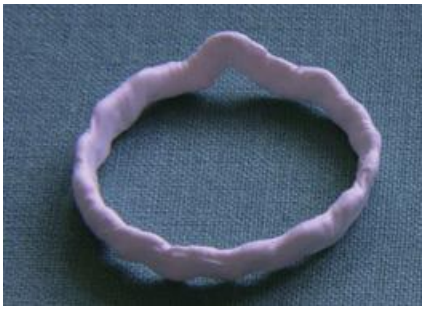

Figure 2.5: Internal annuloplasty ring [31].

Figure 2.6: Rankin's HAART 300 rigid aortic annuloplasty device [32].

In 2013, Rankin et al. designed a rigid internal annuloplasty device (Figure 2.6) to restore a physiologic annular size and geometry during aortic valve repair surgery [32]. The ring was made of titanium with a Dacron cover. The ring was tested in 5 patients with acceptable results, as the ring reduced the aortic valve dilatation as well as the volume of blood leaked through the valve during diastole [32]. However, a rigid internal ring brings about risks of tearing surrounding tissues, as well as calcification. In addition, this design cannot accommodate the frequently irregular shapes found in patients' valves.

As can be gleaned from the previous description, as well as established by discussing with Dr. Boodhwani and in accordance with known concepts of physiology and design of implantable cardiovascular devices, below are basic and functional requirements that need to be satisfied by the annuloplasty ring:

1) The ring should be internal (i.e. fit within the VAJ) to avoid access and positioning issues encountered with external annuloplasty rings. Further, the ring should be of relatively small thickness (e.g. on the order of 1 mm) to not interfere with the blood flow;

2) The ring must be biocompatible to minimize issues of rejection by the body. As discussed, many material options, flexible or rigid, are available;

3) The ring must be able to sustain millions of cardiac cycles because the heart beats more than 80 million times each year;

4) The ring should not promote tears or calcification of neighboring structures. One key aspect to achieve this goal is to ensure that the ring accommodates deformations that are of the same order as those that would occur naturally at the base of the aortic valve. Namely, a value of 3% for the radial flexibility of the ring during cardiac cycles has been found to be compatible with normal human physiology [30];

5) The ring should have a feature (cuff) that allows for sowing into place;

6) The ring should allow for patient-specific shaping of triangular projections along the circumference to accommodate the fibrous triangles of the valve (see Fig. 1.3).

Chapter 3 Stainless steel design

3.1 General

In this chapter, the focus is placed on analyses aimed at testing the feasibility of an internal annuloplasty ring made of stainless steel. Although nickel and titanium alloys (Nitinol) could also have been of interest as they are commonly used for cardiovascular stents [33], its price was felt to be prohibitive for this early design study. After a tentative geometry is defined, the different steps of analysis of the design will be presented.

3.2 Ring geometry

The tentative ring design consists of a pattern (Figure 3.1) that is repeated around the circumference of the ring. This design, compared to a solid ring design which would have been very stiff radially, was expected to impart the ring with controllable radial flexibility by promoting flexion in the struts when the ring was submitted to radial loads from the pulsatile blood pressure. A view of the complete ring is shown in Figure 3.2. The ring was assumed to be radially cut from a tube of stainless steel. Based on standard tube dimensions (Appendix 1), the initial outer diameter (OD) of the ring was 22.225 mm, and the thickness (T) of the ring was 0.889 mm. By design, such a ring would satisfy the following requirements from Chapter 2:

1) The ring should be internal (i.e. fit within the VAJ) to avoid access and positioning issues encountered with external annuloplasty rings. Further, the ring should be of relatively small thickness to not interfere with the blood flow;

2) The ring must be biocompatible to minimize issues of rejection by the body.

On the other hand, the following requirements from Chapter 2 would not immediately be met:

3) The ring must be able to sustain millions of cardiac cycles because the heart beats more than 80 million times each year. This issue can be addressed if a successful design satisfying the other requirements was to emerge;

5) The ring should have a feature (cuff) that allows for sowing into place. This requirement can easily be met by covering the ring with a fabric sheath;

6) The ring should allow for patient-specific shaping of triangular projections along the circumference to accommodate the fibrous triangles of the valve (see Fig. 1.3). This requirement could be met by attaching triangular projections where needed around the ring, but this option is considered premature before the elastic behaviour of the proposed ring is complete. Finally,

4) The ring should allow for 3% radial flexibility of the ring during cardiac cycles [30]. Please note that at the time of the study, the target value was still 10% as indicated in [14]. This requirement prompted the parametric analysis of the design, through the process detailed in the following sections.

With a gap between two struts equal to 2B, fillet radii of B (not shown in Fig. 3.1, but implemented in Fig. 3.2) were set at the end of each strut to reduce stress concentrations. The value of B was set to be proportional to that of strut width H, and maximized the fillet radius given the available space. The initial ring design comprised of N = 80 struts. The design dimensions shown in Figure 3.1 are those on the outer diameter of the ring, for an example design.

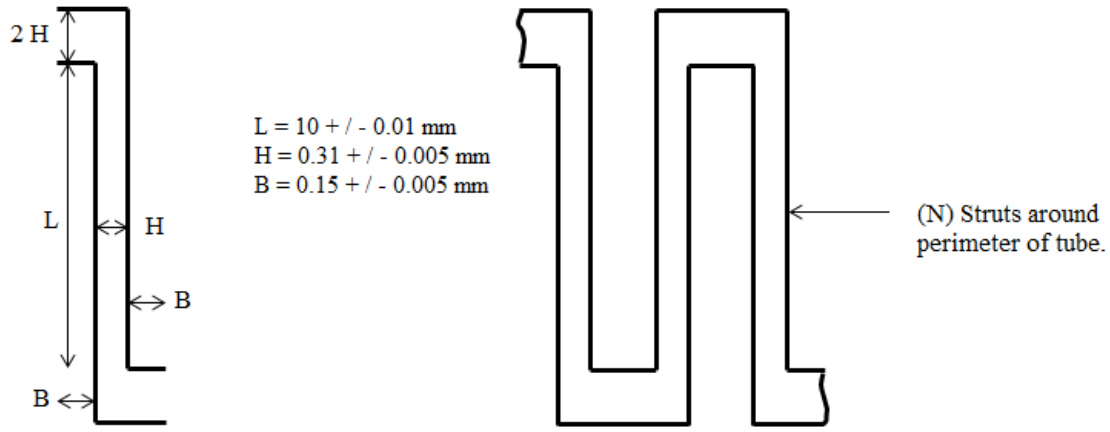

Figure 3.1: Initial schematic of individual struts constituting the ring.

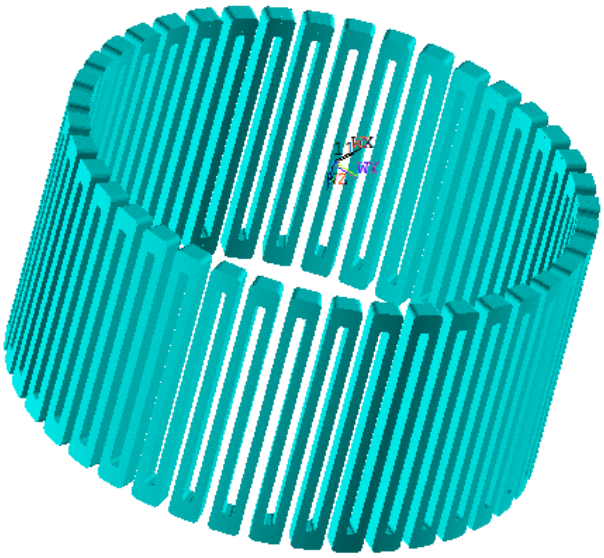

Figure 3.2: ANSYS rendering of the whole internal annuloplasty ring with strut dimensions as in Figure 3.1, and 80 struts. The ring would be inserted just below the aortic leaflets, within the out-flow tract of the left ventricle.

As some level of plastic deformation in the fillet regions turned out to be unavoidable for the loads and geometries of interest, it became clear that the stress and deflection levels within the ring were not going to be described by a simple analytical model. Therefore, it was decided to turn to finite element (FE) analysis.

The ring geometry was generated by writing parameterized commands in ANSYS APDL (ANSYS 15.2, Canonsburg, Pennsylvania, USA) (Appendix 2). Parameterized commands made it easy to change the geometry of the ring (e.g. number and dimensions of struts). As typical in ANSYS geometric modeling, the first step consisted in defining a list of 3D coordinates for the points of interest (keypoints). They were then connected by lines. The lines were used to define areas, and in turn, the areas were used to define volumes (Figure 3.3).

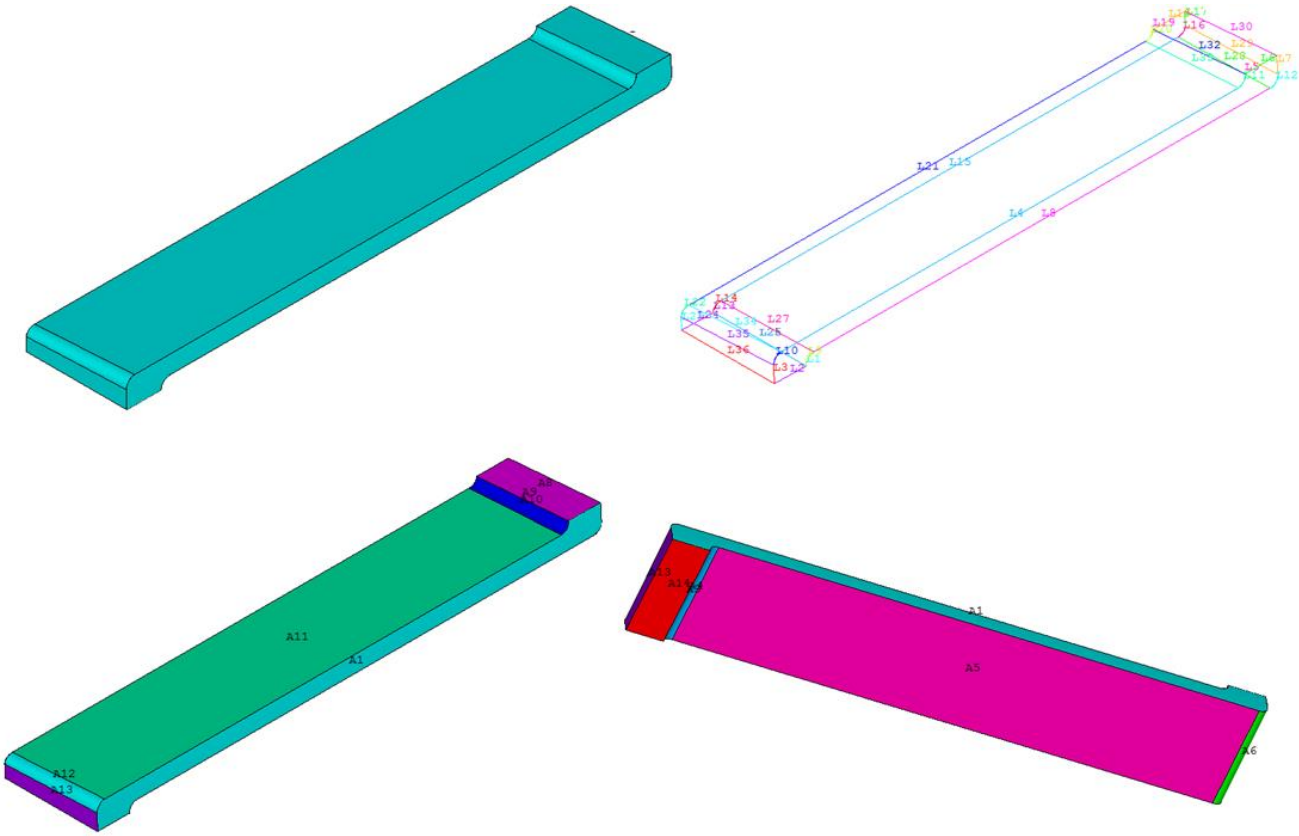

Figure 3.3*:* Schematic of the volume of one individual strut of the ring created in ANSYS APDL with key points, lines and areas.

3.3 Material properties

The candidate material was 316 stainless steel due to the existence of medical, biocompatible versions of it, common availability and general machinability [34]. However, it was necessary to use a material model that could account for the development of plastic deformations at the fillets of the ring struts. One realistic approach to do so is to use the elastoplastic material model, wherein the response of the material is perfectly elastic (characterized by modulus of elasticity and Poisson's ratio) until stresses in the material, combined into Von Mises stress, exceed the yield strength of the material. Further increases in deformations are made to follow a nonlinear stress-strain curve that can be set pointwise (Figure 3.4).

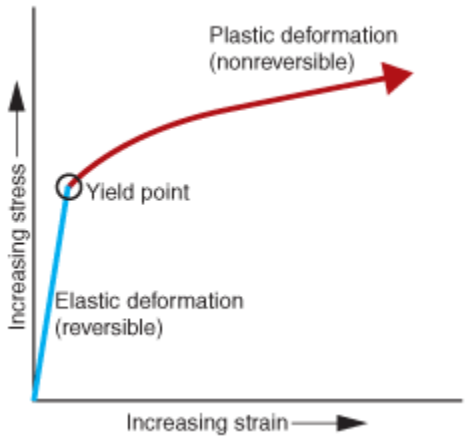

Figure 3.4: Schematic stress-strain curve for an elastoplastic material.

If the load is progressively removed, elastic deformations occur first, as governed by the modulus of elasticity, and the plastic, incompressible strains progressively reveal themselves in the form of the permanent set under no load. In this study using ANSYS, the material properties were input as a linearly elastic and isotropic part with an elastic modulus of 190,000 MPa and a Poisson's ratio of 0.33 [34], as well as a multilinear isotropic plastic part defined by 6 points on a uniaxial stress-strain curve ("tbpt" commands in Appendix 2) [35].

3.4 Finite element mesh, boundary conditions and loading

Element type SOLID185 was used for the three-dimensional modeling of the ring. The element is defined by eight nodes having three degrees of freedom at each node: translations in the nodal x, y, and z directions. This element was chosen because it has plasticity, large deflection, and large strain capabilities. To control the mesh density of the model, four different parameters were defined (Appendix 2): sele, the size of elements along strut ends; self, the size of elements along fillet radius; selL, the size of elements along strut length (L), and nelT, the number of elements across strut thickness (T).

An illustration of the meshed strut is shown in Figure 3.5 for sele = 2*H/10, self = B/8, selL = L/160 and nelT = 20.

Figure 3.5: Hexahedral-dominant mesh used for the ring strut mesh.

As illustrated in Figure 3.6, boundary conditions were applied to relevant areas of the strut to achieve circular symmetry around the ring, while actually only modeling one strut. With X, Y and Z being the radial, circumferential and longitudinal directions, respectively, of a cylindrical coordinate system attached to the strut, all nodes in Area 13 were prohibited from moving in the Z direction, while all nodes in Areas 8 and 14 were prevented from moving in the Y direction. The strut was loaded by a radial displacement imposed on all nodes of Area 1.

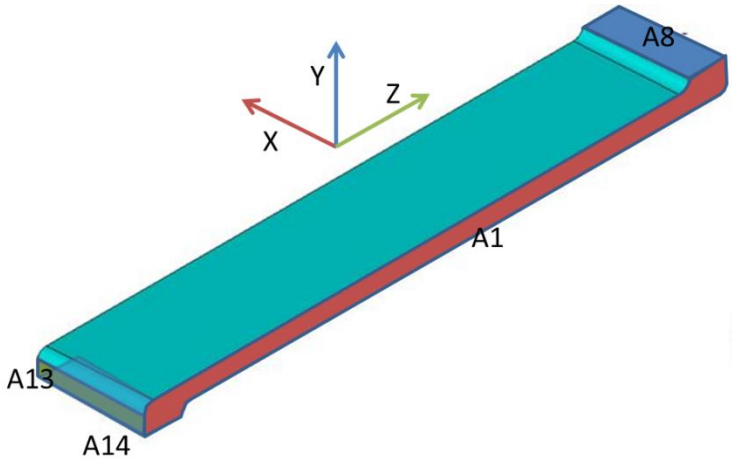

Figure 3.6: Applying loading and boundary conditions.

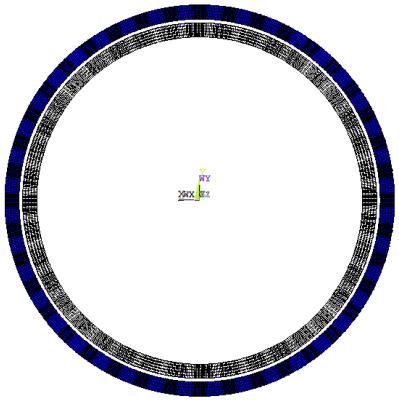

Figure 3.7: End view of the expanded model (owing to symmetry and pattern repetitions) of the whole ring formed by 80 struts. The deformed (blue) and undeformed (black) shapes are represented.

3.5 Method of analysis

The annuloplasty ring is meant to be sown inside the VAJ, just below the aortic valve leaflets to not interfere with them, while preventing the dilatation of the tissues that support them for years to come. For simplicity, the aortic valve may be represented as a cylindrical tube. In real conditions of use, the ring would be implanted in a somewhat dilated aortic valve, meaning that the ring would have to restrain the existing tissues, while preserving some physiological radial flexibility during each cardiac cycle. One central design issue is how much radial flexibility can be afforded by a ring of given geometry, such that, one might be able to tune this radial flexibility to desired values. To try and address this issue, the analysis was carried out as follows.

The first assumption consisted in replacing the actual blood flow within the aorta by its resulting pressure, expected to fluctuate between 80 and 120 mmHg pressures (100 mmHg = 13.3 kPa). Assuming that the inner diameter of the annuloplasty ring sown in the aorta is increased by an arbitrary amount (as a result of the application of such pressure), the finite element model was used to determine the radial force exerted by the ring to resist this diameter increase. The resulting radial force was then distributed over the deformed annular area covered by the ring to determine the corresponding blood pressure.

As an example of the type of results obtained through this analysis, the ANSYS-generated plot of blood pressure vs. ring diameter presented in Figure 3.8 was obtained for an initial annuloplasty ring diameter of 17.3 mm. Because of plastic deformations occurring in the ring upon first

loading, large increases of the ring diameter were observed: as the blood pressure was increased to slightly over 120 mmHg, the ring diameter reached 28.5 mm (loading phase). Such dilatation would only be observed the first time that the ring would be loaded. According to the elastoplastic model, during service as an annuloplasty ring in a patient with diastolic and systolic pressures of 80 and 120 mmHg, respectively, the ring outer diameter would stay on the path described by the unloading phase of the graph: it would elastically vary between 25.9 and 27.66 mm, back and forth. The radial flexibility of the ring can be determined by analyzing the path of the curve during the unloading phase, according to the following equation:

$$Flexibility\ (\%) = \frac{OD_{120} - OD_{80}}{OD_{80}} \times 100, \tag{3.1}$$

where the outer diameter (OD) information is needed under 80 and 120 mmHg pressures. In the case described in Figure 3.8, the radial flexibility was 6.8%. Given that the ring diameter under 80 mmHg was still too large compared to values in the 22-23 mm range as needed to match values in normal aortas, the dimensions of the unpressurized geometry still required modification. However, the research on the stainless steel annuloplasty design was aborted because of what appeared to be a major design flaw, as detailed in the next section.

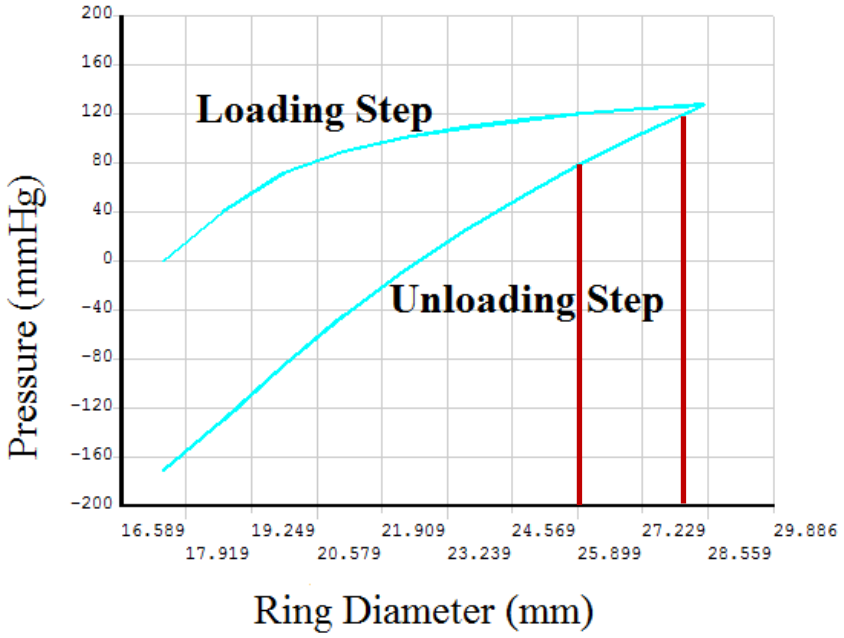

Figure 3.8: Pressure-diameter curve for one candidate annuloplasty ring; in this example, the radial flexibility defined in (3.1) between systole and diastole (red lines) was 6.8 %.

Finally, note that the negative pressure values shown in Figure 3.8 correspond to the hypothetical case where one would "suck in" on the ring to make it reach its original diameter after it has plastically deformed.

3.6 Concluding remarks

While fatigue life calculations would have possible from the stress results available from FE analysis to confirm the design (using for example the modified Goodman fatigue criterion), the results illustrated in Figure 3.8 pointed to a most crucial problem with the proposed ring design: its operating dimensions were very sensitive to the patient's maximum blood pressure (which may be as high as 160 or even 200 mmHg in severe cases, and cannot be predicted to reliably stay below a certain value). For such pressures, the plastic deformations would allow the ring to reach uncontrolled and unwanted dimensions, rendering it useless. In addition, despite many attempts through parametric analyses varying geometric parameters B, H, and N, it did not seem possible to operate purely in the elastic range of deformations and reach a radial flexibility of 10%.

Other issues were also noted regarding potential manufacturing of a ring prototype. It turned out that we could not identify any contractor that had suitable equipment or techniques to make such a prototype out of a stainless tube (or other material). Laser cutting, with its high temperatures, would induce unwanted residual stresses in the design (although they could be removed by heat treatment), and possibly severely distort the ring. For water jet cutting, it was discovered by contacting several independent contractors that the nozzles available were larger than the smallest cuts necessary to achieve the desired pattern. Three-dimensional printing by laser sintering was not considered because of the inhomogeneous nature of the material obtained by the process, which would make the fatigue life of the ring challenging to assess and guarantee. Electrical discharge machining, because of its lack of speed, and given the extensive cutting required to make a ring, was not considered either.

When these realizations finally sank in, it was decided to consider another design.

Chapter 4 Biomaterial ring design

4.1 General

At the same time as major roadblocks were faced with the stainless steel annuloplasty ring design, seven different biomaterials had just been mechanically characterized using planar biaxial testing in Dr. Labrosse's laboratory at the University of Ottawa Heart Institute [36]. These biomaterials are typically used by cardiac surgeons for creating patches to seal or repair heart valves, heart chambers or arteries. They present themselves in thin sheets and are inherently biocompatible, meaning that they will not be rejected by the body; in addition, because they are soft, they can be cut with scissors and formed into shape during the operation, such that the shaping of patient-specific triangular projections along the circumference to accommodate the fibrous triangles of the valve would not be an issue. However, because they usually only measure about half a millimeter in thickness, several layers will be necessary in the context of an annuloplasty ring to achieve enough strength. By design, such a ring would satisfy the following requirements from Chapter 2:

1) The ring should be internal (i.e. fit within the VAJ) to avoid access and positioning issues encountered with external annuloplasty rings. Further, the ring should be of relatively small thickness to not interfere with the blood flow;

2) The ring must be biocompatible to minimize issues of rejection by the body;

5) The ring should have a feature (cuff) that allows for sewing into place. In fact, the biomaterial constituting the ring itself would be amenable to suturing, removing the need for an additional cuff.

6) The ring should allow for patient-specific shaping of triangular projections along the circumference to accommodate the fibrous triangles of the valve (see Fig. 1.3), as detailed later.

On the other hand, the following requirements from Chapter 2 would not immediately be met:

3) The ring must be able to sustain millions of cardiac cycles because the heart beats more than 80 million times each year. This issue can be addressed later if a successful design satisfying the other requirements was to emerge;

4) The ring should allow for 3% radial flexibility of the ring during cardiac cycles [30]. By the time of the biomaterial ring design was considered, the target value of 10% as indicated in [14] had been corrected according to new published data [30]. This requirement still needed attention. The next sections will present the different steps leading to the flexibility analysis under physiological loads.

4.2 Ring geometry

The proposed design for the internal annuloplasty ring is shown in Figure 4.1 as a simple hollow cylinder whose upper end could easily be tailored by the surgeon to match the VAJ geometry of a specific patient without interfering with the aortic leaflets. This would be achieved by scalloping the upper end of the ring to match the crown-like geometry of the fibrous triangles represented in Figure 1.3.

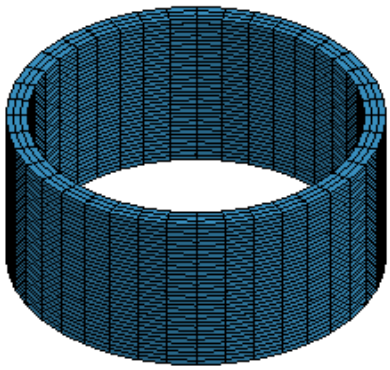

Figure 4.1: Schematic of the proposed annuloplasty ring, obtained by wrapping several layers of a cardiovascular biomaterial. One end of the ring will be scalloped to match the VAJ geometry of the patient, and the ring will be sutured in place to shrink the base diameter of the aortic valve.

4.3 Material properties

Most of the biomaterials considered in this study were provided by manufacturers, and resulted from various and proprietary chemical treatments of pericardial tissue, a leather-like biological material. Pericardium is a sack wrapping the heart and the roots of the great vessels (Figure 4.2).

It is found at the back of the breastbone, attached to the diaphragm. Enclosed between the pericardium and the heart muscle is a thin layer of lubricant to minimize friction loss during the cardiac contractions [2].

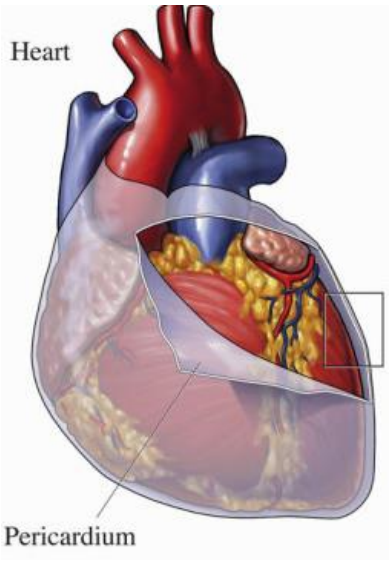

Figure 4.2: The heart shown with its pericardium cover [37].

Specifically, the biomaterials initially considered were [36]: 1) fresh autologous porcine pericardium (APP), 2) glutaraldehyde fixed porcine pericardium (GPP), 3) St Jude Medical pericardial patch (SJM; St Jude Medical, St Paul, Minnesota, USA), 4) CardioCel patch (CC; Admedus, Minneapolis, Minnesota, USA), 5) PeriGuard (PG; Synovis, St Paul, Minnesota, USA) and 6) Supple PeriGuard (SPG; Synovis, St Paul, Minnesota, USA). APP and GPP were used as surrogates for the fresh or glutaraldehyde fixed autologous human pericardium samples that have been used in the operating room as cusp replacements [38-40]. The porcine tissues were harvested on hearts from adult pigs weighing approximately 105 kg obtained from a local abattoir within hours of slaughter, and stored in saline solution at 4 ^{o}C. The GPP samples were dipped in 0.6% glutaraldehyde for 20 minutes before testing [41].

Nine samples of each material were initially tested. The samples were cut using parallel steel razor blades into 6.5×6.5 mm^2 squares whose sides were aligned with, or orthogonal to, the direction of fibre reinforcement, as determined by back-lighting and careful visual inspection. In addition, the three AV leaflets in each of two porcine hearts were tested (PC). The details of the methods and data processing can be found in [36].

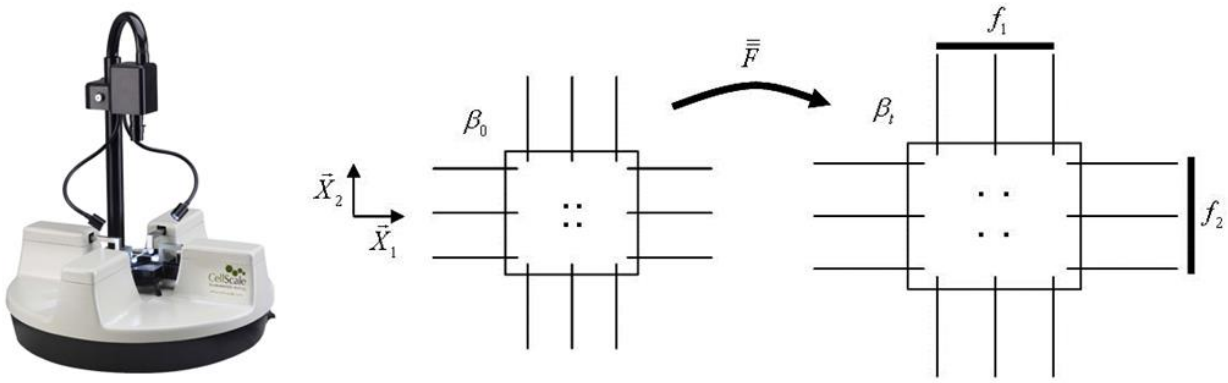

Figure 4.3: CellScale biaxial tester (left), and schematic of the sample under biaxial testing (right). Please refer to text for notations.

For all samples, an electronic thickness gauge was used to evaluate the material's thickness in three different locations and averaged (Model 700-118-20, Mitutoyo, Japan), according to the recommended procedure [42], before it was mounted on the 5-N capacity biaxial testing equipment (Biotester, CellScale, Waterloo, Canada; Figure 4.3) using four tungsten rakes, each fitted with five 0.7 mm spaced tines. The samples were immersed in a temperature-controlled saline bath at 37 ^{o}C for 10 minutes before testing, but were tested out of the bath to mitigate reflections impairing image tracking.

Figure 4.4 shows the summary of the stress-strain curves obtained under equibiaxial tension for all seven materials [36]. As can be seen, the fibre and cross-fibre directions presented with very distinct elastic properties (anisotropic material), and the stress-strain curves were consistent with large elastic deformations (hyperelastic material). It can also be seen that different materials exhibit radically different elastic responses, presenting a wide range of possibilities for design purposes. For example, the SJM material had almost the same stiff behaviour in both directions, while the SPG material extended much more in the cross-fibre direction than the fibre direction.

Regardless of the exact material to be selected, the analysis of anisotropic hyperelastic materials is especially challenging. Because of large deformations, linear elasticity is no longer valid, and some background in continuum mechanics for finite deformations is required.

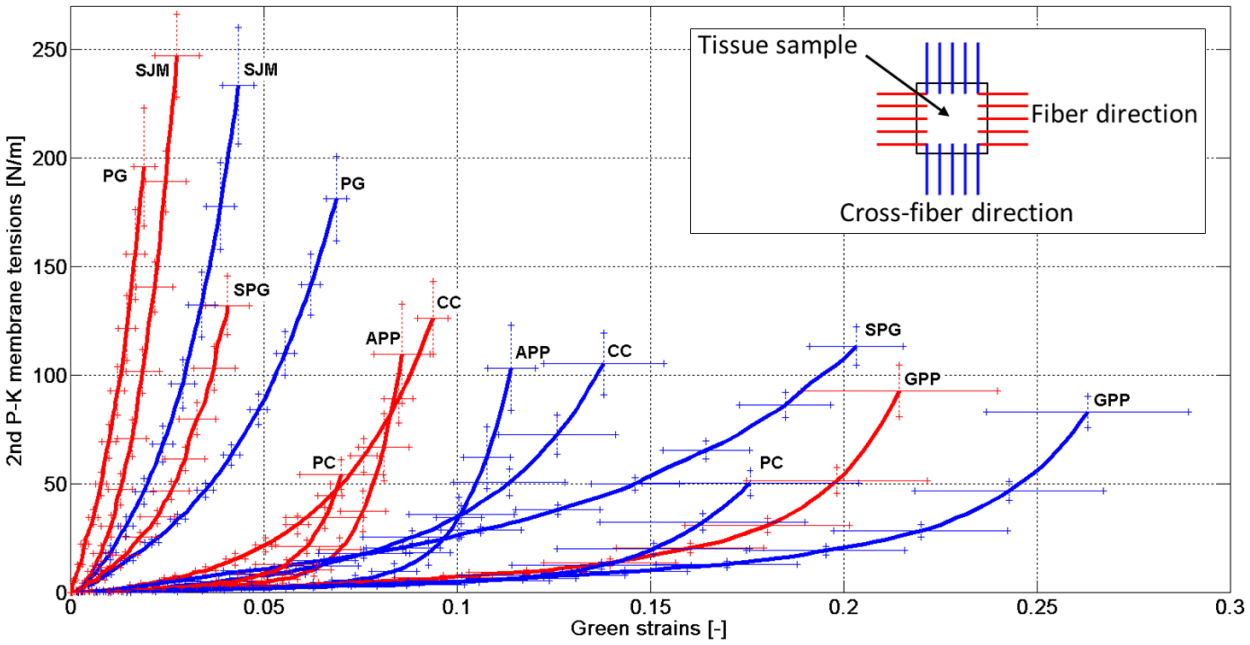

Figure 4.4: Summary of the averaged experimental results for all the materials tested, in the equi-biaxial protocol. Both the fibre and cross-fibre direction are represented, for two curves per material. P-K: Piola-Kirchhoff [36].

Focusing on a rectangular biomaterial sample under biaxial testing (Figure 4.3), let the original domain (within the grips of the apparatus) be defined as: $-L_1/2 \leq X_1 \leq L_1/2$, $-L_2/2 \leq X_2 \leq L_2/2$, and $-H/2 \leq X_3 \leq H/2$, where H is the undeformed thickness. After deformation, the material originally at location X_1, X_2, X_3 in the unloaded, stress-free configuration can be mapped to x_1, x_2, x_3 as follows: $x_1 = \lambda_1 X_1 + F_{12} X_2$, $x_2 = F_{21} X_1 + \lambda_2 X_2$, $x_3 = (h/H) X_3$. The biaxial testing equipment allows one to monitor stretch ratios λ_1, λ_2, as well as the forces applied in each direction, say f_1 and f_2. Assuming the material to be incompressible (due to its large water content), the determinant of the transformation gradient tensor $\bar{\bar{\boldsymbol{F}}} = \partial \boldsymbol{x} / \partial \boldsymbol{X}$ associated with general planar biaxial testing must be equal to 1. Therefore, unknown current thickness h can be expressed in terms of measurable quantities as $h = H/J_{2D}$, where $J_{2D} = \lambda_1 \lambda_2 - F_{12} F_{21}$ and the Cartesian components of $\bar{\bar{\boldsymbol{F}}}$ are given as

$$[\bar{\bar{\boldsymbol{F}}}] = \begin{bmatrix} \lambda_1 & F_{12} & 0 \\ F_{21} & \lambda_2 & 0 \\ 0 & 0 & 1/J_{2D} \end{bmatrix}.$$

Stretch ratios λ_1, λ_2 as well as components F_{12} and F_{21} over a region of interest of the sample can be obtained by following the procedure outlined in [43,36]. The Green (or St Venant, or Lagrangian) strain tensor can then be derived from $\overline{\overline{\boldsymbol{F}}}$ by $\overline{\overline{\boldsymbol{E}}} = 1/2\left(\overline{\overline{\boldsymbol{F}}}^{\mathrm{T}}.\overline{\overline{\boldsymbol{F}}} - \overline{\overline{\boldsymbol{I}}}\right)$, where "." denotes the dot or scalar product, and "T" means transpose. Note that by definition, $\overline{\overline{\boldsymbol{E}}}$ is symmetric.

The components of second P-K stress resultant (or membrane tension, in N/m) tensor are $T_{11}^S = \lambda_2 f_1/(J_{2D}L_2)$, $T_{22}^S = \lambda_1 f_2/(J_{2D}L_1)$ and, owing to the symmetry of $\overline{\overline{\boldsymbol{S}}}$, $T_{12}^S = -F_{21}f_1/(J_{2D}L_2) = T_{21}^S = -F_{12}f_2/(J_{2D}L_1)$, where external forces f_1 and f_2 are applied in directions 1 and 2.

Assuming that a repeatable mechanical response is achieved after preconditioning (according to the pseudo-hyperelasticity concept introduced by Fung [44]), and focusing here on the loading part of it, a 3-D strain energy functions W may be postulated, relating the second PK stress tensor to the Green strain tensor by $\overline{\overline{\boldsymbol{S}}} = \partial W/\partial\overline{\overline{\boldsymbol{E}}}$. Consistent with in-plane stress conditions, W only depends on E_{11}, E_{22}, E_{12} and possibly E_{33}, such that $W = W(E_{11}, E_{22}, E_{12}, E_{33})$ [24]. Because of the assumed material incompressibility, E_{33} may be directly expressed in terms of E_{11}, E_{22} and E_{12}. Therefore, a reduced strain energy function $\widehat{W}$ may be introduced, such that $\widehat{W} = \widehat{W}(E_{11}, E_{22}, E_{12}) = W(E_{11}, E_{22}, E_{12}, E_{33})$. However, it is not possible to identify a suitable form for $\widehat{W}$ just from planar biaxial testing [45]. Instead, a practical form for $\widehat{W}$ is postulated to depend only on E_{11}, E_{22}, E_{12} and not on E_{33}, such that

$$[\overline{\overline{\boldsymbol{S}}}] = \begin{bmatrix} \partial\widehat{W}/\partial E_{11} & \partial\widehat{W}/\partial E_{12} & 0 \\ \partial\widehat{W}/\partial E_{21} & \partial\widehat{W}/\partial E_{22} & 0 \\ 0 & 0 & 0 \end{bmatrix}.$$

Introducing a 2-D strain energy function $w = H\widehat{W}$, the second PK membrane tensions can also be written as $T_{11}^S = \partial w/\partial E_{11}, T_{22}^S = \partial w/\partial E_{22}$ and, owing to the symmetry of $\overline{\overline{\boldsymbol{S}}}$, $T_{12}^S = \partial w/\partial E_{12} = T_{21}^S = \partial w/\partial E_{21}$, all expressions that are independent of the thickness of the sample. The mathematical formulation of such 2-D strain energy functions should ideally be based on a whole range of experimental tests and theoretical considerations [45]. However, as a shortcut, one often uses popular strain energy functions, as done here.

For example, Sacks proposed a seven-parameter Fung model in terms of the Green strain tensor components such that $w = \frac{c_1}{2}[\exp(Q) - 1]$, where $Q = c_2E_{11}^2 + c_3E_{22}^2 + 2c_4E_{11}E_{22} + c_5E_{12}^2 + 2c_6E_{11}E_{12} + 2c_7E_{22}E_{12}$ [46]. Alternatively, we can also consider four-parameter Guccione et al.'s material model [47], in the form: $w = \frac{c_1}{2}[\exp(Q) - 1]$, where $Q = c_2E_{11}^2 + c_3\left[E_{22}^2 + \frac{1}{4}(\frac{1}{\Delta} - 1)^2\right] + 2c_4E_{12}^2$, with $\Delta = (2E_{11} + 1)(2E_{22} + 1)$. One advantage of Guccione et al.'s material model is that it has been implemented in commercial FE software LS-Dyna (LSTC, Livermore, California, USA), which will prove convenient later on in the study.

One can ensure that the experimental curves for second P-K membrane tensions vs. Green strains are recovered by the model using nonlinear optimization of the material constants c_i, e.g by minimizing the objective function $\left\|\left|T_{11\_\text{exp}}^S - T_{11\_\text{theo}}^S\right| + \left|T_{22\_\text{exp}}^S - T_{22\_\text{theo}}^S\right| + \left|T_{12\_\text{exp}}^S - T_{12\_\text{theo}}^S\right|\right\|^2$, where each entity is a vector array of all the relevant data points, and $\|.\|$ represents the Euclidian norm. In these notations, the experimental and theoretical membrane tensions (noted _exp and _theo, respectively) are:

$$T_{11\_\text{exp}}^S = \lambda_2 f_1/(J_{2D}L_2) \text{ and } T_{11\_\text{theo}}^S = c_1\exp(Q)[c_2E_{11} - \frac{c_3}{2\Delta(2E_{11}+1)}(\frac{1}{\Delta} - 1)],$$

$$T_{22\_\text{exp}}^S = \lambda_1 f_2/(J_{2D}L_1) \text{ and } T_{22\_\text{theo}}^S = c_1\exp(Q)[c_3E_{22} - \frac{c_3}{2\Delta(2E_{22}+1)}(\frac{1}{\Delta} - 1)], \text{ as well as}$$

$$T_{12\_\text{exp}}^S = -\frac{F_{21}f_1}{J_{2D}L_2} \text{ and } T_{12\_\text{exp}}^S = c_1\exp(Q)c_4E_{12}.$$

In [36], the material constants were determined by nonlinear optimization based on all biaxial protocols simultaneously, after averaging the results from several samples for each protocol (see Figure 4.5). The data were analyzed using the post-preconditioning state as the reference state.

Table 4.1 lists the thicknesses of all the materials tested and the number of samples retained for determination of the material constants. Indeed, due to some tearing near the tines, or due to image tracking issues, some samples had to be discarded. The values in parentheses report the standard deviation.

The material constants for all the biomaterials considered are listed in Table 4.2, along with the half span of the 95% confidence interval (in parentheses), and the Pearson correlation coefficients between the experimental and predicted membrane tensions in the fibre direction (FD) and cross-fibre direction (XD).

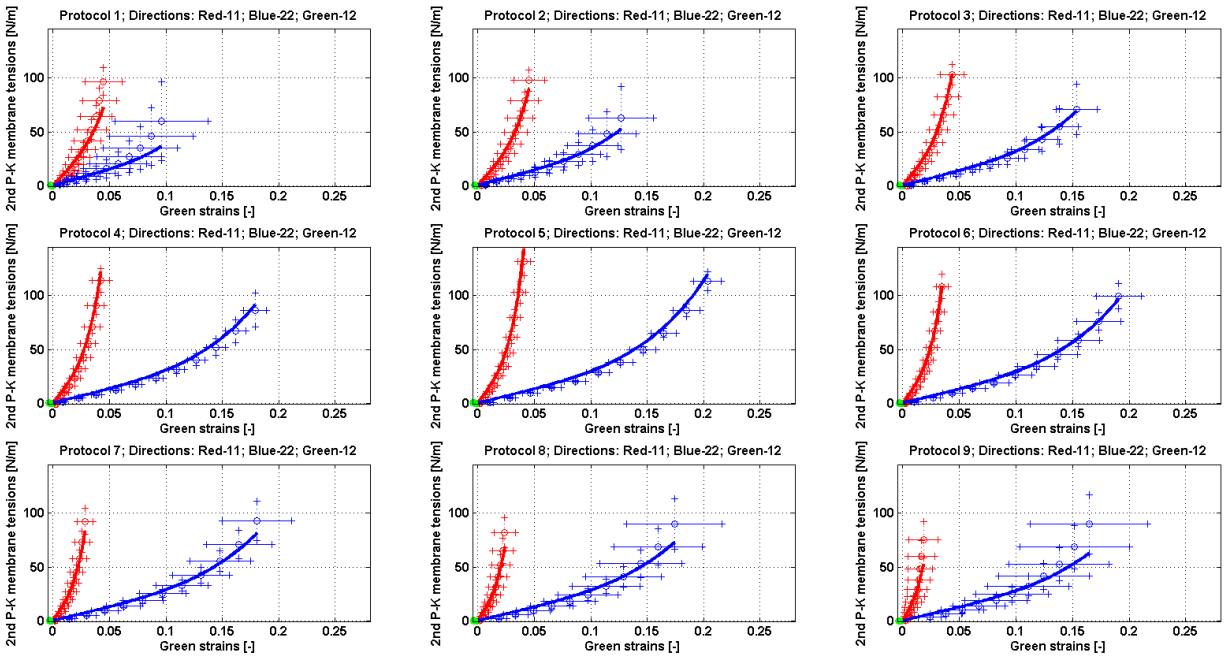

Figure 4.5: Experimental data and model fit with Guccione et al.'s model for material SPG.

Table 4.1: Final sample size and thickness of the seven candidate biomaterials [36].

Material	**APP**	**GPP**	**SJM**	**CC**	**PG**	**SPG**	**PC**
N	7	9	6	7	7	6	6
Thickness [mm]	0.22 (0.07)	0.20 (0.06)	0.23 (0.02)	0.41 (0.02)	0.39 (0.03)	0.42 (0.01)	0.27 (0.08)
Material	**APP**	**GPP**	**SJM**	**CC**	**PG**	**SPG**	**PC**
N	7	9	6	7	7	6	6
Thickness [mm]	0.22 (0.07)	0.20 (0.06)	0.23 (0.02)	0.41 (0.02)	0.39 (0.03)	0.42 (0.01)	0.27 (0.08)

Table 4.2: Material properties of the seven candidate biomaterials [36].

Material	**APP**	**GPP**	**SJM**	**CC**	**PG**	**SPG**	**PC**
c_1 **[N/m]**	0.90 (0.11)	2.06 (0.13)	4.81 (0.19)	3.04 (0.14)	6.97 (0.22)	8.69 (0.25)	0.90 (0.08)
c_2 **[-]**	43.77 (3.61)	14.73 (0.45)	348.57 (9.48)	54.03 (1.46)	432.30 (9.89)	86.02 (1.79)	74.38 (3.47)
c_3 **[-]**	53.34 (2.52)	10.99 (0.30)	160.83 (3.56)	27.24 (0.61)	78.90 (1.50)	14.80 (0.25)	24.64 (0.84)
c_4 **[-]**	0.00 (73.87)	0.13 (24.20	0.00 (18.80)	0.00 (13.10)	0.00 (3.47)	0.00 (6.98)	0.72 (52.29)
R^2-FD	0.88	0.94	0.97	0.96	0.99	0.98	0.91
R^2-XD	0.87	0.92	0.99	0.96	0.99	0.98	0.96

4.4 Method of analysis

As will be described in the next section, the material constants determined for the biomaterials were used in combination with an analytical model describing the elastic behaviour of a pressurized cylinder made of anisotropic hyperelastic material (the annuloplasty ring model). This was done in an effort to trim the list of candidate materials down to only those that were capable of achieving a radial flexibility of about 3% between systolic and diastolic pressures, according to Criterion 4 in Chapter 2. Indeed, if the ring alone cannot produce the desired radial flexibility, the assembly ring + VAJ will not either. If anything, the radial flexibility of the assembly is expected to be less than that of the ring itself, as the assembly contains more material resisting pulsatile dilatation.

This rationale led to the necessity of establishing an analytical model for the VAJ as well. It was simplified into a portion of hollow cylinder whose properties were borrowed from the human ascending aorta, and the model was considered validated when its radial flexibility was also shown to be about 3% between systolic and diastolic pressures.

However, there was no analytical model available to represent an annuloplasty ring sutured into a dilated VAJ and evaluate the radial flexibility of the assembly. This step required FE analysis, as will be detailed in Chapter 5. Therefore, in preparation of the FE modeling of the assembly, careful validation of the FE modeling of the ring and the VAJ, as independent entities, was required, and was established by comparison with the results from the respective analytical models.

4.5 Analytical modeling of an anisotropic hyperelastic pressurized cylinder

The equations for the pressurization of a thick-walled, anisotropic, incompressible hyperelastic cylinder under closed end, free extension conditions are as follows [44,48]:

$$P_{\text{theo}} = \int_{r_i}^{r_o} \left[\left(\frac{r}{R}\right)^{\mathbf{2}} \frac{\partial W}{\partial E_\Theta} - \left(\frac{R}{r\lambda}\right)^{\mathbf{2}} \frac{\partial W}{\partial E_R} \right] \frac{dr}{r} ,$$

$$F_{Z\text{theo}} \equiv 0 = \pi \int_{r_i}^{r_o} \left[2\lambda^{\mathbf{2}} \frac{\partial W}{\partial E_Z} - \left(\frac{r}{R}\right)^{\mathbf{2}} \frac{\partial W}{\partial E_\Theta} - \left(\frac{R}{r\lambda}\right)^{\mathbf{2}} \frac{\partial W}{\partial E_R} \right] r dr ,$$

with radial, circumferential and longitudinal Green strains

$$E_R = \frac{1}{2}\left[\left(\frac{R}{r\lambda}\right)^{\mathbf{2}} - 1\right], E_\Theta = \frac{1}{2}\left[\left(\frac{r}{R}\right)^{\mathbf{2}} - 1\right] \text{ and } E_Z = \frac{1}{2}[\lambda^{\mathbf{2}} - 1],$$

and

$$R^2 = R_i^2 + \lambda(r^2 - {r_i}^2).$$

In these expressions, r_i and r_o are the current inner and outer radii of the cylinder under pressure P_{theo}, and λ is the current longitudinal (or axial) stretch ratio under closed end, free extension conditions characterized by a null axial external force $F_{Z\text{theo}}$ being applied on the end cap of the cylinder. R_i and R_o are the unpressurized inner and outer radii of the cylinder, respectively.

With a view to simulating the behaviour of a cylinder of known material properties and geometry under a known pressure range, one can use nonlinear optimization tools to determine inner radius r_i and longitudinal stretch λ at each pressure value and minimize the objective function $\left\| \left| P_{\text{exp}} - P_{\text{theo}} \right| + \left| F_{\text{Zexp}} - F_{\text{Ztheo}} \right| \right\|^2$, where each entity is a vector array of all the relevant data points, and $\|.\|$ represents the Euclidian norm [44,48].

The calculations were implemented in a MATLAB code (similar to that in Appendix 3; only the material constants and the diameter need changing). When different biomaterials were tested for their radial flexibility performance once formed into a cylindrical ring of about 22 mm in diameter, it was decided to focus only on reliably sourceable materials CC, SJM, PG and SPG. The analytical model was used to predict the flexibility of an annuloplasty ring based on the diameter and thickness (related to the number of layers) of the ring. An additional parameter that was investigated was the fibre or cross-fibre orientation of the material with respect to the circumferential direction of the ring.

As can be seen from Figure 4.4, material SPG, in the cross-fibre direction, is the most extensible of all four materials. According to Table 4.3, several design possibilities emerged with this material when its cross-fibre direction was aligned circumferentially to the ring, such that the ring diameter under 80 mmHg pressure would be in the 22-24 mm range suitable for surgical applications. As can been seen from the table, the number of layers of biomaterial constituting the ring did not markedly affect the radial flexibility, nor did the initial diameter of the ring. In addition, the radial flexibility stayed on the low end of the target value of 3%. Yet, at about 2%, this was the largest value that could be reached from all the materials considered.

Table 4.3: Radial flexibility for annuloplasty ring with SPG material.

Initial Inner Diameter (mm)	Number of layers	ID_{80} (mm)	ID_{120} (mm)	Flexibility (%)
20	7	21.43	21.88	2.09
20	5	21.73	22.18	2.06
21	7	22.54	23.02	2.09
21	5	22.86	23.33	2.06
22	7	23.66	24.16	2.09
22	5	23.97	24.49	2.05

For the analytical model of the VAJ corresponding to the aortic root where the annuloplasty ring is meant to be used, material constants for Guccione et al.'s model that best describe experimental pressurization data (i.e. inner diameter vs. pressure, and longitudinal stretch vs. pressure

curves) were used, as determined in [48] from human ascending aortas. The same analytical model as above (Appendix 3) was run to predict the diameter and longitudinal stretch under pressures ranging between 0 and 150 mmHg (Figure 4.6).

As can be seen from Figure 4.6, when the VAJ model was pressurized under closed end conditions that matched in-vivo conditions [48], its diameter changed and so did its length. In addition, the change in VAJ diameter observed between 80 and 120 mmHg exhibited a radial flexibility on the order of 3.3%, which was deemed consistent with published values [30].

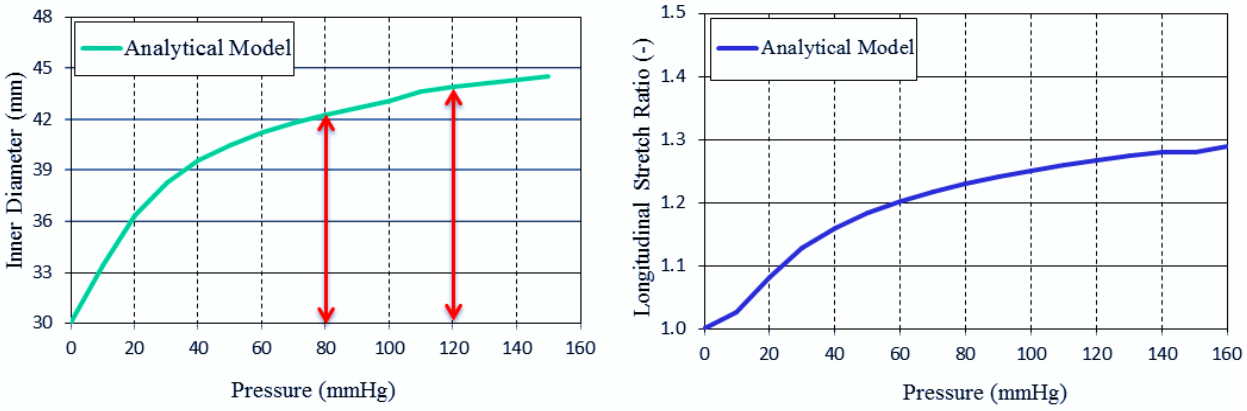

Figure 4.6: Analytical simulation reproducing in-vivo behaviour of the VAJ under pressure.

4.6 FE element modeling: wrapped vs. cylindrical configurations

As mentioned previously, commercial FE software LS-Dyna includes an implementation of Guccione et al.'s material model for anisotropic, hyperelastic tissues. LS-Dyna, however, is not user friendly for geometry creation, and it was preferred to turn to MATLAB to generate LS-Dyna input decks automatically. The MATLAB code that was created to do so (Appendix 4) contains information about the analysis, material properties, node coordinates and connectivity table for creating the elements and outputting a .dyn file that is an LS-Dyna input deck. Eight-noded brick elements were used as required for implementation in combination with Guccione et al.'s material model.

Two configurations were initially considered: the continuous wrapping of an SPG material sheet into a cylinder, and a purely cylindrical configuration of equivalent thickness, as an idealization of the former (Figure 4.7).

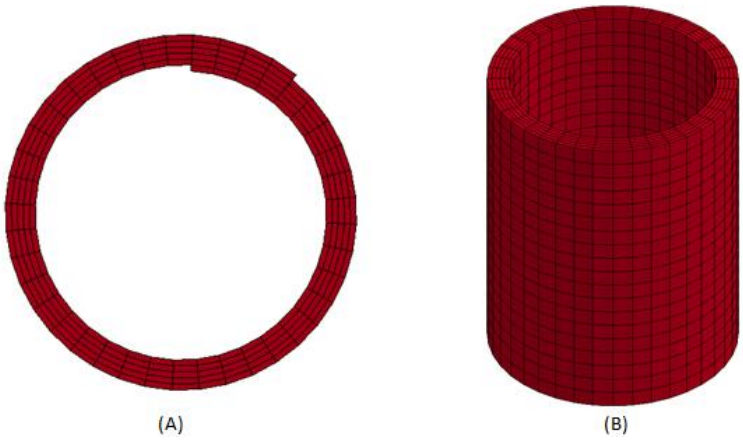

Figure 4.7: Two different options for the ring geometry: (A) Wrap, (B) Cylinder.

For both geometries, the inner diameter and total length as functions of time (note that the pressure is applied as a ramp; therefore time is proportional to pressure) were compared (Figure 4.8). According to Figure 4.8, there was no noticeable difference between the wrapped and cylindrical configurations, and, for simplicity, it was decided to only consider the idealized cylindrical configuration in the next simulations.

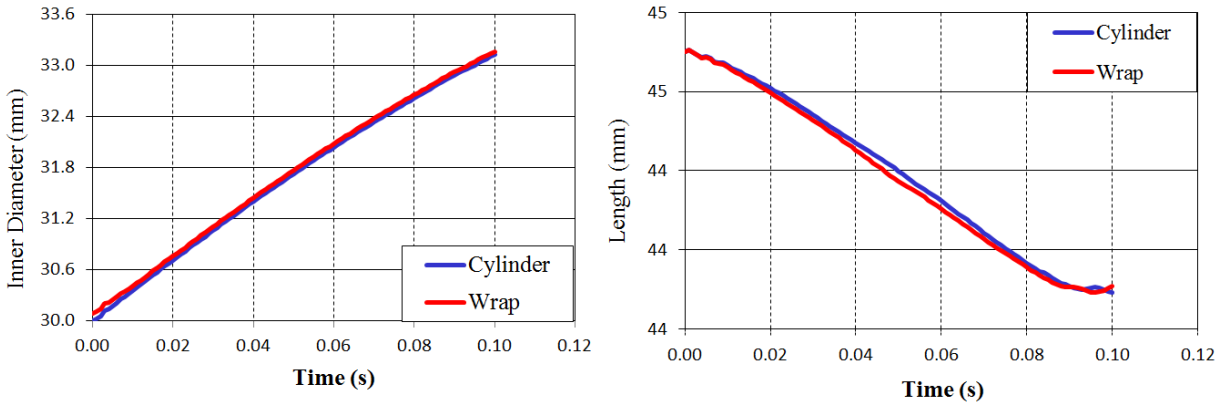

Figure 4.8: Comparisons between the pressurization results obtained for the wrapped and purely cylindrical geometries: inner diameter (left), and total length (right). Time 0 corresponds to 0 pressure, while Time 0.10 sec corresponds to 160 mmHg.

4.7 Finite element modeling vs. analytical modeling

For the VAJ (Figure 4.9) and the ring (Figure 4.10), the inner diameter and longitudinal stretch ratio were obtained independently as functions of pressure in the range of 0 to 160 mmHg, from FE analysis and the analytical models. In the FE analysis, two parameters could be adjusted to

fine-tune the results: the value of the penalty factor *P* used in the material model to numerically enforce the incompressibility of the material, and parameter elemL, the longitudinal dimension of the brick elements. After exhaustive analyses, it was found that 3,210 MPa for the penalty factor and 1 mm for the element longitudinal dimension generated results that were most similar to those from the analytical model.

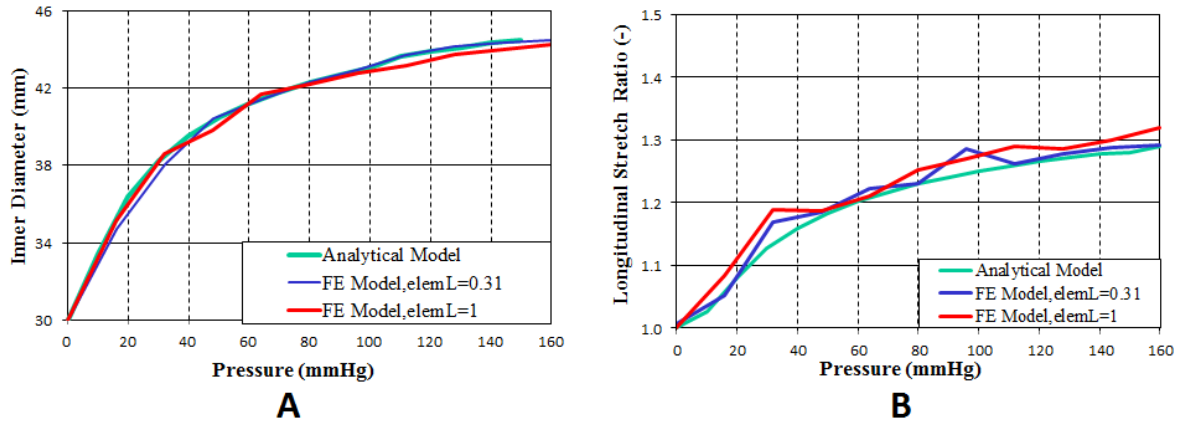

Figure 4.9: Comparison between FE and analytical results for the VAJ: (A) Inner Diameter vs. Pressure, (B) Longitudinal Stretch Ratio vs. Pressure.

For the annuloplasty ring, these values were respectively 18,621 MPa and 0.31 mm, as priority was given to the accuracy in the diameter response over that in the longitudinal extension, because the ultimate outcome of the FE model will be the radial flexibility of the ring-aorta assembly. Still, the percent error in the longitudinal extension was very small whether the element length was 1 or 0.31 mm.

These findings will be useful in the next chapter where the ring will be sutured inside the VAJ. One can already remark that, to be able to model the suturing of the ring using FE modeling, node-to-node mesh correspondence will be required between the ring and the VAJ. This means that the mesh size will need to be the same for both components, and therefore, the element longitudinal dimension will be set at 0.31 mm.

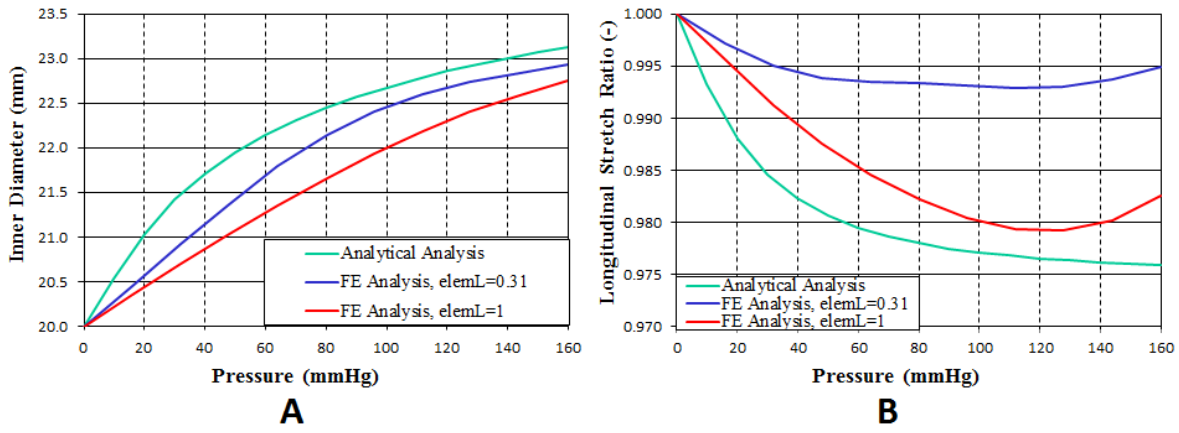

Figure 4.10: Comparison between the FE and analytical results for the ring: (A) Inner Diameter vs. Pressure, (B) Longitudinal Stretch Ratio vs. Pressure.

Chapter 5 Modeling the combined ring and VAJ

5.1 Geometry

The FE model allowing the suturing of an annuloplasty ring inside a dilated VAJ (as a plausible example, say 30 mm diameter) remains to be discussed. As in the previous chapter, MATLAB was used to generate an input deck to be run for FE analysis in LS-Dyna (Appendix 5). The MATLAB code manages information regarding node creation, connectivity tables for the elements, material properties, loading and boundary conditions. Cylindrical coordinates (r, z, θ) were used to easily control the radial, circumferential, and longitudinal positions of all nodes. Next, connectivity tables were created to define eight-noded brick elements, with arbitrary numbers of elements across the thicknesses of the VAJ and ring. The node numbering convention to be used for brick elements in LS-Dyna is shown in (Figure 5.1).

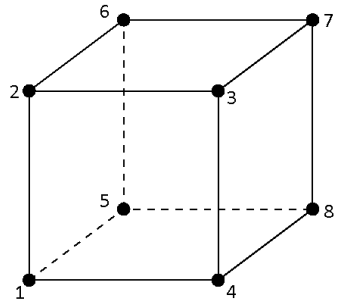

Figure 5.1: LS-Dyna node numbering convention for brick element.

Similarly to the algorithm for node creation and numbering, the algorithm for creating and numbering elements started in the radial direction, then proceeded in the longitudinal direction, and finally in the circumferential direction. The VAJ model was meshed before the ring. Arbitrary numbers of elements can be set in the radial, longitudinal, and circumferential directions, respectively (Appendix 5).

5.2 Load and boundary conditions

Starting from the unpressurized configuration, a pressure of up to 120 mmHg was applied as a ramp over 0.24 seconds. LS-Dyna requires the user to define the faces of the elements that are affected by pressure using the LOAD_SEGMENT command. To create the load segments, a list of surface elements were defined as the interfaces between what would be blood and the aortic wall of the ring.

The VAJ was modelled with one end closed with a virtual rigid cap, while the other end was fixed longitudinally, and free to radially expand so as to not introduce significant end effects. Such boundary conditions were previously shown to be reasonable estimates of the physiological conditions [49]. This was achieved using the BOUNDARY_SPC_NODE command in LS-Dyna for the radial and longitudinal kinematic constraints, along with time-wise controlled forces applied longitudinally to one end of the aorta to represent the force resulting from the pressure applied to the rigid cap.

5.3 Introducing sutures into the model

Rigid attachment, through sutures, of two deformable components such as the VAJ model and the annuloplasty ring, results in an assembly whose geometry is impossible to predict without numerical tools. Luckily, a possibility in LS-Dyna is to use so-called SEATBELT elements, which are designed to shrink by a controlled amount as the simulation is started. As can be seen in Figure 5.2, such elements joining corresponding nodes between the VAJ and the annuloplasty ring can be instructed to shrink by an amount corresponding to the gap between the two components, effectively mimicking the suturing process before pressurization of the assembly starts. This approach was already successfully followed in a study of individual aortic valve leaflet corrections using sutures in the context of aortic valve repair [50]. Practically, SEATBELT elements are defined by two nodes, one of them being on the outer surface of the annuloplasty ring, and the other facing it on the inner side of the VAJ model.

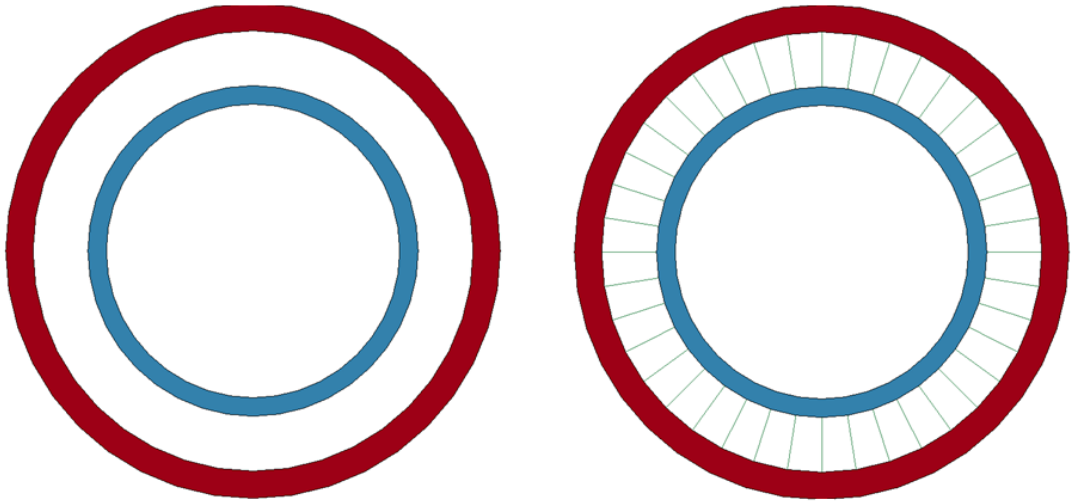

Figure 5.2: The assembly process. There is a gap between the ring and the dilated VAJ (left); sutures are created (right), and by shrinking, will remove the gap between both geometries.

5.4 Parametric quarter-model of combined annuloplasty ring and VAJ model

After assembly, and given the fine mesh required, the number of elements increased dramatically, which led to computation times of a couple of days. The machine used was a workstation with two Intel Xeon E5640 2.67 GHz 4-core processors and 6 GB of RAM. Therefore, to save resources, and given existing symmetries, a quarter-model of the combined ring and aorta was created (Figure 5.3). However, this reduction of the model introduced difficulties with the modeling of the closed end condition, namely the occurrence of highly distorted elements where axial forces were applied. As a work-around, the closed-end condition was replaced by an arbitrary and equivalent longitudinal stretch determined from the analysis of the VAJ model alone. This fixed the issue completely (Appendix 6), as numerical simulations in LS-Dyna are generally more stable if displacement-controlled boundary conditions are applied, rather than force-controlled ones. Yet, if they end up with the same displacements, as enforced here, they are equivalent.

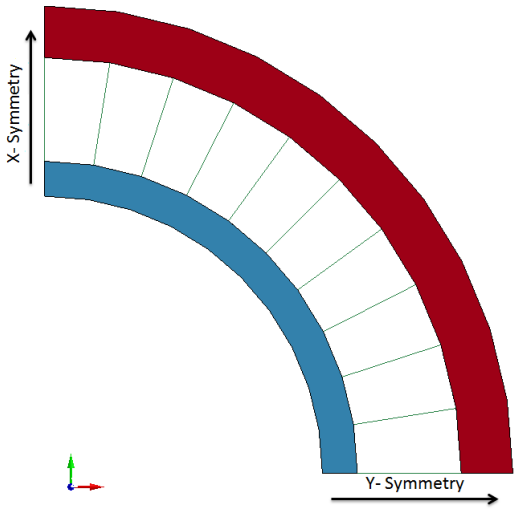

Figure 5.3: Symmetry conditions for the quarter-model of the combined ring and VAJ model.

Figure 5.4 illustrates the quarter of the whole geometry when the ring restricts the diameter of the VAJ model.

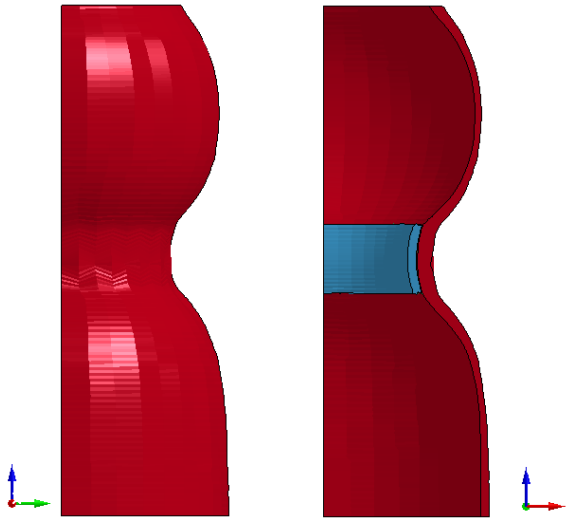

Figure 5.4: External view of the quarter-model of the ring and VAJ model assembly when the sutures are tight (left); inside view of the quarter-model showing the ring in blue, and the VAJ model red (right).

5.5 Results

Figure 5.5 presents the diameter-pressure curves for the dilated VAJ model alone, the annuloplasty ring alone, and both combined with sutures. From the curves, the radial flexibility value of the

assembly between 80 and 120 mmHg can be extracted, yielding a value of 1.2%. Although the target of 3% was somewhat missed, the tools developed through the present work may be used to investigate additional materials and configurations.

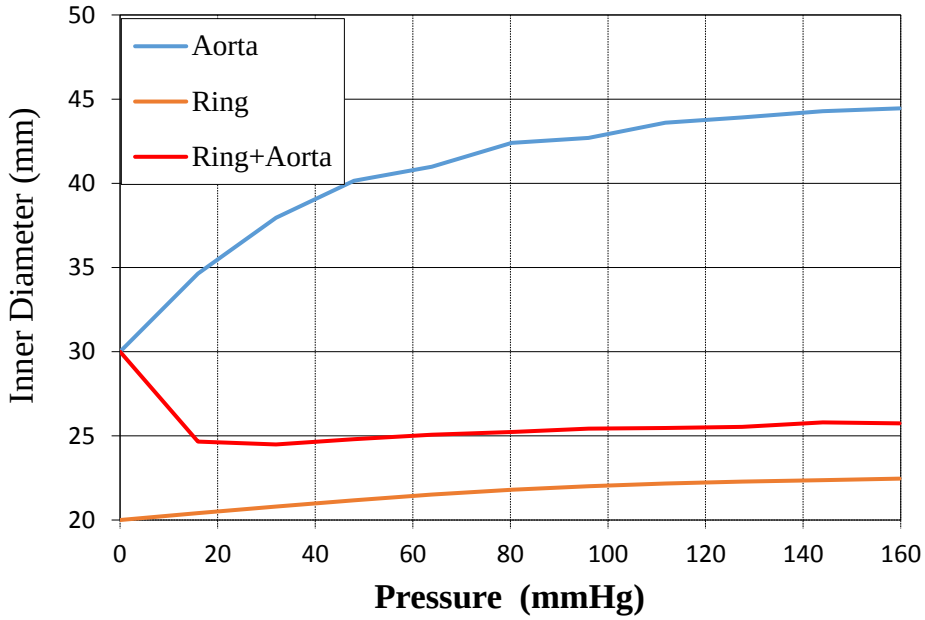

Figure 5.5: Inner Diameter vs. with respect to Pressure for the VAJ model and ring, separately, and combined.

Chapter 6 Conclusion

6.1 Summary

In this study, a new type of internal annuloplasty ring was designed that could be tailored to each valve's shape by simple use of scissors, and sutured inside the ventriculo-arterial junction. The proposed design was formed by wrapping a biocompatible and surgical biomaterial into a ring. As such, this ring would meet the design requirements regarding internal placement, biocompatibility, suturability, and customizability. Both analytical and numerical studies were carried out to confirm the estimation of the dilatational properties of such a ring under physiological pressures. Supple Peri-Guard (SPG) biomaterial used in the transverse orientation, emerged as the most suitable candidate, but could only achieve a level of radial flexibility of 1.2%, which is significantly lower than the targeted 3%. While different configurations (number of layers and ring diameters) were explored, this was the best performance that could be obtained. Although the radial flexibility achieved by the ring was not quite as large as expected, the special FE model developed to simulate the suturing of the biomaterial ring inside a dilated VAJ may be used to study yet other materials to meet the design requirements.

6.2 Recommendations for future work

Assuming a biomaterial can be found that can achieve more physiological radial flexibility, the internal annuloplasty ring will have to be tested in the laboratory, for example inside aortic valves obtained from pigs, as they are very similar to humans. This will make it possible to evaluate the actual radial flexibility of the ring, under pressurized conditions, and to assess the practicality of tailoring the ring to the shape of the valve. In addition, it will be important to determine the minimum number of sutures necessary to ensure that the ring controls the aortic diameter as required. If the tests are successful, simple tabulated instructions may be communicated to the surgeons to let them know how to achieve rings with specific properties (e.g. x layers of such material, for a given inner diameter). Alternatively, a manufacturer may decide to pre-wrap rings and sell them in different sizes. Before this can happen, the in-vitro fatigue and durability properties of device

will need to be assessed, and if promising, the ring will need to be implanted in live animals to test for absence/presence of calcification, as well as in-vivo durability.

About the stainless steel annuloplasty ring design considered in Chapter 3, it would be interesting to revisit it to verify the impact of reducing the radial flexibility target from 10% to 3%. If plastic deformations can be completely ruled out, this design could become promising again.

References

[1] Heart disease – heart health, retrieved Jan. 26, 2017 https://www.canada.ca/en/public-health/services/diseases/heart-disease-heart-health.html

[2] Cheitlin, M.D., Sokolow, M. and McIlroy, M.B., 1993. Clinical cardiology, 6th edition. Appleton & Lange, Norwalk, Connecticut.

[3] Blood flow through the heart, retrieved Jan. 26, 2017 http://imgkid.com/blood-flow-through-the-heart-oxygenated-and-deoxygenated.shtml.

[4] Heart anatomy, retrieved Jan. 26, 2017 http://cnx.org/contents/Y5T_wVSC@4/Heart-Anatomy

[5] Gray, H., 1918. Anatomy of the human body, 20th edition.

[6] Nishimura, R.A., 2002. Aortic Valve Disease. Circulation 106:770–772.

[7] Boodhwani, M., de Kerchove, L., Glineur, D., Poncelet, A., Rubay, J., Astarci, P., Verhelst, R., Noirhomme, P. and El Khoury, G., 2009. Repair-oriented classification of aortic insufficiency: impact on surgical techniques and clinical outcomes. The Journal of Thoracic and Cardiovascular Surgery, 137(2):286–294.

[8] Aortic valve replacement: before your surgery, retrieved Jan. 26, 2017 https://myhealth.alberta.ca/health/AfterCareInformation/pages/conditions.aspx?hwid=abk2162

[9] Vesely, I., 2003. The evolution of bioprosthetic heart valve design and its impact on durability. Cardiovascular Pathology, 12(5):277–286.

[10] Johnston, D.R., Soltesz, E.G., Vakil, N., Rajeswaran, J., Roselli, E.E., Sabik, J.F., Smedira, N.G., Svensson, L.G., Lytle, B.W. and Blackstone, E.H., 2015. Long-term durability of bioprosthetic aortic valves: implications from 12,569 implants. The Annals of thoracic surgery, 99(4):1239–1247.

[11] Vojáček, J., Žáček, P. and Dominik, J., 2017. Aortic valve repair and valve sparing procedures. Cor et Vasa, 59(1):e77–e84.

[12] Gott, V.L., Alejo, D.E. and Cameron, D.E., 2003. Mechanical heart valves: 50 years of evolution. The Annals of thoracic surgery, 76(6):S2230–S2239.

[13] Piazza, N., Bleiziffer, S., Brockmann, G., Hendrick, R., Deutsch, M.A., Opitz, A., Mazzitelli, D., Tassani-Prell, P., Schreiber, C. and Lange, R., 2011. Transcatheter aortic valve implantation for failing surgical aortic bioprosthetic valve: from concept to clinical application and evaluation (part 1). JACC: Cardiovascular Interventions, 4(7):721–732.

[14] Lansac, E., Di Centa, I., Raoux, F., et al., 2009. An expansible aortic ring for a physiological approach to conservative aortic valve surgery. Journal of Thoracic and Cardiovascular Surgery 138(3):718–724.

[15] Bonow, R.O., Carabello, B.A., Chatterjee, K. et al., 2006. ACC/AHA 2006 Guidelines for the management of patients with valvular heart disease. Circulation 114:e84–e231.

[16] Madaric, J., Watripont, P., Bartunek, J. et al., 2010. Exercise pulmonary hypertension in asymptomatic degenerative mitral regurgitation. Circulation 122(1):33–41.

[17] Egbe, A.C., Connolly, H.M., Pellikka, P.A., Schaff, H.V., Hanna, R., Maleszewski, J.J., Nkomo, V.T. and Pislaru, S.V., 2017. Outcomes of warfarin therapy for bioprosthetic valve thrombosis of surgically implanted valves: a prospective study. JACC: Cardiovascular Interventions, 10(4):379–387.

[18] Masri, A., Gillinov, A.M., Johnston, D.M., Sabik, J.F., Svensson, L.G., Rodriguez, L.L., Kapadia, S.R., Stewart, W.J., Grimm, R.A., Griffin, B.P. and Desai, M.Y., 2017. Anticoagulation versus antiplatelet or no therapy in patients undergoing bioprosthetic valve implantation: a systematic review and meta-analysis. Heart, 103(1):40–48.

[19] Chan, V., Levac-Martinho, O., Sohmer, B., Elmistekawy, E., Ruel, M. and Mesana, T.G., 2017. When Should the Mitral Valve Be Repaired or Replaced in Patients With Ischemic Mitral Regurgitation? The Annals of thoracic surgery, 103(3):742–747.

[20] Morrel, W.G., Ge, L., Zhang, Z., Grossi, E.A., Guccione, J.M. and Ratcliffe, M.B., 2014. Effect of mitral annuloplasty device shape and size on leaflet and myofibre stress following repair of posterior leaflet prolapse: a patient-specific finite element simulation. The Journal of heart valve disease, 23(6):727–734.

[21] Baxter, I. Finite element modeling of the mitral valve and mitral valve repair. MASc thesis, Université d'Ottawa/University of Ottawa, December 2011.

[22] Alfieri, O., De Bonis, M. and La Canna, G. eds., 2015. Edge-to-Edge Mitral Repair: From a Surgical to a Percutaneous Approach. Springer.

[23] Schoch, N., Kißler, F., Stoll, M., Engelhardt, S., Simone, R., Wolf, I., Bendl, R. and Heuveline, V., 2016. Comprehensive patient-specific information preprocessing for cardiac surgery simulations. International journal of computer assisted radiology and surgery, 11(6):1051–1059.

[24] Maisano, F., Skantharaja, R., Denti, P. et al., 2009. Mitral annuloplasty. Multimedia Manual Cardio-Thoracic Surgery, Volume 2009, Issue 0918.

[25] Chee, T., Haston, R., Togo, A., et al., 2008. Is a flexible mitral annuloplasty ring superior to a semi-rigid or rigid ring in terms of improvement in symptoms and survival? Interact CardioVasc Thorac Sur 7(3):477–484.

[26] Olson, L.J., Subramanian, R. and Edwards, W.D., 1984. Surgical pathology of pure aortic insufficiency: a study of 225 cases. Circulation 59(12):835–841.

[27] David, T.E., Feindel, C.M. and Bos, J., 1995. Repair of the aortic valve in patients with aortic insufficiency and aortic root aneurysm. Circulation 109(2):345–351.

[28] Sarsam, M.A. and Yacoub, M., 1993. Remodeling of the aortic valve annulus. Circulation 105(3):435–438.

[29] Lansac, E., Di Centa, I., Arnaud-Crozat, E., Bouchot, O., Doguet, F., Hacini, R., Demaria, R., Chatel, D., Sleilaty, G. and Debauchez, M., 2011. Remodeling of the aortic root combined to an expansible aortic ring annuloplasty. Multimedia manual of cardiothoracic surgery: MMCTS, 2011(401), pp.mmcts-2006.

[30] Holubec, T., Higashigaito, K., Belobradek, Z., Dergel, M., Harrer, J., Alkadhi, H., Zacek, P. and Vojacek, J., 2017. An expansible aortic ring in aortic root remodeling: exact position, pulsatility, effectiveness, and stability in three-dimensional CT study. The Annals of Thoracic Surgery, 103(1):83–90.

[31] Scharfschwerdt, M., Pawlik, M., Sievers, H.-F., et al., 2011. In vitro investigation of aortic valve annuloplasty using prosthetic ring devices, Eur J Cardiothorac Surg. 40(5):1127–1130.

[32] Mazzitelli, D., Nöbauer, C., Rankin, J.S. et al., 2013. Early results after implantation of a new geometric anuloplasty ring for aortic valve repair. Ann Thorac Surg. 95(1):94–97.

[33] Berreklouw, E., Koene, B., De Somer, F., Bouchez, S., Chiers, K., Taeymans, Y. and Van Nooten, G.J., 2011. Sutureless replacement of aortic valves with St Jude Medical mechanical valve prostheses and Nitinol attachment rings: Feasibility in long-term (90-day) pig experiments. The Journal of thoracic and cardiovascular surgery, 141(5):1231–1237.

[34] Black, J. and Hastings, G. eds., 2013. Handbook of biomaterial properties. Springer Science & Business Media.

[35] Rasmussen, K.J., 2003. Full-range stress–strain curves for stainless steel alloys. Journal of constructional steel research, 59(1):47–61.

[36] Labrosse, M.R., Jafar, R., Ngu, J. and Boodhwani, M., 2016. Planar biaxial testing of heart valve cusp replacement biomaterials: Experiments, theory and material constants. Acta Biomaterialia 45:303–320.

[37] Pericardium, retrieved Jan. 26, 2017
http://www.cardiachealth.org/your-pericardium

[38] Fattouch, K., Murana, G., Castrovinci, S., Nasso, G., Mossuto, C., Corrado, E., Ruvolo, G. and Speziale, G., 2012. Outcomes of aortic valve repair according to valve morphology and surgical techniques. Interactive cardiovascular and thoracic surgery, p.ivs195.

[39] Doss, M., Sirat, S., Risteski, P., Martens, S. and Moritz, A., 2008. Pericardial patch augmentation for repair of incompetent bicuspid aortic valves at midterm. European Journal of Cardio-Thoracic Surgery, 33(5):881–884.

[40] Lausberg, H.F., Aicher, D., Langer, F. and Schäfers, H.J., 2006. Aortic valve repair with autologous pericardial patch. European journal of cardio-thoracic surgery, 30(2):244–249.

[41] Ozaki, S., Kawase, I., Yamashita, H., Nozawa, Y., Takatoh, M., Hagiwara, S. and Kiyohara, N., 2014. Aortic valve reconstruction using autologous pericardium for patients aged less than 60 years. The Journal of thoracic and cardiovascular surgery, 148(3):934–938.

[42] O'Leary, S.A., Doyle, B.J. and McGloughlin, T.M., 2013. Comparison of methods used to measure the thickness of soft tissues and their influence on the evaluation of tensile stress. Journal of biomechanics, 46(11):1955–1960.

[43] Humphrey, J.D., Vawter, D.L. and Vito, R.P., 1987. Quantification of strains in biaxially tested soft tissues. Journal of Biomechanics, 20(1):59–65.

[44] Humphrey, J.D., 2013. Cardiovascular solid mechanics: cells, tissues, and organs. Springer Science & Business Media.

[45] Holzapfel, G.A. and Ogden, R.W., 2009. On planar biaxial tests for anisotropic nonlinearly elastic solids. A continuum mechanical framework. Mathematics and Mechanics of Solids, 14(5):474–489.

[46] Sacks, M.S., 2014. Engineering A Method for Planar Biaxial Mechanical Testing That Includes In-Plane Shear. J Biomech Eng, 121:551–555.

[47] Guccione, J.M., McCulloch, A.D. and Waldman, L.K., 1991. Passive material properties of intact ventricular myocardium determined from a cylindrical model. J Biomech Eng, 113(1):42–55.

[48] Labrosse, M.R., Gerson, E.R., Veinot, J.P. and Beller, C.J., 2013. Mechanical characterization of human aortas from pressurization testing and a paradigm shift for circumferential residual stress. Journal of the mechanical behavior of biomedical materials, 17:44–55.

[49] Labrosse, M.R., Beller, C.J., Mesana, T. and Veinot, J.P., 2009. Mechanical behavior of human aortas: Experiments, material constants and 3-D finite element modeling including residual stress. Journal of biomechanics, 42(8):996–1004.

[50] Labrosse, M.R., Boodhwani, M., Sohmer, B. and Beller, C.J., 2011. Modeling leaflet correction techniques in aortic valve repair: a finite element study. Journal of biomechanics, 44(12):2292–2298.

Appendix 1: Sample standard tube dimensions for 316 Stainless Steel

(https://www.twmetals.com retrieved Jan 26, 2017)

Product	Grade	Mfg Method	Outside Dia (mm)	Wall Thickness (mm)	Specification	SKU Length (cm)	Price Per Length
12890-1 (SELECT)	304	Seamless	41.28	9.52	ASTM A269	30	$59.13
12890-2 (SELECT)	304	Seamless	41.28	9.52	ASTM A269	61	$78.27
12890-3 (SELECT)	304	Seamless	41.28	9.52	ASTM A269	91	$97.40
12890-4 (SELECT)	304	Seamless	41.28	9.52	ASTM A269	122	$116.54
12890-5 (SELECT)	304	Seamless	41.28	9.52	ASTM A269	152	$135.67
12890-6 (SELECT)	304	Seamless	41.28	9.52	ASTM A269	183	$154.81
12890-7 (SELECT)	304	Seamless	41.28	9.52	ASTM A269	213	$173.94
12890-8 (SELECT)	304	Seamless	41.28	9.52	ASTM A269	244	$193.07
33206-1 (SELECT)	304/L	Seamless	177.80	9.52	ASTM A269	30	$116.27
33206-2 (SELECT)	304/L	Seamless	177.80	9.52	ASTM A269	61	$192.53
33206-3 (SELECT)	304/L	Seamless	177.80	9.52	ASTM A269	91	$268.80
33206-4 (SELECT)	304/L	Seamless	177.80	9.52	ASTM A269	122	$345.07
33206-5 (SELECT)	304/L	Seamless	177.80	9.52	ASTM A269	152	$421.33
33206-6 (SELECT)	304/L	Seamless	177.80	9.52	ASTM A269	183	$497.60
33206-7 (SELECT)	304/L	Seamless	177.80	9.52	ASTM A269	213	$573.86
33206-8 (SELECT)	304/L	Seamless	177.80	9.52	ASTM A269	244	$650.13
34740-1 (SELECT)	304/L	Seamless	215.90	25.40	ASTM A269	30	$405.95
34740-2 (SELECT)	304/L	Seamless	215.90	25.40	ASTM A269	61	$771.90
34740-3 (SELECT)	304/L	Seamless	215.90	25.40	ASTM A269	91	$1,137.86
34740-4 (SELECT)	304/L	Seamless	215.90	25.40	ASTM A269	122	$1,503.81
34740-5 (SELECT)	304/L	Seamless	215.90	25.40	ASTM A269	152	$1,869.76
34740-6 (SELECT)	304/L	Seamless	215.90	25.40	ASTM A269	183	$2,235.71
34740-7 (SELECT)	304/L	Seamless	215.90	25.40	ASTM A269	213	$2,601.66
34740-8 (SELECT)	304/L	Seamless	215.90	25.40	ASTM A269	244	$2,967.62
37249-1 (SELECT)	304/L	Seamless	31.75	4.78	ASTM A269	30	$47.84
37249-2 (SELECT)	304/L	Seamless	31.75	4.78	ASTM A269	61	$55.67
37249-3 (SELECT)	304/L	Seamless	31.75	4.78	ASTM A269	91	$63.51
37249-4 (SELECT)	304/L	Seamless	31.75	4.78	ASTM A269	122	$71.34
37249-5 (SELECT)	304/L	Seamless	31.75	4.78	ASTM A269	152	$79.18
37249-6 (SELECT)	304/L	Seamless	31.75	4.78	ASTM A269	183	$87.01
37249-7 (SELECT)	304/L	Seamless	31.75	4.78	ASTM A269	213	$94.85
37249-8 (SELECT)	304/L	Seamless	31.75	4.78	ASTM A269	244	$102.69
37251-1 (SELECT)	304/L	Seamless	31.75	6.35	ASTM A269	30	$49.55
37251-2 (SELECT)	304/L	Seamless	31.75	6.35	ASTM A269	61	$59.10
37251-3 (SELECT)	304/L	Seamless	31.75	6.35	ASTM A269	91	$68.66
37251-4 (SELECT)	304/L	Seamless	31.75	6.35	ASTM A269	122	$78.21
37251-5 (SELECT)	304/L	Seamless	31.75	6.35	ASTM A269	152	$87.76
37251-6 (SELECT)	304/L	Seamless	31.75	6.35	ASTM A269	183	$97.31

Appendix 2: ANSYS APDL code for 316 Stainless steel ring

```
finish
/cle
stop = 0
pi = 4*atan(1)
!/filname,OD2222w124N80L10alpha05maxdisp6 ! change name to represent your parameters
!!!!!!!! List of parameters to play with
OD = 19.05              ! outside diameter of tube, in mm
T= 1.65     ! tube thickness, in mm
N =83                   ! number of struts around the ring
L = 10      ! length of strut, in mm
alpha = .5  ! alpha is such that B = alpha*H
maxdisp = 4             ! arbitrary radial initially outward displacement, in mm
!!!!!!!! End of parameters to play with
H = pi*OD/(N*(2*alpha+1))
B = alpha*H
nh = 2      ! ratio of strut end height to strut width
nn = 10     ! number of steps during loading or unloading
b_deg=B/(OD/2)*180/pi
h_deg=H/(OD/2)*180/pi
theta=2*b_deg+h_deg
sele = 2*H/10           ! size of elements along strut ends
self = B/8              ! size of elements along fillet curves
selL = L/160            ! size of elements along strut length L
nelT = 20               ! size of elements across strut thickness w
*dim,disp,table,2*nn,1
*dim,diam,table,2*nn,1
*dim,rad_force,table,2*nn,1
*dim,pressure,table,2*nn,1
*dim,data,table,2*nn,4
*dim,maxVM,table,2*nn,1
 disp(0,1) = 1
 diam(0,1) = 1
pressure(0,1) = 1
data(0,1) = 1
data(0,2) = 2
data(0,3) = 3
data(0,4) = 4
maxVM(0,1) = 1
*do,i,1,nn,1
```

```
disp(i,1) = maxdisp*(i-1)/(nn-1)
disp(i+nn,1) = maxdisp-maxdisp*(i-1)/(nn-1)
*enddo
*do,i,1,2*nn
disp(i,0) = i
diam(i,0) = i
pressure(i,0) = i
data(i,0) = i
maxVM(i,0) = i
rad_force(i,0) = i
diam(i,1) = 2*(OD/2+disp(i,1))
*enddo
/prep7
! Element types
et,1,mesh200,6
et,2,solid185
! Material properties (316 stainless steel)
mp,ex,1,190000          ! elastic modulus in MPa
mp,nuxy,1,0.33          ! Poisson's ratio
tb,plastic,1,1,6,miso
tbpt,defi,0,100
tbpt,defi,0.001188,200
tbpt,defi,0.003052,300
tbpt,defi,0.003663,316
tbpt,defi,0.040,400
tbpt,defi,0.080,500
! Geometry
csys,1
K,1,OD/2,0,L+nh*H
k,2,OD/2,b_deg,L+nh*H
K,3,OD/2,0,L+2*nh*H
K,4,OD/2,b_deg+h_deg,L+2*nh*H
K,5,OD/2,b_deg,0
k,6,OD/2,theta,0
K,7,OD/2,theta,nh*H
K,8,OD/2,b_deg+h_deg,nh*H
l,1,2
l,1,3
l,3,4
l,4,8
l,8,7
l,7,6
```

```
l,6,5
l,5,2
lfillt,1,8,B
lfillt,3,4,B
lfillt,5,4,B
lfillt,8,7,B
al,all
type,1
lesize,4,selL
lesize,8,selL
lesize,3,sele
lesize,6,sele
lesize,7,sele
lesize,2,sele
lesize,1,self
lesize,5,self
lesize,9,self
lesize,10,sele
lesize,11,self
lesize,12,sele
allsel
mshape,0,2D
amesh,all
mat,1
type,2
esize,,nelT
voffst,1,-T
! Boundary conditions
csys,1
asel,s,area,,13          ! Selects a subset of areas
nsla,s,1                 ! Selects a subset of nodes
d,all,uz,0
asel,s,area,,14
nsla,s,1
d,all,uy,0
clocal,11,1,0,0,0,theta ! Defines a local coord. system relative to the active coordinate system.
asel,s,area,,8
nsla,s,1
lsel,s,line,,6
nsll,u,1
nrotat,all
d,all,uy,0
```

```
lsel,s,line,,6
nsll,s,1
nrotat,all
d,all,uy,0
csys,1
allsel
finish
/solu                ! Enters the solution processor.
antype,static        ! Specifies the analysis type.
solcontrol,on        ! Specifies solution algorithm and controls.
nlgeom,on            ! Includes large deformation effects.
*do,i,1,nn,1
time,i
! Loading
asel,s,area,,1
nsla,s,1             ! Selects a subset of nodes
lsel,s,line,,6       ! Selects a subset of lines
nsll,u,1             ! Selects those nodes associated with the selected lines.
d,all,ux,disp(i,1)
outres,all,last
lswrite,i
allsel
solve
*enddo
*do,i,1,nn,1
time,i+nn
asel,s,area,,1
nsla,s,1             ! Selects a subset of nodes
lsel,s,line,,6       ! Selects a subset of lines
nsll,u,1             ! Selects those nodes associated with the selected lines.
d,all,ux,disp(i+nn,1)
outres,all,last
lswrite,i+nn
allsel
solve
*enddo
finish
/post1
*do,i,1,2*nn
set,,,,,i
rsys,1
asel,s,area,,1
```

```
nsla,s,1
fsum,rsys,f
*get,rad_force(i,1),fsum,,item,fx
plnsol,s,eqv,0,1
*get,maxVM(i,1),plnsol,0,max
pressure(i,1) = -rad_force(i,1)*N/(pi*diam(i,1)*(L+2*nh*H))
pressure(i,1) = pressure(i,1)*100/0.0133                    ! conversion from MPa to mmHg
data(i,1) = -rad_force(i,1)
data(i,2) = pressure(i,1)
data(i,3) = diam(i,1)
data(i,4) = maxVM(i,1)
*enddo
/axlab,x,Ring diameter [mm]
/axlab,y,Pressure [mmHg]
/xrange,OD*(0.95),(OD+2*maxdisp)*1.05
/yrange,-200,200
*vplot,diam,pressure
save
*if,stop,eq,1,then
*endif
/Expand,N,polar,half,0,theta,0
CSYS,0
VSYMM,y,ALL,0,0    ! generates volumes from a volume pattern by symmetry reflection.
CSYS,1
VGEN,N/2,all, , , ,2*theta, , ,0    ! generates additional volumes from a pattern of volumes.
```

Appendix 3: MATLAB code to predict the elastic response of a human ascending aorta under closed end, free-extension conditions, for a pressure range between 0 and 160 mmHg.

```
function mainprogram_Neda()

    clc;
    clear             % clears all variables
    format long
    N = 1;            % number of turns (-)
    Ri = 15;          % stress-free inner radius (mm)
    % humman
    t = 1.86;         % thickness of one layer (mm)
    Constants = [0.02069,14.80,86.02];
    % No need to change anything below this line
    Ro = Ri + N*t;    % stress-free outer radius (mm)
    theta0 = 180;     % opening angle (deg)
    theta0 = theta0*pi/180; % opening angle (rad)
    nPoints = 160;
    Pexp = linspace(0,200,nPoints)*0.0133/100; % pressure (MPa)
    Pexp = Pexp';
    Fexp = zeros(nPoints,1); % longitudinal force (N)
    riexp = Ri*ones(nPoints,1);
    lambdaexp = ones(nPoints,1)
    % options for Levenberg-Marquardt method of solution
    options = optimset('largescale','off','MaxFunEvals',1e100,'tolFun',1e-30,'TolX',1e-30,'Max-
Iter',5e3,'Algorithm','levenberg-marquardt','Display','off');

    % abscissas for Gauss-Legendre integration
    ksi = [-0.238619186083197 -0.661209386466265 -0.932469514203152 0.238619186083197
0.661209386466265 0.932469514203152];
    % weights for Gauss-Legendre integration
    w = [0.467913934572691 0.360761573048139 0.171324492379170 0.467913934572691
0.360761573048139 0.171324492379170];

    model = 'guccione';

    iniguess = [riexp lambdaexp]; % initial guesses for theoretical inner radius and longitudinal
stretch
    RadLamb = lsqnonlin(@(x) errPF(Con-
stants,x,Pexp,Fexp,Ro,Ri,theta0,ksi,w,model),iniguess,[],[],options) % the optimizer calls the
@errPF m-file
    [Pressure,~] = PF(Constants,RadLamb,Ro,Ri,theta0,ksi,w,model) % uses optimized values to get
theoretical pressure and force

    r80 = RadLamb(81,1)
    r120 = RadLamb(121,1)
    flex = (r120 - r80)/r80*100   % flexibility in percent
    figure(1)
    subplot(2,1,1)
    plot(Pressure.*1000,RadLamb(:,1),'+k')
    ylabel('Inner Radius (mm)')

    subplot(2,1,2)
    plot(Pressure.*1000,RadLamb(:,2),'+k')
    ylabel('Longitudinal Stretch Ratio (-)')
    xlabel('Inner Pressure (kPa)')

end

function error = errPF(C,RadLamb,Pexp,Fexp,Ro,Ri,theta0,ksi,w,model)
    [Pt,Ft] = PF(C,RadLamb,Ro,Ri,theta0,ksi,w,model);
    errp=(Pt-Pexp)*Ri^2; % use of 1, Ri, Ri^2 or Ri^3 as weight
    errf=(Ft-Fexp);
    error=[errp;errf]; % combines errp and errf into one vector
end

function [Pt,Ft] = PF(C,RadLamb,Ro,Ri,theta0,ksi,w,model)
    ri=RadLamb(:,1);
    lambda=RadLamb(:,2);
```

```
    P=zeros(length(ri),1); % initial pressure
    F=zeros(length(ri),1); % initial force
    ro=sqrt(((Ro^2-Ri^2)./(pi*lambda))*theta0+ri.^2); % outer radius in current state
    for i=1:length(ksi) % Gauss-Legendre points
            r=(ro+ri)./2+(ro-ri)./2.*ksi(i); % current radius
            R=sqrt(Ri.^2+(((pi.*lambda)./theta0).*(r.^2-ri.^2)));
            Ezz=0.5*(lambda.^2-1);
            Ett=0.5*(((pi.*r)./(theta0.*R)).^2-1);
            calcPartials = str2func(model);
            [dWtt,dWzz] = calcPartials(C,Ett,Ezz); % calculates partial derivatives for current
model
            P=P+w(i).*(((pi.*r)./(theta0.*R)).^2.*dWtt)./r; % sums pressure
            F=F+w(i).*(2.*lambda.^2.*dWzz-((pi.*r)./(theta0.*R)).^2.*dWtt).*r; % sums force
    end
    Pt=((ro-ri)./2).*P; % theoretical pressure (Nmm-2)
    Ft=pi.*((ro-ri)./2).*F; % theoretical force (N)
end

function [dWtt,dWzz] = guccione(C,Ett,Ezz)
% Computes the partial derivatives of W for the Guccione model
    delta=(1+2.*Ett).*(1+2.*Ezz);
    q=C(2).*Ett.^2+C(3).*(Ezz.^2+(0.5.*(1./delta-1)).^2);
    dWtt=2.*C(2).*Ett-C(3).*(1./delta-1)./(delta.*(1+2.*Ett));
    dWtt=0.5.*C(1).*dWtt.*exp(q);
    dWzz=2.*C(3).*Ezz-C(3).*(1./delta-1)./(delta.*(1+2.*Ezz));
    dWzz=0.5.*C(1).*dWzz.*exp(q);
end
```

Appendix 4: MATALB code to create a wrapped finite element model in LS-Dyna

```
% This program creates a pressurized cylindrically wrapped structure for analysis with LS-Dyna,
with:
%       1) closed end conditions;
% or    2) enforced constant longitudinal stretch.

% Preferred units are mm, mmHg. Results are in N, and Nmm-2

clc;
clear;

Di = 20;        % initial inner diameter [mm]
h = 0.42;       % SPG sheet thickness [mm]
nt = 5;         % number of layers

% The parameters below do not need to be changed

option = 1;     % case 1) or 2 ) above

l = 1.5*Di;     % length of the cylinder
pmax = 160;     % maximum pressure (a ramp from 0 to pmax is applied between times 0 and endtime)
endtime = 0.1;  % end time of the analysis

% Guccione's model constants, for SPG in transverse orientation
c = 0.02069;    % in MPa
b1 = 14.80;     % constant describing behaviour in direction N1-N2, which is circumferential
b2 = 86.02;     % constant describing behaviour in direction N1-N4, which is longitudinal
b3 = 0.1*b2;    % default value describing unknown behaviour in shear
p = 15*100000*c;% Lagrange multiplier

nc = 40;        % number of elements along circumference

nl = round(l*nc/(pi*Di)); % number of elements along cylinder, chosen for good aspect ratio

Do = 2*(nt+1)*h + Di;

npart = 1;
part = cell(1,npart);
part(1) = cellstr('Wrap');

% Create all nodes and their coordinates
nnode = ((nt+1)*nc + 5)*(nl+1);
n = zeros(1,nnode);
xn = zeros(1,nnode);
yn = zeros(1,nnode);
zn = zeros(1,nnode);
for k = 1:(nt+1)*nc + 5
    theta = pi*Di/h + (k-1)*2*pi/nc - 4*pi/nc;
    for j = 1:nl+1
        n(j + (k-1)*(nl+1)) = j + (k-1)*(nl+1);
        z = (j-1)*l/nl;
        xn(j + (k-1)*(nl+1)) = h*theta*cos(theta)/(2*pi);
        yn(j + (k-1)*(nl+1)) = h*theta*sin(theta)/(2*pi);
        zn(j + (k-1)*(nl+1)) = z;
    end
end

% plot3(xn(:),yn(:),zn(:),'+-');
% axis 'equal';

% Create brick elements and their connectivity tables
nelembrick = (nt*nc + 4)*nl;
e = zeros(1,nelembrick);
m = zeros(1,nelembrick);
n1 = zeros(1,nelembrick);
n2 = zeros(1,nelembrick);
```

```
n3 = zeros(1,nelembrick);
n4 = zeros(1,nelembrick);
n5 = zeros(1,nelembrick);
n6 = zeros(1,nelembrick);
n7 = zeros(1,nelembrick);
n8 = zeros(1,nelembrick);
for k = 1:nt*nc + 4
    for j = 1:nl
        e(j + (k-1)*nl) = j + (k-1)*nl;
        m(j + (k-1)*nl) = 1;
        n1(j + (k-1)*nl) = j + (k-1)*(nl+1);
        n2(j + (k-1)*nl) = j + k*(nl+1);
        n3(j + (k-1)*nl) = j + 1 + k*(nl+1);
        n4(j + (k-1)*nl) = j + 1 + (k-1)*(nl+1);
        n5(j + (k-1)*nl) = j + (k-1)*(nl+1) + nc*(nl+1);
        n6(j + (k-1)*nl) = j + k*(nl+1) + nc*(nl+1);
        n7(j + (k-1)*nl) = j + 1 + k*(nl+1) + nc*(nl+1);
        n8(j + (k-1)*nl) = j + 1 + (k-1)*(nl+1) + nc*(nl+1);
    end
end

% Create load segments as shell elements to be pressurized
neleminterior = nc*nl;
n1s = zeros(1,neleminterior);
n2s = zeros(1,neleminterior);
n3s = zeros(1,neleminterior);
n4s = zeros(1,neleminterior);
i = 1;
for k = 1:nc
    for j = 1:nl
        n1s(i) = j + (k-1)*(nl+1);
        n2s(i) = j + k*(nl+1);
        n3s(i) = j + 1 + k*(nl+1);
        n4s(i) = j + 1 + (k-1)*(nl+1);
        i = i + 1;
    end
end

% List of proximal nodes of cylinder
dnode1 = (nt+1)*nc + 5;
dn1 = zeros(1,dnode1);
j = 1;
for k = 1:(nt+1)*nc + 5
    dn1(j) = 1 + (k-1)*(nl+1);
    j = j + 1;
end

% List of distal nodes of cylinder
fnode = (nt+1)*nc + 5;
fn = zeros(1,fnode);
j = 1;
for k = 1:(nt+1)*nc + 5
    fn(j) = k*(nl+1);
    j = j + 1;
end

savefile = 'Wrap.dyn';
fid = fopen(savefile, 'wt');
fprintf(fid, '*KEYWORD\n');
fprintf(fid, '$---+----1----+----2----+----3----+----4----+----5----+----6----+----7----+----
8\n');
fprintf(fid, '$                    TITLE CARD\n');
fprintf(fid, '$---+----1----+----2----+----3----+----4----+----5----+----6----+----7----+----
8\n');
fprintf(fid, '*TITLE\n');
fprintf(fid, 'Wrap\n');
fprintf(fid, '$---+----1----+----2----+----3----+----4----+----5----+----6----+----7----+----
8\n');
fprintf(fid, '$                    CONTROL CARDS\n');
fprintf(fid, '$---+----1----+----2----+----3----+----4----+----5----+----6----+----7----+----
8\n');
```

```
fprintf(fid, '*CONTROL_TERMINATION\n');
fprintf(fid, '$   ENDTIM    ENDCYC     DTMIN    ENDNEG    ENDMAS\n');
fprintf(fid, '%10f         0       0.0       0.0       0.0\n', endtime);
fprintf(fid, '*CONTROL_TIMESTEP\n');
fprintf(fid, '$   DTINIT      SCFT      ISDO    TSLIMT      DTMS      LCTM     ERODE
MS1ST\n');
fprintf(fid, '      0.00       0.9         0\n');
fprintf(fid, '*CONTROL_HOURGLASS\n');
fprintf(fid, '$      IHQ        QH\n');
fprintf(fid, '         1       0.1\n');
fprintf(fid, '*CONTROL_BULK_VISCOSITY\n');
fprintf(fid, '$       Q2        Q1\n');
fprintf(fid, ' 0.150E+01 0.600E-01\n');
fprintf(fid, '*CONTROL_OUTPUT\n');
fprintf(fid, '$    NPOPT    NEECHO    NREFUP    IACCOP     OPIFS    IPNINT    IKEDIT\n');
fprintf(fid, '         0         0         0         0 0.000E+00         0         0\n');
fprintf(fid, '*CONTROL_ENERGY\n');
fprintf(fid, '$     HGEN      RWEN    SLNTEN     RYLEN\n');
fprintf(fid, '         1         2         1         1\n');
fprintf(fid, '$---+----1----+----2----+----3----+----4----+----5----+----6----+----7----+----
8\n');
fprintf(fid, '$                     DATABASE CONTROL CARDS FOR ASCII FILE\n');
fprintf(fid, '$---+----1----+----2----+----3----+----4----+----5----+----6----+----7----+----
8\n');
fprintf(fid, '*DATABASE_GLSTAT\n');
fprintf(fid, '   0.12E-3\n');
fprintf(fid, '*DATABASE_RCFORC\n');
fprintf(fid, '   0.12E-3\n');
fprintf(fid, '$---+----1----+----2----+----3----+----4----+----5----+----6----+----7----+----
8\n');
fprintf(fid, '$                     DATABASE CONTROL CARDS FOR BINARY FILE\n');
fprintf(fid, '$---+----1----+----2----+----3----+----4----+----5----+----6----+----7----+----
8\n');
fprintf(fid, '*DATABASE_BINARY_D3PLOT\n');
fprintf(fid, '%10f \n', endtime/100);
fprintf(fid, '*DATABASE_BINARY_D3THDT\n');
fprintf(fid, '%10f \n', endtime/100);
fprintf(fid, '*DATABASE_EXTENT_BINARY\n');
fprintf(fid, '         0         0         3         0         1         1         1
1\n');
fprintf(fid, '         0         0         0         0         0         0\n');
fprintf(fid, '$---+----1----+----2----+----3----+----4----+----5----+----6----+----7----+----
8\n');
fprintf(fid, '$                     DEFINE PARTS CARDS\n');
fprintf(fid, '$---+----1----+----2----+----3----+----4----+----5----+----6----+----7----+----
8\n');
for i = 1:npart
   fprintf(fid, '*PART\n');
   fprintf(fid, '$ HEADING\n');
   fprintf(fid, ' PART PID =      %2i PART NAME : %s\n', i,char(part(i)));
   fprintf(fid, '$      PID       SID       MID     EOSID      HGID      GRAV    ADPOPT
TMID\n');
   fprintf(fid, '%10i %9i %9i\n', i,i,i);
end
fprintf(fid, '$---+----1----+----2----+----3----+----4----+----5----+----6----+----7----+----
8\n');
fprintf(fid, '$                     MATERIAL CARDS\n');
fprintf(fid, '$---+----1----+----2----+----3----+----4----+----5----+----6----+----7----+----
8\n');
for i = 1:npart
   fprintf(fid, '*MAT_HEART_TISSUE\n');
   fprintf(fid, '$ MATERIAL NAME :%s\n', char(part(i)));
   fprintf(fid, '$      MID        RO         C        B1        B2        B3         P\n');
   fprintf(fid, '%10i    0.1E-8 %9.2E %9.2E %9.2E %9.2E %9.2E \n', i,c,b1,b2,b3,p);
   fprintf(fid, '$     AOPT\n');
   fprintf(fid, '         0\n');
   fprintf(fid, '$       XP        YP        ZP        A1        A2        A3\n\n');
   fprintf(fid, '$       V1        V2        V3        D1        D2        D3      BETA\n\n');
end
% for i = 1:npart
%     fprintf(fid, '*MAT_ELASTIC\n');
```

```
%    fprintf(fid, '$ MATERIAL NAME :%s\n', char(part(i)));
%    fprintf(fid, '$      MID        RO         E        PR        DA        DB         K\n');
%    fprintf(fid, '%10i    0.1E-8  %9.2E %9.2E\n', i,2,0.45);
% end
fprintf(fid, '$---+----1----+----2----+----3----+----4----+----5----+----6----+----7----+----
8\n');
fprintf(fid, '$                    SECTION CARDS\n');
fprintf(fid, '$---+----1----+----2----+----3----+----4----+----5----+----6----+----7----+----
8\n');
for i = 1:npart
   fprintf(fid, '*SECTION_SOLID\n');
   fprintf(fid, '$    SECID    ELFORM       AET\n');
   fprintf(fid, '%10i %9i\n', i,1); % 1 means constant stress elements; 2 would mean constant
pressure elements
end
fprintf(fid, '$---+----1----+----2----+----3----+----4----+----5----+----6----+----7----+----
8\n');
fprintf(fid, '$                    NODAL POINT CARDS\n');
fprintf(fid, '$---+----1----+----2----+----3----+----4----+----5----+----6----+----7----+----
8\n');
fprintf(fid, '*NODE\n');
fprintf(fid, '$   NODE               X               Y               Z      TC      RC\n');
for i = 1:nnode
    fprintf(fid, '%8i %15.9f %15.9f %15.9f\n',n(i),xn(i),yn(i),zn(i));
end
fprintf(fid, '$---+----1----+----2----+----3----+----4----+----5----+----6----+----7----+----
8\n');
fprintf(fid, '$                    SOLID ELEMENT CARDS\n');
fprintf(fid, '$---+----1----+----2----+----3----+----4----+----5----+----6----+----7----+----
8\n');
fprintf(fid, '*ELEMENT_SOLID\n');
fprintf(fid, '$    EID     PID      N1      N2      N3      N4      N5      N6      N7
N8\n');
repeat = 1;
for i = 1:nelembrick
    fprintf(fid, '%8i %7i %7i %7i %7i %7i %7i %7i %7i
%7i\n',e(i),m(i),n1(i),n2(i),n3(i),n4(i),n5(i),n6(i),n7(i),n8(i));
end
fprintf(fid, '*LOAD_SEGMENT\n');
fprintf(fid, '$     LCID        SF        AT        N1        N2        N3        N4\n');
for i = 1:neleminterior
    fprintf(fid, '%10i %9.1f %9.1i %9i %9i %9i %9i\n',1,-1,0,n1s(i),n2s(i),n3s(i),n4s(i));
end
if option == 1
    fprintf(fid, '*LOAD_NODE_POINT\n');
    fprintf(fid, '$     NODE       DOF      LCID        SF       CID        M1        M2
M3\n');
    for i = 1:fnode
        fprintf(fid, '%10i %9i %9i %9.1f\n',fn(i),3,2,1);
    end
end
fprintf(fid, '$---+----1----+----2----+----3----+----4----+----5----+----6----+----7----+----
8\n');
fprintf(fid, '$                    BOUNDARY CONDITION CARDS\n');
fprintf(fid, '$---+----1----+----2----+----3----+----4----+----5----+----6----+----7----+----
8\n');
fprintf(fid, '*BOUNDARY_SPC_NODE\n');
fprintf(fid, '$ NID/NSID       CID      DOFX      DOFY      DOFZ     DOFRX     DOFRY
DOFRZ\n');
for i = 1:dnode1
    fprintf(fid, '%10i %9i %9i %9i %9i \n',dn1(i),0,0,0,1);     % no displacement in z-direction
end
for i = 1:fnode
    fprintf(fid, '%10i %9i %9i %9i %9i \n',fn(i),0,1,1,0);      % no displacement in x- and y-
directions
end
if option == 2
    fprintf(fid, '*BOUNDARY_PRESCRIBED_MOTION_NODE\n');
    fprintf(fid, '$      NID       DOF       VAD      LCID        SF       VID     DEATH
BIRTH\n');
    for i = 1:fnode
```

```
        fprintf(fid, '%10i %9i %9i %9i\n',fn(i),3,2,2);
    end
end

% Load Curves
fprintf(fid, '*DEFINE_CURVE\n');
fprintf(fid, '$     LCID      SIDR      SCLA      SCLO      OFFA      OFFO\n');
fprintf(fid, '%10i          %10.4f\n',1,1);
fprintf(fid, '$                 A1                  O1\n');
fprintf(fid, '%20.4f %19.4f\n',0,0*0.0133/100);
fprintf(fid, '%20.4f %19.4f\n',endtime,pmax*0.0133/100);

if option == 1
    fprintf(fid, '*DEFINE_CURVE\n');
    fprintf(fid, '$     LCID      SIDR      SCLA      SCLO      OFFA      OFFO\n');
    fprintf(fid, '%10i          %10.4f\n',2,1);
    fprintf(fid, '$                 A1                  O1\n');
    fprintf(fid, '%20.4f %19.4f\n',0,0*0.0133/100);
    fprintf(fid, '%20.4f %19.4f\n',endtime,pmax*0.0133/100*pi*0.25*Di^2/fnode);
end
if option == 2
    fprintf(fid, '*DEFINE_CURVE\n');
    fprintf(fid, '$     LCID      SIDR      SCLA      SCLO      OFFA      OFFO\n');
    fprintf(fid, '%10i          %10.4f\n',2,1);
    fprintf(fid, '$                 A1                  O1\n');
    fprintf(fid, '%20.4f %19.4f\n',0,0);
    fprintf(fid, '%20.4f %19.4f\n',endtime/100,1*(lambda-1));
    fprintf(fid, '%20.4f %19.4f\n',endtime,1*(lambda-1));
end

fprintf(fid, '*END\n');
fclose(fid);
```

Appendix 5: MATLAB code for FE modeling of assembly ring + VAJ model

```
% This program creates a ring in cylinder geometry for analysis with LS-Dyna, with:

%       1) closed end conditions;
% or    2) enforced constant longitudinal stretch.

clc;
clear;

nc = 40;                % number of elements along cylinder and ring circumference
option = 1;             % case 1) or 2 ) above

%%%%%%%%%%%%%%%%%%%%%%%%%%
% Ring
%%%%%%%%%%%%%%%%%%%%%%%%%%

DiR = 20;               % ring inner diameter (mm)
elemL =0.31;            % element longitudinal dimension (tentative, mm)
LR = 10;                % ring length (tentative, mm)
hR = 0.42;              % individual layer thickness (mm)
nrR = 3;                % number of layers (and elements) in ring wall thickness

nlR =ceil(LR/elemL)     % number of elements along ring
DoR = 2*nrR*hR + DiR;   % ring outer diameter

%%%%%%%%%%%%%%%%%%%%%%%%%%
% Cylinder
%%%%%%%%%%%%%%%%%%%%%%%%%%

DiC = 30;               % cylinder inner diameter (mm)
Lratio = 2              % cylinder length divided by ring length (tentative)
hC = 1.86;              % cylinder wall thickness (mm)
nrC = 5;                % number of elements across cylinder wall thickness

LC = max([Lratio*LR,2*DiC])   % cylinder length (tentative)
nn = ceil((LC-LR)/(2*elemL)); % number of elements along cylinder above or below ring
LC = (nlR + 2*nn)*elemL       % cylinder length (final)
LR = nlR*elemL                % ring length (final)
nlC = nlR + 2*nn              % number of elements along cylinder
elemL = LC/nlC
DoC = DiC + 2*hC;              % cylinder outer diameter

%%%%%%%%%%%%%%%%%%%%%%%%%%
% Sutures
%%%%%%%%%%%%%%%%%%%%%%%%%%

gap = 1;                % circumferential node interval between longitudinal sutures
                        % must be an integral divider of nc

%%%%%%%%%%%%%%%%%%%%%%%%%%%%%%%%%%%%%%%%%%%%%%%%%%%%%%%%
% The parameters below do not need to be changed
%%%%%%%%%%%%%%%%%%%%%%%%%%%%%%%%%%%%%%%%%%%%%%%%%%%%%%%%

pmax = 160;     % maximum pressure (mmHg)(a ramp from 0 to pmax is applied between times 0 and
endtime)
endtime = 0.24; % end time (sec) of the analysis

% Cylinder material
% Guccione's model constants, for human ascending aortic tissue
c(1) = 21.4/1000;  % in MPa
b1(1) = 3.7448;    % constant describing behaviour in direction N1-N2, which is circumferential
b2(1) = 3.3958;    % constant describing behaviour in direction N1-N4, which is longitudinal
b3(1) = 0.1*b2(1); % default value describing unknown behaviour in shear
p(1) = 3210;       % Lagrange multiplier

% Ring material
```

```
% Guccione's model constants, for SPG in transverse orientation
c(2) = 0.02069;    % in MPa
b1(2) = 14.80;     % constant describing behaviour in direction N1-N2, which is circumferential
b2(2) = 86.02;     % constant describing behaviour in direction N1-N4, which is longitudinal
b3(2) = 0.1*b2(2); % default value describing unknown behaviour in shear
p(2) =  18621;     % Lagrange multiplier

npart = 3;
part = cell(1,npart);           % returns an n-by-n cell array of empty matrices
part(1) = cellstr('Cylinder');  % C = cellstr(S) converts array S to a cell array
part(2) = cellstr('Ring');
part(3) = cellstr('Sutures');

%%%%%%%%%%%%%%%%%%%%%%%%%%%%%%%%%%%%%%%%%%%%%%%%%%%%%%%
% Create all nodes and their coordinates
%%%%%%%%%%%%%%%%%%%%%%%%%%%%%%%%%%%%%%%%%%%%%%%%%%%%%%%

nnodeC = nc*(nrC+1)*(nlC+1); % number of nodes in the cylinder
nnodeR = nc*(nrR+1)*(nlR+1); % number of nodes in the ring

nnode = nnodeC + nnodeR;     % total number of nodes
n = zeros(1,nnode);
xn = zeros(1,nnode);
yn = zeros(1,nnode);
zn = zeros(1,nnode);

listC = zeros(1,nc*(nlR+1));
listR = zeros(1,nc*(nlR+1));

% Cylinder
for k = 1:nc
    for j = 1:nlC+1
        for i = 1:nrC+1

            n(i + (j-1)*(nrC+1) + (k-1)*(nrC+1)*(nlC+1)) = i + (j-1)*(nrC+1) + (k-
1)*(nrC+1)*(nlC+1);
            r = 0.5*DiC + (i-1)*0.5*(DoC - DiC)/nrC;
            z = (j-1)*elemL;
            theta = (k-1)*2*pi/nc;

            xn(i + (j-1)*(nrC+1) + (k-1)*(nrC+1)*(nlC+1)) = r*cos(theta);
            yn(i + (j-1)*(nrC+1) + (k-1)*(nrC+1)*(nlC+1)) = r*sin(theta);
            zn(i + (j-1)*(nrC+1) + (k-1)*(nrC+1)*(nlC+1)) = z;

        end
    end
end

% List of cylinder nodes that will be sutured
i = 1;
for k = 1:gap:nc
    for j = nn + 1:nn + nlR + 1
        listC(i) = 1 + (j-1)*(nrC+1) + (k-1)*(nrC+1)*(nlC+1);
        i = i + 1;
    end
end
nsutures = i-1;

% Ring
for k = 1:nc
    for j = 1:nlR+1
        for i = 1:nrR+1

            n(nnodeC + i + (j-1)*(nrR+1) + (k-1)*(nrR+1)*(nlR+1)) = nnodeC + i + (j-1)*(nrR+1) +
(k-1)*(nrR+1)*(nlR+1);
            r = 0.5*DiR + (i-1)*0.5*(DoR - DiR)/nrR;
            z = (j-1)*elemL  + nn*elemL;
            theta = (k-1)*2*pi/nc;

            xn(nnodeC + i + (j-1)*(nrR+1) + (k-1)*(nrR+1)*(nlR+1)) = r*cos(theta);
            yn(nnodeC + i + (j-1)*(nrR+1) + (k-1)*(nrR+1)*(nlR+1)) = r*sin(theta);
```

```
            zn(nnodeC + i + (j-1)*(nrR+1) + (k-1)*(nrR+1)*(nlR+1)) = z;

        end
    end
end

% List of ring nodes that will be sutured
i = 1;
for k = 1:gap:nc
    for j = 1:nlR+1
        listR(i) = nnodeC + nrR + 1 + (j-1)*(nrR+1) + (k-1)*(nrR+1)*(nlR+1);
        i = i + 1;
    end
end

plot3(xn(1:nnodeC),yn(1:nnodeC),zn(1:nnodeC),'+')
hold on
plot3(xn(nnodeC+1:nnode),yn(nnodeC+1:nnode),zn(nnodeC+1:nnode),'+')
axis 'equal'

% Create brick elements and their connectivity tables
nelembrickC = nc*nrC*nlC; % number of brick elements in the cylinder
nelembrickR = nc*nrR*nlR; % number of brick elements in the ring

nelembrick = nelembrickC + nelembrickR; % total number of brick elements
e = zeros(1,nelembrick);
m = zeros(1,nelembrick);
n1 = zeros(1,nelembrick);
n2 = zeros(1,nelembrick);
n3 = zeros(1,nelembrick);
n4 = zeros(1,nelembrick);
n5 = zeros(1,nelembrick);
n6 = zeros(1,nelembrick);
n7 = zeros(1,nelembrick);
n8 = zeros(1,nelembrick);

% Cylinder
for k = 1:nc-1
    for j = 1:nlC
        for i = 1:nrC
            e(i + (j-1)*nrC + (k-1)*nrC*nlC) = i + (j-1)*nrC + (k-1)*nrC*nlC;
            m(i + (j-1)*nrC + (k-1)*nrC*nlC) = 1;
            n1(i + (j-1)*nrC + (k-1)*nrC*nlC) = i + (j-1)*(nrC+1) + (k-1)*(nrC+1)*(nlC+1);
            n2(i + (j-1)*nrC + (k-1)*nrC*nlC) = i + (j-1)*(nrC+1) + k*(nrC+1)*(nlC+1);
            n3(i + (j-1)*nrC + (k-1)*nrC*nlC) = i + j*(nrC+1) + k*(nrC+1)*(nlC+1);
            n4(i + (j-1)*nrC + (k-1)*nrC*nlC) = i + j*(nrC+1) + (k-1)*(nrC+1)*(nlC+1);
            n5(i + (j-1)*nrC + (k-1)*nrC*nlC) = i + 1 + (j-1)*(nrC+1) + (k-1)*(nrC+1)*(nlC+1);
            n6(i + (j-1)*nrC + (k-1)*nrC*nlC) = i + 1 + (j-1)*(nrC+1) + k*(nrC+1)*(nlC+1);
            n7(i + (j-1)*nrC + (k-1)*nrC*nlC) = i + 1 + j*(nrC+1) + k*(nrC+1)*(nlC+1);
            n8(i + (j-1)*nrC + (k-1)*nrC*nlC) = i + 1 + j*(nrC+1) + (k-1)*(nrC+1)*(nlC+1);
        end
    end
end
for j = 1:nlC
    for i = 1:nrC
        e(i + (j-1)*nrC + (nc-1)*nrC*nlC) = i + (j-1)*nrC + (nc-1)*nrC*nlC;
        m(i + (j-1)*nrC + (nc-1)*nrC*nlC) = 1;
        n1(i + (j-1)*nrC + (nc-1)*nrC*nlC) = i + (j-1)*(nrC+1) + (nc-1)*(nrC+1)*(nlC+1);
        n2(i + (j-1)*nrC + (nc-1)*nrC*nlC) = i + (j-1)*(nrC+1);
        n3(i + (j-1)*nrC + (nc-1)*nrC*nlC) = i + j*(nrC+1);
        n4(i + (j-1)*nrC + (nc-1)*nrC*nlC) = i + j*(nrC+1) + (nc-1)*(nrC+1)*(nlC+1);
        n5(i + (j-1)*nrC + (nc-1)*nrC*nlC) = i + 1 + (j-1)*(nrC+1) + (nc-1)*(nrC+1)*(nlC+1);
        n6(i + (j-1)*nrC + (nc-1)*nrC*nlC) = i + 1 + (j-1)*(nrC+1);
        n7(i + (j-1)*nrC + (nc-1)*nrC*nlC) = i + 1 + j*(nrC+1);
        n8(i + (j-1)*nrC + (nc-1)*nrC*nlC) = i + 1 + j*(nrC+1) + (nc-1)*(nrC+1)*(nlC+1);
    end
end

% Ring
for k = 1:nc-1
    for j = 1:nlR
```

```
        for i = 1:nrR
            e(nelembrickC + i + (j-1)*nrR + (k-1)*nrR*nlR) = nelembrickC + i + (j-1)*nrR + (k-
1)*nrR*nlR;
            m(nelembrickC + i + (j-1)*nrR + (k-1)*nrR*nlR) = 2;
            n1(nelembrickC + i + (j-1)*nrR + (k-1)*nrR*nlR) = nnodeC + i + (j-1)*(nrR+1) + (k-
1)*(nrR+1)*(nlR+1);
            n2(nelembrickC + i + (j-1)*nrR + (k-1)*nrR*nlR) = nnodeC + i + (j-1)*(nrR+1) +
k*(nrR+1)*(nlR+1);
            n3(nelembrickC + i + (j-1)*nrR + (k-1)*nrR*nlR) = nnodeC + i + j*(nrR+1) +
k*(nrR+1)*(nlR+1);
            n4(nelembrickC + i + (j-1)*nrR + (k-1)*nrR*nlR) = nnodeC + i + j*(nrR+1) + (k-
1)*(nrR+1)*(nlR+1);
            n5(nelembrickC + i + (j-1)*nrR + (k-1)*nrR*nlR) = nnodeC + i + 1 + (j-1)*(nrR+1) +
(k-1)*(nrR+1)*(nlR+1);
            n6(nelembrickC + i + (j-1)*nrR + (k-1)*nrR*nlR) = nnodeC + i + 1 + (j-1)*(nrR+1) +
k*(nrR+1)*(nlR+1);
            n7(nelembrickC + i + (j-1)*nrR + (k-1)*nrR*nlR) = nnodeC + i + 1 + j*(nrR+1) +
k*(nrR+1)*(nlR+1);
            n8(nelembrickC + i + (j-1)*nrR + (k-1)*nrR*nlR) = nnodeC + i + 1 + j*(nrR+1) + (k-
1)*(nrR+1)*(nlR+1);
        end
    end
end
for j = 1:nlR
    for i = 1:nrR
        e(nelembrickC + i + (j-1)*nrR + (nc-1)*nrR*nlR) = nelembrickC + i + (j-1)*nrR + (nc-
1)*nrR*nlR;
        m(nelembrickC + i + (j-1)*nrR + (nc-1)*nrR*nlR) = 2;
        n1(nelembrickC + i + (j-1)*nrR + (nc-1)*nrR*nlR) = nnodeC + i + (j-1)*(nrR+1) + (nc-
1)*(nrR+1)*(nlR+1);
        n2(nelembrickC + i + (j-1)*nrR + (nc-1)*nrR*nlR) = nnodeC + i + (j-1)*(nrR+1);
        n3(nelembrickC + i + (j-1)*nrR + (nc-1)*nrR*nlR) = nnodeC + i + j*(nrR+1);
        n4(nelembrickC + i + (j-1)*nrR + (nc-1)*nrR*nlR) = nnodeC + i + j*(nrR+1) + (nc-
1)*(nrR+1)*(nlR+1);
        n5(nelembrickC + i + (j-1)*nrR + (nc-1)*nrR*nlR) = nnodeC + i + 1 + (j-1)*(nrR+1) + (nc-
1)*(nrR+1)*(nlR+1);
        n6(nelembrickC + i + (j-1)*nrR + (nc-1)*nrR*nlR) = nnodeC + i + 1 + (j-1)*(nrR+1);
        n7(nelembrickC + i + (j-1)*nrR + (nc-1)*nrR*nlR) = nnodeC + i + 1 + j*(nrR+1);
        n8(nelembrickC + i + (j-1)*nrR + (nc-1)*nrR*nlR) = nnodeC + i + 1 + j*(nrR+1) + (nc-
1)*(nrR+1)*(nlR+1);
    end
end

% Create load segments as shell elements to be pressurized
neleminterior = nc*nlC;
n1s = zeros(1,neleminterior);
n2s = zeros(1,neleminterior);
n3s = zeros(1,neleminterior);
n4s = zeros(1,neleminterior);
i = 1;

% on the inside of the ring
for k = 1:nc-1
    for j = 1:nlR
        n1s(i) = nnodeC + 1 + (j-1)*(nrR+1) + (k-1)*(nrR+1)*(nlR+1);
        n2s(i) = nnodeC + 1 + j*(nrR+1) + (k-1)*(nrR+1)*(nlR+1);
        n3s(i) = nnodeC + 1 + j*(nrR+1) + k*(nrR+1)*(nlR+1);
        n4s(i) = nnodeC + 1 + (j-1)*(nrR+1) + k*(nrR+1)*(nlR+1);
        i = i + 1;
    end
end
for j = 1:nlR
    n1s(i) = nnodeC + 1 + (j-1)*(nrR+1) + (nc-1)*(nrR+1)*(nlR+1);
    n2s(i) = nnodeC + 1 + j*(nrR+1) + (nc-1)*(nrR+1)*(nlR+1);
    n3s(i) = nnodeC + 1 + j*(nrR+1);
    n4s(i) = nnodeC + 1 + (j-1)*(nrR+1);
    i = i + 1;
end

% on the inside of the difference bewteen the cylinder and the ring
```

```
for k = 1:nc-1
    for j = 1:nn
        n1s(i) = 1 + (j-1)*(nrC+1) + (k-1)*(nrC+1)*(nlC+1);
        n2s(i) = 1 + j*(nrC+1) + (k-1)*(nrC+1)*(nlC+1);
        n3s(i) = 1 + j*(nrC+1) + k*(nrC+1)*(nlC+1);
        n4s(i) = 1 + (j-1)*(nrC+1) + k*(nrC+1)*(nlC+1);
        i = i + 1;
    end
end
for j = 1:nn
    n1s(i) = 1 + (j-1)*(nrC+1) + (nc-1)*(nrC+1)*(nlC+1);
    n2s(i) = 1 + j*(nrC+1) + (nc-1)*(nrC+1)*(nlC+1);
    n3s(i) = 1 + j*(nrC+1);
    n4s(i) = 1 + (j-1)*(nrC+1);
    i = i + 1;
end

for k = 1:nc-1
    for j = nn + nlR + 1:nlC;
        n1s(i) = 1 + (j-1)*(nrC+1) + (k-1)*(nrC+1)*(nlC+1);
        n2s(i) = 1 + j*(nrC+1) + (k-1)*(nrC+1)*(nlC+1);
        n3s(i) = 1 + j*(nrC+1) + k*(nrC+1)*(nlC+1);
        n4s(i) = 1 + (j-1)*(nrC+1) + k*(nrC+1)*(nlC+1);
        i = i + 1;
    end
end
for j = nn + nlR + 1:nlC;
    n1s(i) = 1 + (j-1)*(nrC+1) + (nc-1)*(nrC+1)*(nlC+1);
    n2s(i) = 1 + j*(nrC+1) + (nc-1)*(nrC+1)*(nlC+1);
    n3s(i) = 1 + j*(nrC+1);
    n4s(i) = 1 + (j-1)*(nrC+1);
    i = i + 1;
end

% List of bottom nodes of cylinder
dnode1 = nc*(nrC+1);
dn1 = zeros(1,dnode1);
j = 1;
for k = 1:nc
    for i = 1:(nrC+1)
            dn1(j) = i + (k-1)*(nrC+1)*(nlC+1);
            j = j + 1;
    end
end

% List of top nodes of cylinder
fnode = nc*(nrC+1);
fn = zeros(1,fnode);
j = 1;
for k = 1:nc
    for i = 1:(nrC+1)
            fn(j) = i + nlC*(nrC+1) + (k-1)*(nrC+1)*(nlC+1);
            j = j + 1;
    end
end

savefile = 'Ring_in_Cylinder.dyn';
fid = fopen(savefile, 'wt');
fprintf(fid, '*KEYWORD\n');
fprintf(fid, '$---+----1----+----2----+----3----+----4----+----5----+----6----+----7----+----
8\n');
fprintf(fid, '$                    TITLE CARD\n');
fprintf(fid, '$---+----1----+----2----+----3----+----4----+----5----+----6----+----7----+----
8\n');
fprintf(fid, '*TITLE\n');
fprintf(fid, 'Ring in Cylinder\n');
fprintf(fid, '$---+----1----+----2----+----3----+----4----+----5----+----6----+----7----+----
8\n');
fprintf(fid, '$                    CONTROL CARDS\n');
fprintf(fid, '$---+----1----+----2----+----3----+----4----+----5----+----6----+----7----+----
8\n');
```

```
fprintf(fid, '*CONTROL_TERMINATION\n');
fprintf(fid, '$   ENDTIM    ENDCYC     DTMIN    ENDNEG    ENDMAS\n');
fprintf(fid, '%10f         0       0.0       0.0       0.0\n', endtime);
fprintf(fid, '*CONTROL_TIMESTEP\n');
fprintf(fid, '$   DTINIT      SCFT      ISDO    TSLIMT      DTMS      LCTM     ERODE
MS1ST\n');
fprintf(fid, '      0.00       0.9         0\n');
fprintf(fid, '*CONTROL_HOURGLASS\n');
fprintf(fid, '$      IHQ        QH\n');
fprintf(fid, '         1       0.1\n');
fprintf(fid, '*CONTROL_BULK_VISCOSITY\n');
fprintf(fid, '$       Q2        Q1\n');
fprintf(fid, ' 0.150E+01 0.600E-01\n');
fprintf(fid, '*CONTROL_OUTPUT\n');
fprintf(fid, '$    NPOPT    NEECHO    NREFUP    IACCOP     OPIFS    IPNINT    IKEDIT\n');
fprintf(fid, '         0         0         0         0 0.000E+00         0         0\n');
fprintf(fid, '*CONTROL_ENERGY\n');
fprintf(fid, '$     HGEN      RWEN    SLNTEN     RYLEN\n');
fprintf(fid, '         1         2         1         1\n');
fprintf(fid, '$---+----1----+----2----+----3----+----4----+----5----+----6----+----7----+----
8\n');
fprintf(fid, '$                     DATABASE CONTROL CARDS FOR ASCII FILE\n');
fprintf(fid, '$---+----1----+----2----+----3----+----4----+----5----+----6----+----7----+----
8\n');
fprintf(fid, '*DATABASE_GLSTAT\n');
fprintf(fid, '   0.12E-3\n');
fprintf(fid, '*DATABASE_RCFORC\n');
fprintf(fid, '   0.12E-3\n');
fprintf(fid, '$---+----1----+----2----+----3----+----4----+----5----+----6----+----7----+----
8\n');
fprintf(fid, '$                     DATABASE CONTROL CARDS FOR BINARY FILE\n');
fprintf(fid, '$---+----1----+----2----+----3----+----4----+----5----+----6----+----7----+----
8\n');
fprintf(fid, '*DATABASE_BINARY_D3PLOT\n');
fprintf(fid, '%10f \n', endtime/100);
fprintf(fid, '*DATABASE_BINARY_D3THDT\n');
fprintf(fid, '%10f \n', endtime/100);
fprintf(fid, '*DATABASE_EXTENT_BINARY\n');
fprintf(fid, '         0         0         3         0         1         1         1
1\n');
fprintf(fid, '         0         0         0         0         0         0\n');
fprintf(fid, '$---+----1----+----2----+----3----+----4----+----5----+----6----+----7----+----
8\n');
fprintf(fid, '$                     DEFINE PARTS CARDS\n');
fprintf(fid, '$---+----1----+----2----+----3----+----4----+----5----+----6----+----7----+----
8\n');
for i = 1:npart
   fprintf(fid, '*PART\n');
   fprintf(fid, '$ HEADING\n');
   fprintf(fid, ' PART PID =      %2i PART NAME : %s\n', i,char(part(i)));
   fprintf(fid, '$      PID       SID       MID     EOSID      HGID      GRAV    ADPOPT
TMID\n');
   fprintf(fid, '%10i %9i %9i\n', i,i,i);
end
fprintf(fid, '$---+----1----+----2----+----3----+----4----+----5----+----6----+----7----+----
8\n');
fprintf(fid, '$                     MATERIAL CARDS\n');
fprintf(fid, '$---+----1----+----2----+----3----+----4----+----5----+----6----+----7----+----
8\n');
for i = 1:npart-1
   fprintf(fid, '*MAT_HEART_TISSUE\n');
   fprintf(fid, '$ MATERIAL NAME :%s\n', char(part(i)));
   fprintf(fid, '$      MID        RO         C        B1        B2        B3         P\n');
   fprintf(fid, '%10i    0.1E-8 %9.2E %9.2E %9.2E %9.2E %9.2E \n',
i,c(i),b1(i),b2(i),b3(i),p(i));
   fprintf(fid, '$     AOPT\n');
   fprintf(fid, '         0\n');
   fprintf(fid, '$       XP        YP        ZP        A1        A2        A3\n\n');
   fprintf(fid, '$       V1        V2        V3        D1        D2        D3      BETA\n\n');
end
% for i = 1:npart
```

```
%    fprintf(fid, '*MAT_ELASTIC\n');
%    fprintf(fid, '$ MATERIAL NAME :%s\n', char(part(i)));
%    fprintf(fid, '$      MID        RO         E        PR        DA        DB         K\n');
%    fprintf(fid, '%10i    0.1E-8  %9.2E %9.2E\n', i,2,0.45);
% end
fprintf(fid, '*MAT_SEATBELT\n');
fprintf(fid, '$ MATERIAL NAME :%s\n', char(part(3)));
fprintf(fid, '$      MID      MPUL     LLCID     ULCID      LMIN\n');
fprintf(fid, '%10i  %1.1i %9.1i %9.1i\n', 3,5.59e-12,3,4);
fprintf(fid, '$---+----1----+----2----+----3----+----4----+----5----+----6----+----7----+----
8\n');
fprintf(fid, '$                    SECTION CARDS\n');
fprintf(fid, '$---+----1----+----2----+----3----+----4----+----5----+----6----+----7----+----
8\n');
for i = 1:npart-1
   fprintf(fid, '*SECTION_SOLID\n');
   fprintf(fid, '$    SECID    ELFORM       AET\n');
   fprintf(fid, '%10i %9i\n', i,1); % 1 means constant stress elements; 2 would mean constant
pressure elements
end
fprintf(fid, '*SECTION_SEATBELT\n');
fprintf(fid, '$    SECID\n');
fprintf(fid, '%10i\n', 3);
fprintf(fid, '$---+----1----+----2----+----3----+----4----+----5----+----6----+----7----+----
8\n');
fprintf(fid, '$                    NODAL POINT CARDS\n');
fprintf(fid, '$---+----1----+----2----+----3----+----4----+----5----+----6----+----7----+----
8\n');
fprintf(fid, '*NODE\n');
fprintf(fid, '$   NODE              X               Y               Z      TC      RC\n');
for i = 1:nnode
    fprintf(fid, '%8i %15.9f %15.9f %15.9f\n',n(i),xn(i),yn(i),zn(i));
end
fprintf(fid, '$---+----1----+----2----+----3----+----4----+----5----+----6----+----7----+----
8\n');
fprintf(fid, '$                    SOLID ELEMENT CARDS\n');
fprintf(fid, '$---+----1----+----2----+----3----+----4----+----5----+----6----+----7----+----
8\n');
fprintf(fid, '*ELEMENT_SOLID\n');
fprintf(fid, '$    EID     PID      N1      N2      N3      N4      N5      N6      N7
N8\n');
repeat = 1;
for i = 1:nelembrick
    fprintf(fid, '%8i %7i %7i %7i %7i %7i %7i %7i %7i
%7i\n',e(i),m(i),n1(i),n2(i),n3(i),n4(i),n5(i),n6(i),n7(i),n8(i));
end
fprintf(fid, '*ELEMENT_SEATBELT\n');
fprintf(fid, '$    EID     PID      N1      N2   SBRID    SLEN      N3      N4\n');
for i = 1:nsutures
    fprintf(fid, '%8i %7i %7i %7i %15.3f\n',i,3,listC(i),listR(i),-0.95*0.5*(DiC-DoR));
end
fprintf(fid, '*LOAD_SEGMENT\n');
fprintf(fid, '$     LCID        SF        AT        N1        N2        N3        N4\n');
for i = 1:neleminterior
    fprintf(fid, '%10i %9.1f %9.1i %9i %9i %9i %9i\n',1,1,0,n1s(i),n2s(i),n3s(i),n4s(i));
end
if option == 1
    fprintf(fid, '*LOAD_NODE_POINT\n');
    fprintf(fid, '$     NODE       DOF      LCID        SF       CID        M1        M2
M3\n');
    for i = 1:fnode
        fprintf(fid, '%10i %9i %9i %9.1f\n',fn(i),3,2,1);
    end
end
fprintf(fid, '$---+----1----+----2----+----3----+----4----+----5----+----6----+----7----+----
8\n');
fprintf(fid, '$                    BOUNDARY CONDITION CARDS\n');
fprintf(fid, '$---+----1----+----2----+----3----+----4----+----5----+----6----+----7----+----
8\n');
fprintf(fid, '*BOUNDARY_SPC_NODE\n');
```

```
fprintf(fid, '$ NID/NSID       CID      DOFX      DOFY      DOFZ     DOFRX     DOFRY
DOFRZ\n');
for i = 1:dnode1
    fprintf(fid, '%10i %9i %9i %9i %9i \n',dn1(i),0,0,0,1);     % no displacement in z-direction
end
for i = 1:fnode
    fprintf(fid, '%10i %9i %9i %9i %9i \n',fn(i),0,1,1,0);      % no displacement in x- and y-
directions
end
if option == 2
    fprintf(fid, '*BOUNDARY_PRESCRIBED_MOTION_NODE\n');
    fprintf(fid, '$      NID       DOF       VAD      LCID        SF       VID     DEATH
BIRTH\n');
    for i = 1:fnode
        fprintf(fid, '%10i %9i %9i %9i\n',fn(i),3,2,2);
    end
end

% Load Curves
fprintf(fid, '*DEFINE_CURVE\n');
fprintf(fid, '$     LCID      SIDR      SCLA      SCLO      OFFA      OFFO\n');
fprintf(fid, '%10i          %10.4f\n',1,1);
fprintf(fid, '$                  A1                  O1\n');
fprintf(fid, '%20.4f %19.4f\n',0,0*0.0133/100);
fprintf(fid, '%20.4f %19.4f\n',1.01*endtime,pmax*0.0133/100);

if option == 1
    fprintf(fid, '*DEFINE_CURVE\n');
    fprintf(fid, '$     LCID      SIDR      SCLA      SCLO      OFFA      OFFO\n');
    fprintf(fid, '%10i          %10.4f\n',2,1);
    fprintf(fid, '$                  A1                  O1\n');
    fprintf(fid, '%20.4f %19.4f\n',0,0*0.0133/100);
    fprintf(fid, '%20.4f %19.4f\n',1.01*endtime,pmax*0.0133/100*pi*0.25*DiC^2/(nc*(nrC+1)));
elseif option == 2
    fprintf(fid, '*DEFINE_CURVE\n');
    fprintf(fid, '$     LCID      SIDR      SCLA      SCLO      OFFA      OFFO\n');
    fprintf(fid, '%10i          %10.4f\n',2,1);
    fprintf(fid, '$                  A1                  O1\n');
    fprintf(fid, '%20.4f %19.4f\n',0,0);
    fprintf(fid, '%20.4f %19.4f\n',endtime/100,LR*(lambda-1));
    fprintf(fid, '%20.4f %19.4f\n',1.01*endtime,LR*(lambda-1));
end
fprintf(fid, '*DEFINE_CURVE\n');
fprintf(fid, '$     LCID      SIDR      SCLA      SCLO      OFFA      OFFO\n');
fprintf(fid, '         3         0\n');
fprintf(fid, '$                  A1                  O1\n');
fprintf(fid, '%20.4f %19.4f\n',0,0);
fprintf(fid, '%20.4f %19.4f\n',endtime/10,0.1);
fprintf(fid, '*DEFINE_CURVE\n');
fprintf(fid, '$     LCID      SIDR      SCLA      SCLO      OFFA      OFFO\n');
fprintf(fid, '         4         0\n');
fprintf(fid, '$                  A1                  O1\n');
fprintf(fid, '%20.4f %19.4f\n',0,0);
fprintf(fid, '%20.4f %19.4f\n',endtime/10,0.1);
fprintf(fid, '*END\n');
fclose(fid);
```

Appendix 6: Parametric quarter-model of combined ring and VAJ model

```
% This program creates a quarter of a ring in cylinder geometry for analysis with LS-Dyna, with:
%       1) closed end conditions;
% or    2) enforced constant longitudinal stretch.

clc;
clear;

nc = 10;                % number of elements along cylinder and ring circumference
option = 2;             % case 1) or 2 ) above
lambda = 1.19;

%%%%%%%%%%%%%%%%%%%%%%%%%
% Ring
%%%%%%%%%%%%%%%%%%%%%%%%%

DiR = 20;               % ring inner diameter (mm)
elemL =0.31;            % element longitudinal dimension (tentative, mm)
LR = 10;                % ring length (tentative, mm)
hR = 0.42;              % individual layer thickness (mm)
nrR = 3;                % number of layers (and elements) in ring wall thickness

nlR =ceil(LR/elemL)     % number of elements along ring
DoR = 2*nrR*hR + DiR;   % ring outer diameter

%%%%%%%%%%%%%%%%%%%%%%%%%
% Cylinder
%%%%%%%%%%%%%%%%%%%%%%%%%

DiC = 30;               % cylinder inner diameter (mm)
Lratio = 2              % cylinder length divided by ring length (tentative)
hC = 1.86;              % cylinder wall thickness (mm)
nrC = 5;                % number of elements across cylinder wall thickness

LC = max([Lratio*LR,2*DiC])   % cylinder length (tentative)
nn = ceil((LC-LR)/(2*elemL)); % number of elements along cylinder above or below ring
LC = (nlR + 2*nn)*elemL       % cylinder length (final)
LR = nlR*elemL                % ring length (final)
nlC = nlR + 2*nn              % number of elements along cylinder
elemL = LC/nlC
DoC = DiC + 2*hC;             % cylinder outer diameter

%%%%%%%%%%%%%%%%%%%%%%%%%
% Sutures
%%%%%%%%%%%%%%%%%%%%%%%%%

gap = 1;                % circumferential node interval between longitudinal sutures
                        % must be an integral divider of nc

%%%%%%%%%%%%%%%%%%%%%%%%%%%%%%%%%%%%%%%%%%%%%%%%%%%%%%%%
% The parameters below do not need to be changed
%%%%%%%%%%%%%%%%%%%%%%%%%%%%%%%%%%%%%%%%%%%%%%%%%%%%%%%%

pmax = 160;     % maximum pressure (mmHg)(a ramp from 0 to pmax is applied between times 0 and
endtime)
endtime = 0.24; % end time (sec) of the analysis

% Cylinder material
% Guccione's model constants, for human ascending aortic tissue
c(1) = 21.4/1000;  % in MPa
b1(1) = 3.7448;    % constant describing behaviour in direction N1-N2, which is circumferential
b2(1) = 3.3958;    % constant describing behaviour in direction N1-N4, which is longitudinal
b3(1) = 0.1*b2(1); % default value describing unknown behaviour in shear
p(1) = 3210;       % Lagrange multiplier
```

```
% Ring material
% Guccione's model constants, for SPG in transverse orientation
c(2) = 0.02069;    % in MPa
b1(2) = 14.80;     % constant describing behaviour in direction N1-N2, which is circumferential
b2(2) = 86.02;     % constant describing behaviour in direction N1-N4, which is longitudinal
b3(2) = 0.1*b2(2); % default value describing unknown behaviour in shear
p(2) =  18621;     % Lagrange multiplier

npart = 3;
part = cell(1,npart);           % returns an n-by-n cell array of empty matrices
part(1) = cellstr('Cylinder');  % C = cellstr(S) converts array S to a cell array
part(2) = cellstr('Ring');
part(3) = cellstr('Sutures');

%%%%%%%%%%%%%%%%%%%%%%%%%%%%%%%%%%%%%%%%%%%%%%%%%%%%%%%%
% Create all nodes and their coordinates
%%%%%%%%%%%%%%%%%%%%%%%%%%%%%%%%%%%%%%%%%%%%%%%%%%%%%%%%

nnodeC = (nc+1)*(nrC+1)*(nlC+1); % number of nodes in the cylinder
nnodeR = (nc+1)*(nrR+1)*(nlR+1); % number of nodes in the ring

nnode = nnodeC + nnodeR;     % total number of nodes
n = zeros(1,nnode);
xn = zeros(1,nnode);
yn = zeros(1,nnode);
zn = zeros(1,nnode);

listC = zeros(1,nc*(nlR+1));
listR = zeros(1,nc*(nlR+1));

% Cylinder
for k = 1:nc+1
    for j = 1:nlC+1
        for i = 1:nrC+1

            n(i + (j-1)*(nrC+1) + (k-1)*(nrC+1)*(nlC+1)) = i + (j-1)*(nrC+1) + (k-
1)*(nrC+1)*(nlC+1);
            r = 0.5*DiC + (i-1)*0.5*(DoC - DiC)/nrC;
            z = (j-1)*elemL;
            theta = (k-1)*0.5*pi/nc;

            xn(i + (j-1)*(nrC+1) + (k-1)*(nrC+1)*(nlC+1)) = r*cos(theta);
            yn(i + (j-1)*(nrC+1) + (k-1)*(nrC+1)*(nlC+1)) = r*sin(theta);
            zn(i + (j-1)*(nrC+1) + (k-1)*(nrC+1)*(nlC+1)) = z;

        end
    end
end

% List of cylinder nodes that will be sutured
i = 1;
for k = 1:gap:nc+1
    for j = nn + 1:nn + nlR + 1
        listC(i) = 1 + (j-1)*(nrC+1) + (k-1)*(nrC+1)*(nlC+1);
        i = i + 1;
    end
end
nsutures = i-1;

% Ring
for k = 1:nc+1
    for j = 1:nlR+1
        for i = 1:nrR+1

            n(nnodeC + i + (j-1)*(nrR+1) + (k-1)*(nrR+1)*(nlR+1)) = nnodeC + i + (j-1)*(nrR+1) +
(k-1)*(nrR+1)*(nlR+1);
            r = 0.5*DiR + (i-1)*0.5*(DoR - DiR)/nrR;
            z = (j-1)*elemL  + nn*elemL;
            theta = (k-1)*0.5*pi/nc;
```

```
            xn(nnodeC + i + (j-1)*(nrR+1) + (k-1)*(nrR+1)*(nlR+1)) = r*cos(theta);
            yn(nnodeC + i + (j-1)*(nrR+1) + (k-1)*(nrR+1)*(nlR+1)) = r*sin(theta);
            zn(nnodeC + i + (j-1)*(nrR+1) + (k-1)*(nrR+1)*(nlR+1)) = z;

        end
    end
end

% List of ring nodes that will be sutured
i = 1;
for k = 1:gap:nc+1
    for j = 1:nlR+1
        listR(i) = nnodeC + nrR + 1 + (j-1)*(nrR+1) + (k-1)*(nrR+1)*(nlR+1);
        i = i + 1;
    end
end

plot3(xn(1:nnodeC),yn(1:nnodeC),zn(1:nnodeC),'+')
hold on
plot3(xn(nnodeC+1:nnode),yn(nnodeC+1:nnode),zn(nnodeC+1:nnode),'+')
axis 'equal'

% Create brick elements and their connectivity tables
nelembrickC = nc*nrC*nlC; % number of brick elements in the cylinder
nelembrickR = nc*nrR*nlR; % number of brick elements in the ring

nelembrick = nelembrickC + nelembrickR; % total number of brick elements
e = zeros(1,nelembrick);
m = zeros(1,nelembrick);
n1 = zeros(1,nelembrick);
n2 = zeros(1,nelembrick);
n3 = zeros(1,nelembrick);
n4 = zeros(1,nelembrick);
n5 = zeros(1,nelembrick);
n6 = zeros(1,nelembrick);
n7 = zeros(1,nelembrick);
n8 = zeros(1,nelembrick);

% Cylinder
for k = 1:nc
    for j = 1:nlC
        for i = 1:nrC
            e(i + (j-1)*nrC + (k-1)*nrC*nlC) = i + (j-1)*nrC + (k-1)*nrC*nlC;
            m(i + (j-1)*nrC + (k-1)*nrC*nlC) = 1;
            n1(i + (j-1)*nrC + (k-1)*nrC*nlC) = i + (j-1)*(nrC+1) + (k-1)*(nrC+1)*(nlC+1);
            n2(i + (j-1)*nrC + (k-1)*nrC*nlC) = i + (j-1)*(nrC+1) + k*(nrC+1)*(nlC+1);
            n3(i + (j-1)*nrC + (k-1)*nrC*nlC) = i + j*(nrC+1) + k*(nrC+1)*(nlC+1);
            n4(i + (j-1)*nrC + (k-1)*nrC*nlC) = i + j*(nrC+1) + (k-1)*(nrC+1)*(nlC+1);
            n5(i + (j-1)*nrC + (k-1)*nrC*nlC) = i + 1 + (j-1)*(nrC+1) + (k-1)*(nrC+1)*(nlC+1);
            n6(i + (j-1)*nrC + (k-1)*nrC*nlC) = i + 1 + (j-1)*(nrC+1) + k*(nrC+1)*(nlC+1);
            n7(i + (j-1)*nrC + (k-1)*nrC*nlC) = i + 1 + j*(nrC+1) + k*(nrC+1)*(nlC+1);
            n8(i + (j-1)*nrC + (k-1)*nrC*nlC) = i + 1 + j*(nrC+1) + (k-1)*(nrC+1)*(nlC+1);
        end
    end
end

% Ring
for k = 1:nc
    for j = 1:nlR
        for i = 1:nrR
            e(nelembrickC + i + (j-1)*nrR + (k-1)*nrR*nlR) = nelembrickC + i + (j-1)*nrR + (k-
1)*nrR*nlR;
            m(nelembrickC + i + (j-1)*nrR + (k-1)*nrR*nlR) = 2;
            n1(nelembrickC + i + (j-1)*nrR + (k-1)*nrR*nlR) = nnodeC + i + (j-1)*(nrR+1) + (k-
1)*(nrR+1)*(nlR+1);
            n2(nelembrickC + i + (j-1)*nrR + (k-1)*nrR*nlR) = nnodeC + i + (j-1)*(nrR+1) +
k*(nrR+1)*(nlR+1);
            n3(nelembrickC + i + (j-1)*nrR + (k-1)*nrR*nlR) = nnodeC + i + j*(nrR+1) +
k*(nrR+1)*(nlR+1);
            n4(nelembrickC + i + (j-1)*nrR + (k-1)*nrR*nlR) = nnodeC + i + j*(nrR+1) + (k-
1)*(nrR+1)*(nlR+1);
```

```
            n5(nelembrickC + i + (j-1)*nrR + (k-1)*nrR*nlR) = nnodeC + i + 1 + (j-1)*(nrR+1) +
(k-1)*(nrR+1)*(nlR+1);
            n6(nelembrickC + i + (j-1)*nrR + (k-1)*nrR*nlR) = nnodeC + i + 1 + (j-1)*(nrR+1) +
k*(nrR+1)*(nlR+1);
            n7(nelembrickC + i + (j-1)*nrR + (k-1)*nrR*nlR) = nnodeC + i + 1 + j*(nrR+1) +
k*(nrR+1)*(nlR+1);
            n8(nelembrickC + i + (j-1)*nrR + (k-1)*nrR*nlR) = nnodeC + i + 1 + j*(nrR+1) + (k-
1)*(nrR+1)*(nlR+1);
        end
    end
end

% Create load segments as shell elements to be pressurized
neleminterior = nc*nlC;
n1s = zeros(1,neleminterior);
n2s = zeros(1,neleminterior);
n3s = zeros(1,neleminterior);
n4s = zeros(1,neleminterior);
i = 1;

% on the inside of the ring
for k = 1:nc
    for j = 1:nlR
        n1s(i) = nnodeC + 1 + (j-1)*(nrR+1) + (k-1)*(nrR+1)*(nlR+1);
        n2s(i) = nnodeC + 1 + j*(nrR+1) + (k-1)*(nrR+1)*(nlR+1);
        n3s(i) = nnodeC + 1 + j*(nrR+1) + k*(nrR+1)*(nlR+1);
        n4s(i) = nnodeC + 1 + (j-1)*(nrR+1) + k*(nrR+1)*(nlR+1);
        i = i + 1;
    end
end

% on the inside of the difference between the cylinder and the ring

for k = 1:nc
    for j = 1:nn
        n1s(i) = 1 + (j-1)*(nrC+1) + (k-1)*(nrC+1)*(nlC+1);
        n2s(i) = 1 + j*(nrC+1) + (k-1)*(nrC+1)*(nlC+1);
        n3s(i) = 1 + j*(nrC+1) + k*(nrC+1)*(nlC+1);
        n4s(i) = 1 + (j-1)*(nrC+1) + k*(nrC+1)*(nlC+1);
        i = i + 1;
    end
end

for k = 1:nc
    for j = nn + nlR + 1:nlC;
        n1s(i) = 1 + (j-1)*(nrC+1) + (k-1)*(nrC+1)*(nlC+1);
        n2s(i) = 1 + j*(nrC+1) + (k-1)*(nrC+1)*(nlC+1);
        n3s(i) = 1 + j*(nrC+1) + k*(nrC+1)*(nlC+1);
        n4s(i) = 1 + (j-1)*(nrC+1) + k*(nrC+1)*(nlC+1);
        i = i + 1;
    end
end

% List of bottom nodes of cylinder
dnode_C = (nc+1)*(nrC+1);
dn_C = zeros(1,dnode_C);
j = 1;
for k = 1:nc+1
    for i = 1:(nrC+1)
            dn_C(j) = i + (k-1)*(nrC+1)*(nlC+1);
            j = j + 1;
    end
end

% List of top nodes of cylinder
fnode_C = (nc+1)*(nrC+1);
fn_C = zeros(1,fnode_C);
j = 1;
for k = 1:nc+1
    for i = 1:(nrC+1)
            fn_C(j) = i + nlC*(nrC+1) + (k-1)*(nrC+1)*(nlC+1);
```

```
            j = j + 1;
    end
end

%list of nodes for cutting edges of the Cylinder(y symmetry)
tnode_C=(nrC+1)*(nlC+1);
tn_C=zeros(1,tnode_C);
k=1;
for j=1:nlC+1
    for i=1:nrC+1
        tn_C(k)=i+(j-1)*(nrC+1);
        k=k+1;
    end
end

%list of nodes for cutting edges of the Cylinder(x symmetry)

bnode_C=(nrC+1)*(nlC+1);
bn_C=zeros(1,bnode_C);
k=1;
for j=1:nlC+1
    for i=1:nrC+1
        bn_C(k)=i+(j-1)*(nrC+1)+(nrC+1)*nc*(nlC+1);
        k=1+k;
    end
end

% list of nodes for cutting edges of the ring(y symmetry)

tnode_R=(nrR+1)*(nlR+1);
tn_R=zeros(1,tnode_R);
k=1;
for j=1:nlR+1
    for i=1:nrR+1
        tn_R(k)= nnodeC + i+(j-1)*(nrR+1);
        k=k+1;
    end
end

% list of nodes for cutting edges of the ring(x symmetry)

bnode_R=(nrR+1)*(nlR+1);
bn_R=zeros(1,bnode_R);
k=1;
for j=1:nlR+1
    for i=1:nrR+1
        bn_R(k)= nnodeC+ i+(j-1)*(nrR+1)+(nrR+1)*nc*(nlR+1);
        k=1+k;
    end
end



savefile = 'Ring_in_Cylinder.dyn';
fid = fopen(savefile, 'wt');
fprintf(fid, '*KEYWORD\n');
fprintf(fid, '$---+----1----+----2----+----3----+----4----+----5----+----6----+----7----+----
8\n');
fprintf(fid, '$                     TITLE CARD\n');
fprintf(fid, '$---+----1----+----2----+----3----+----4----+----5----+----6----+----7----+----
8\n');
fprintf(fid, '*TITLE\n');
fprintf(fid, 'Ring in Cylinder\n');
fprintf(fid, '$---+----1----+----2----+----3----+----4----+----5----+----6----+----7----+----
8\n');
fprintf(fid, '$                     CONTROL CARDS\n');
fprintf(fid, '$---+----1----+----2----+----3----+----4----+----5----+----6----+----7----+----
8\n');
fprintf(fid, '*CONTROL_TERMINATION\n');
fprintf(fid, '$    ENDTIM    ENDCYC     DTMIN    ENDNEG    ENDMAS\n');
fprintf(fid, '%10f         0       0.0       0.0       0.0\n', endtime);
```

```
fprintf(fid, '*CONTROL_TIMESTEP\n');
fprintf(fid, '$    DTINIT      SCFT      ISDO    TSLIMT      DTMS      LCTM     ERODE
MS1ST\n');
fprintf(fid, '       0.00       0.9         0\n');
fprintf(fid, '*CONTROL_HOURGLASS\n');
fprintf(fid, '$       IHQ        QH\n');
fprintf(fid, '         1       0.1\n');
fprintf(fid, '*CONTROL_BULK_VISCOSITY\n');
fprintf(fid, '$        Q2        Q1\n');
fprintf(fid, ' 0.150E+01 0.600E-01\n');
fprintf(fid, '*CONTROL_OUTPUT\n');
fprintf(fid, '$    NPOPT    NEECHO    NREFUP    IACCOP     OPIFS    IPNINT    IKEDIT\n');
fprintf(fid, '         0         0         0         0 0.000E+00         0         0\n');
fprintf(fid, '*CONTROL_ENERGY\n');
fprintf(fid, '$      HGEN      RWEN    SLNTEN     RYLEN\n');
fprintf(fid, '         1         2         1         1\n');
fprintf(fid, '$---+----1----+----2----+----3----+----4----+----5----+----6----+----7----+----
8\n');
fprintf(fid, '$                     DATABASE CONTROL CARDS FOR ASCII FILE\n');
fprintf(fid, '$---+----1----+----2----+----3----+----4----+----5----+----6----+----7----+----
8\n');
fprintf(fid, '*DATABASE_GLSTAT\n');
fprintf(fid, '   0.12E-3\n');
fprintf(fid, '*DATABASE_RCFORC\n');
fprintf(fid, '   0.12E-3\n');
fprintf(fid, '$---+----1----+----2----+----3----+----4----+----5----+----6----+----7----+----
8\n');
fprintf(fid, '$                     DATABASE CONTROL CARDS FOR BINARY FILE\n');
fprintf(fid, '$---+----1----+----2----+----3----+----4----+----5----+----6----+----7----+----
8\n');
fprintf(fid, '*DATABASE_BINARY_D3PLOT\n');
fprintf(fid, '%10f \n', endtime/100);
fprintf(fid, '*DATABASE_BINARY_D3THDT\n');
fprintf(fid, '%10f \n', endtime/100);
fprintf(fid, '*DATABASE_EXTENT_BINARY\n');
fprintf(fid, '         0         0         3         0         1         1         1
1\n');
fprintf(fid, '         0         0         0         0         0         0\n');
fprintf(fid, '$---+----1----+----2----+----3----+----4----+----5----+----6----+----7----+----
8\n');
fprintf(fid, '$                     DEFINE PARTS CARDS\n');
fprintf(fid, '$---+----1----+----2----+----3----+----4----+----5----+----6----+----7----+----
8\n');
for i = 1:npart
   fprintf(fid, '*PART\n');
   fprintf(fid, '$ HEADING\n');
   fprintf(fid, ' PART PID =      %2i PART NAME : %s\n', i,char(part(i)));
   fprintf(fid, '$      PID       SID       MID     EOSID      HGID      GRAV    ADPOPT
TMID\n');
   fprintf(fid, '%10i %9i %9i\n', i,i,i);
end
fprintf(fid, '$---+----1----+----2----+----3----+----4----+----5----+----6----+----7----+----
8\n');
fprintf(fid, '$                     MATERIAL CARDS\n');
fprintf(fid, '$---+----1----+----2----+----3----+----4----+----5----+----6----+----7----+----
8\n');
for i = 1:npart-1
   fprintf(fid, '*MAT_HEART_TISSUE\n');
   fprintf(fid, '$ MATERIAL NAME :%s\n', char(part(i)));
   fprintf(fid, '$      MID        RO         C        B1        B2        B3         P\n');
   fprintf(fid, '%10i    0.1E-8 %9.2E %9.2E %9.2E %9.2E %9.2E \n',
i,c(i),b1(i),b2(i),b3(i),p(i));
   fprintf(fid, '$     AOPT\n');
   fprintf(fid, '          0\n');
   fprintf(fid, '$       XP        YP        ZP        A1        A2        A3\n\n');
   fprintf(fid, '$       V1        V2        V3        D1        D2        D3      BETA\n\n');
end
% for i = 1:npart
%    fprintf(fid, '*MAT_ELASTIC\n');
%    fprintf(fid, '$ MATERIAL NAME :%s\n', char(part(i)));
%    fprintf(fid, '$      MID        RO         E        PR        DA        DB         K\n');
```

```
%    fprintf(fid, '%10i    0.1E-8  %9.2E %9.2E\n', i,2,0.45);
% end
fprintf(fid, '*MAT_SEATBELT\n');
fprintf(fid, '$ MATERIAL NAME :%s\n', char(part(3)));
fprintf(fid, '$      MID      MPUL     LLCID     ULCID      LMIN\n');
fprintf(fid, '%10i  %1.1i %9.1i %9.1i\n', 3,5.59e-12,3,4);
fprintf(fid, '$---+----1----+----2----+----3----+----4----+----5----+----6----+----7----+----
8\n');
fprintf(fid, '$                    SECTION CARDS\n');
fprintf(fid, '$---+----1----+----2----+----3----+----4----+----5----+----6----+----7----+----
8\n');
for i = 1:npart-1
   fprintf(fid, '*SECTION_SOLID\n');
   fprintf(fid, '$    SECID    ELFORM       AET\n');
   fprintf(fid, '%10i %9i\n', i,1); % 1 means constant stress elements; 2 would mean constant
pressure elements
end
fprintf(fid, '*SECTION_SEATBELT\n');
fprintf(fid, '$    SECID\n');
fprintf(fid, '%10i\n', 3);
fprintf(fid, '$---+----1----+----2----+----3----+----4----+----5----+----6----+----7----+----
8\n');
fprintf(fid, '$                    NODAL POINT CARDS\n');
fprintf(fid, '$---+----1----+----2----+----3----+----4----+----5----+----6----+----7----+----
8\n');
fprintf(fid, '*NODE\n');
fprintf(fid, '$   NODE              X               Y               Z      TC      RC\n');
for i = 1:nnode
    fprintf(fid, '%8i %15.9f %15.9f %15.9f\n',n(i),xn(i),yn(i),zn(i));
end
fprintf(fid, '$---+----1----+----2----+----3----+----4----+----5----+----6----+----7----+----
8\n');
fprintf(fid, '$                    SOLID ELEMENT CARDS\n');
fprintf(fid, '$---+----1----+----2----+----3----+----4----+----5----+----6----+----7----+----
8\n');
fprintf(fid, '*ELEMENT_SOLID\n');
fprintf(fid, '$    EID     PID      N1      N2      N3      N4      N5      N6      N7
N8\n');
repeat = 1;
for i = 1:nelembrick
    fprintf(fid, '%8i %7i %7i %7i %7i %7i %7i %7i %7i
%7i\n',e(i),m(i),n1(i),n2(i),n3(i),n4(i),n5(i),n6(i),n7(i),n8(i));
end
fprintf(fid, '*ELEMENT_SEATBELT\n');
fprintf(fid, '$    EID     PID      N1      N2   SBRID    SLEN      N3      N4\n');
for i = 1:nsutures
    fprintf(fid, '%8i %7i %7i %7i %15.3f\n',i,3,listC(i),listR(i),-0.95*0.5*(DiC-DoR));
end
fprintf(fid, '*LOAD_SEGMENT\n');
fprintf(fid, '$     LCID        SF        AT        N1        N2        N3        N4\n');
for i = 1:neleminterior
    fprintf(fid, '%10i %9.1f %9.1i %9i %9i %9i %9i\n',1,1,0,n1s(i),n2s(i),n3s(i),n4s(i));
end
if option == 1
    fprintf(fid, '*LOAD_NODE_POINT\n');
    fprintf(fid, '$     NODE       DOF      LCID        SF       CID        M1        M2
M3\n');
    for i = 1:fnode_C
        fprintf(fid, '%10i %9i %9i %9.1f\n',fn_C(i),3,2,1);
    end
end
fprintf(fid, '$---+----1----+----2----+----3----+----4----+----5----+----6----+----7----+----
8\n');
fprintf(fid, '$                    BOUNDARY CONDITION CARDS\n');
fprintf(fid, '$---+----1----+----2----+----3----+----4----+----5----+----6----+----7----+----
8\n');
fprintf(fid, '*BOUNDARY_SPC_NODE\n');
fprintf(fid, '$ NID/NSID       CID      DOFX      DOFY      DOFZ     DOFRX     DOFRY
DOFRZ\n');

% Boundary condition for the Cylinder
```

```
for i = 1:dnode_C
    fprintf(fid, '%10i %9i %9i %9i %9i \n',dn_C(i),0,0,0,1);  % no displacement in z-direction
end
for i = 1:fnode_C
    fprintf(fid, '%10i %9i %9i %9i %9i \n',fn_C(i),0,1,1,0);  % no displacement in x- and y-di-
rections
end
for i=1:tnode_C
    fprintf(fid, '%10i %9i %9i %9i %9i \n',tn_C(i),0,0,1,0);  % no displacement in y-direction
end

for i=1:bnode_C
    fprintf(fid, '%10i %9i %9i %9i %9i \n',bn_C(i),0,1,0,0);  % no displacement in x-direction
end


% Boundary condition for the Ring

for i=1:tnode_R
    fprintf(fid, '%10i %9i %9i %9i %9i \n',tn_R(i),0,0,1,0);  % no displacement in y-direction
end

for i=1:bnode_R
     fprintf(fid, '%10i %9i %9i %9i %9i \n',bn_R(i),0,1,0,0); % no displacement in x-direction
end

if option == 2
    fprintf(fid, '*BOUNDARY_PRESCRIBED_MOTION_NODE\n');
    fprintf(fid, '$      NID       DOF       VAD      LCID        SF       VID     DEATH
BIRTH\n');
    for i = 1:fnode_C
        fprintf(fid, '%10i %9i %9i %9i\n',fn_C(i),3,2,2);
    end
end

% Load Curves
fprintf(fid, '*DEFINE_CURVE\n');
fprintf(fid, '$     LCID      SIDR      SCLA      SCLO      OFFA      OFFO\n');
fprintf(fid, '%10i          %10.4f\n',1,1);
fprintf(fid, '$                A1                  O1\n');
fprintf(fid, '%20.4f %19.4f\n',0,0*0.0133/100);
fprintf(fid, '%20.4f %19.4f\n',1.01*endtime,pmax*0.0133/100);

if option == 1
    fprintf(fid, '*DEFINE_CURVE\n');
    fprintf(fid, '$     LCID      SIDR      SCLA      SCLO      OFFA      OFFO\n');
    fprintf(fid, '%10i          %10.4f\n',2,1);
    fprintf(fid, '$                A1                  O1\n');
    fprintf(fid, '%20.4f %19.4f\n',0,0*0.0133/100);
    fprintf(fid, '%20.4f %19.4f\n',1.01*endtime,pmax*0.0133/100*pi*1/16*DiC^2/((nc+1)*(nrC+1)));
elseif option == 2
    fprintf(fid, '*DEFINE_CURVE\n');
    fprintf(fid, '$     LCID      SIDR      SCLA      SCLO      OFFA      OFFO\n');
    fprintf(fid, '%10i          %10.4f\n',2,1);
    fprintf(fid, '$                A1                  O1\n');
    fprintf(fid, '%20.4f %19.4f\n',0,0);
    fprintf(fid, '%20.4f %19.4f\n',endtime/10,LC*(lambda-1));
    fprintf(fid, '%20.4f %19.4f\n',1.01*endtime,LC*(lambda-1));
end
fprintf(fid, '*DEFINE_CURVE\n');
fprintf(fid, '$     LCID      SIDR      SCLA      SCLO      OFFA      OFFO\n');
fprintf(fid, '         3         0\n');
fprintf(fid, '$                A1                  O1\n');
fprintf(fid, '%20.4f %19.4f\n',0,0);
fprintf(fid, '%20.4f %19.4f\n',endtime/10,0.1);
fprintf(fid, '*DEFINE_CURVE\n');
fprintf(fid, '$     LCID      SIDR      SCLA      SCLO      OFFA      OFFO\n');
fprintf(fid, '         4         0\n');
fprintf(fid, '$                A1                  O1\n');
fprintf(fid, '%20.4f %19.4f\n',0,0);
fprintf(fid, '%20.4f %19.4f\n',endtime/10,0.1);
```

```
fprintf(fid, '*END\n');
```